Design of Tall-Coupled-Wall Timber Building: Energy Dissipating Coupling Beams

PRINCIPAL INVESTIGATOR

Dr. Solomon Tesfamariam, P.Eng.

(Professor, UBC Okanagan Campus)

HQP

Konstantinos Skandalos

(PhD Candidate, UBC Okanagan Campus)

Biniam Tekle Teweldebrhan

(PhD Student, UBC Okanagan Campus)

December 2021

THE UNIVERSITY OF BRITISH COLUMBIA

FACULTY OF APPLIED SCIENCE, SCHOOL OF ENGINEERING

Prepared for

Forestry Innovation Investment Ltd.
1200 - 1130 West Pender Street, Vancouver, BC Canada V6E 4A4

by

Dr. Solomon Tesfamariam, P.Eng.
School of Engineering
The University of British Columbia, Okanagan Campus, BC, Canada
3333 University Way, Kelowna, BC Canada V1V 1V7

Disclaimers

This report includes seismic design of High-rise timber building coupled with dampers consisting CLT walls, glulam columns and beams, and steel coupling beams. Other analysis models, types and design methods for coupled shear walls are possible, and they may result in different demands on the building. The connections detailing in this report were chosen to represent the use of off-the shelf solutions, and other ways of connection detailing are available. The report has no intention of promoting or endorsing any particular proprietary connection or building system. The authors have taken reasonable actions and due diligence to ensure the accuracy of the information provided in this report; however, THE AUTHORS, UNIVERSITY OF BRITISH COLUMBIA, OR OTHER CONTRIBUTORS ASSUME NO LIABILITY FOR ANY DIRECT OR INDIRECT DAMAGE, INJURY, LOSS OR EXPENSE THAT MAY BE INCURRED OR SUFFERED AS A RESULT OF THE USE OF THIS REPORT INCLUDING WITHOUT LIMITATION PRODUCTS, BUILDING TECHNIQUES OR PRACTICES. The authors do not guarantee the completeness of the information published in this report. Users of this report agree to use the information in this report (analysis suggestions, design procedures, detailing, etc.) at their own risk. We will not be liable for any errors, inaccuracies, omissions or damages arising from the use of the information presented in this report, nor any action taken in reliance to the presented information. Building science, products and construction practices change and improve over time and rather than relying on this report, it is advisable to: (a) regularly consult up-to-date technical publications on products and practices, (b) seek specific information and professional advice on the use of products mentioned in this report from manufacturers or suppliers of the products and consultants with appropriate qualifications and experience, and (c) review and comply with the specific requirements of the applicable building codes for each construction project.

Acknowledgements

Development of the design guideline in this project was supported through the BC Forestry Innovation Investment's (FII) Wood First Program. The financial support through NSERC Alliance is acknowledged. Under the supervision of Dr. Tesfamariam, various students have contributed to the knowledge presented in this report:

- Konstantinos Skandalos (PhD candidate) was actively involved in OpenSees modelling and initial report writing.
- Biniam Tekle Teweldebrhan (PhD student) was actively involved in the performance-based design implementation and final report writing.

Contents

List of Figures

List of Tables

Chapter 1

Introduction

1.1 Motivation

Rapid growth of urban populations and associated environmental concerns challenged city planners and developers to consider sustainable building systems. A decision on the selection of mass timber building, one such sustainable alternative, by different stakeholders, should consider economics, aesthetics, technology, regulations, and political factors (Moon et al., 2007; Tesfamariam et al., 2019b). The political factors are indeed satisfied as the Canadian timber industry and Natural Resources Canada are backing design and construction of tall-timber buildings. One such initiative in British Columbia (BC), for example, is Forest Innovation Investment (FII) Wood First program. Canadian engineers and designers are at the forefront and are pushing the limit of tall-timber design. In Canada, an 18-storey UBC's Brock common (the tallest hybrid wood building in the world in 2017, Fig. 1.1) and 13-storey Origine (the tallest all-wood condominium building in North America in 2017) buildings are constructed in the city of Vancouver and Quebec City, respectively (Dubois et al., 2020; Veilleux et al., 2015). The UBC's Brock common building showed the technical viability of tall mass-timber buildings. With the use of mass timber, such as cross-laminated timber (CLT), the current National Building Code of Canada (NBC 2020) has increased the timber-based building height from 6 to 12 stories (Dubois et al., 2020; Tesfamariam et al., 2021; Veilleux et al., 2015). With this increase in building height, however, timber being lighter and flexible material, wind and earthquake loads should be considered (Tesfamariam et al., 2019b). In combination with steel or concrete hybrid systems, CLT buildings are shown to be feasible solution for tall timber structures in

a high seismic zone (Tesfamariam et al., 2015, 2019a). One possible innovative and readily available structural system is to use coupled-wall (CW) systems.

Figure 1.1: UBC's Brock Common 18-storey timber-RC hybrid building; "Photo: UBC Media Relations"

CW structural system uses multiple structural walls connected at all storeys with coupling beams. The coupling beams can be moment-resisting or shear-resisting, depending on their depth-to-length ratio (El-Tawil et al., 2010). Coupling beams enhance strength and stiffness of the system by providing an additional lateral load resistance frame-resisting mechanism. Specifically, in this frame-resisting mechanism, part of the base moments of the individual walls are converted to wall axial forces by means of shear forces developed in the coupling beams (El-Tawil et al., 2010). The analysis and design of this system is a classical problem whose evolution goes back as early as the late 1940s (Chitty, 1947). CW systems have been used in conventional coupled-wall (CCW), hybrid coupled wall (HCW), and replaceable coupled wall (RCW) systems. In this report, CW system is extended to timber buildings by using CLT shear-walls. For tall buildings, platform construction is challenging due to the large perpendicular-to-grain compressive loads that are transferred to the CLT floor panels at the lower story levels (Chen and Popovski, 2020). Moreover, with the

platform type system, the energy dissipation and kinematics is not efficient for CW system (Tesfamariam et al., 2021). Hence, a balloon type CLT walls is used and design guideline for 10-, 15-, and 20-storey CLT coupled-wall (CLT-CW) system is developed. 20-storey tall-mass-timber building with CW system is shown in Figure 1.2. Coupling beams with replaceable shear links and buckling-restrained brace (BRB) hold-downs are proposed as energy dissipation elements of the system. This system enables the timber buildings to respond in-elastically when subjected to design seismic loads where the coupling beams yield first and incur the largest portion of ductility and energy dissipation demand of the system. The behavior of the CLT-CW system is investigated under different coupling ratio (CR) and combined seismic modification factors ($R_o R_d$) conditions. It is believed that the availability of design guideline would enhance the confidence of architects, structural engineers, owners, and contractors towards tall mass-timber buildings. Outcome of the proposed research would increase the volume of wood in buildings, which will support the forestry business in Canada.

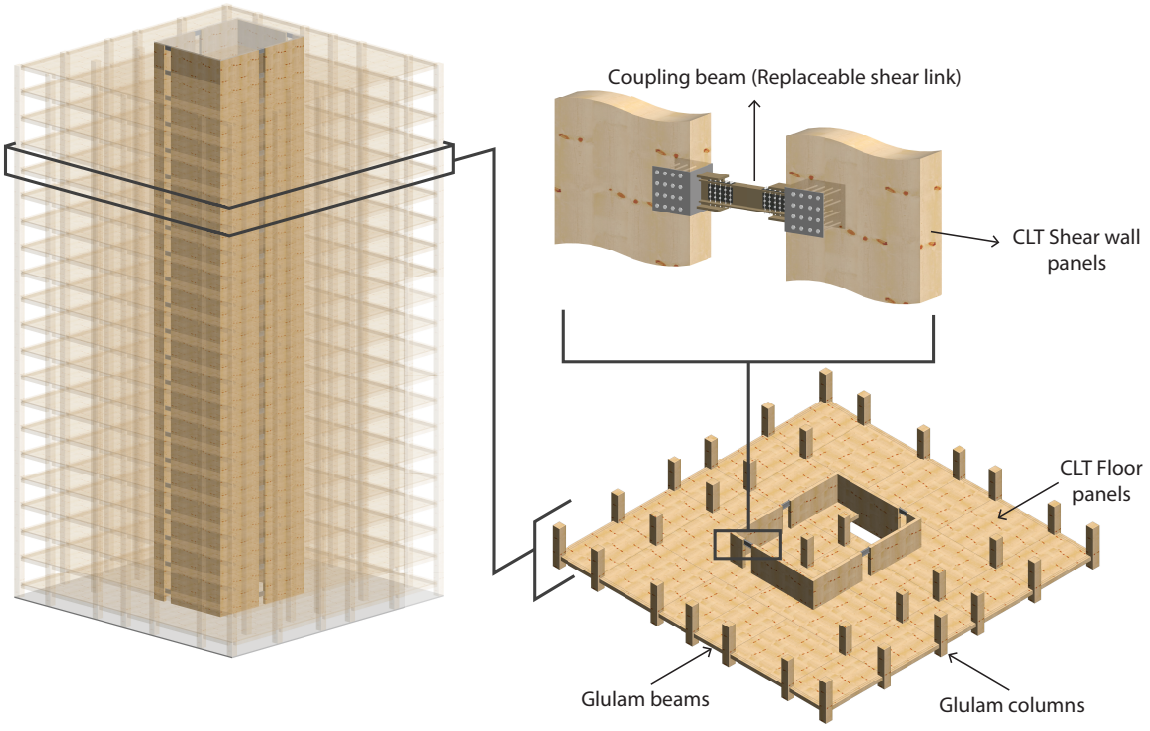

Figure 1.2: 3D view of the proposed CLT-CW system

1.2 Seismic design methods

Force-based design (FBD), displacement-based design (DBD) and performance-based design (PBD) method are alternate design methods that have be used in the design of buildings. The FBD is predominantly used by building codes worldwide and it is based on conducting linear-elastic analyses of the system. In this method, the elastic design forces are reduced by a ductility R_d and overstrength R_o force reduction factors to account for the ductility and energy dissipation, and over-strength of the system, respectively (NBC, 2015). Linear elastic analysis, either the equivalent static load analysis (ESLA) or the response spectrum analysis (RSA) method, can be used. The proposition of seismic modification factors for a new structural system is not an easy task, as extensive experimental and analytical studies are required to ensure their validity, e.g. (Tesfamariam et al., 2021). These factors account for uncertainty in seismic motion from future earthquakes, thus their values are generally conservative. Furthermore, they are generally independent of the fundamental period and the geometrical configuration of the specified structural system, therefore leading to non-uniform risk designs (Baltzopoulos et al., 2021; Vamvatsikos et al., 2020). Notwithstanding the simplicity and wide use of FBD in practice, several disadvantages have been identified with respect to its underlying assumptions (Priestley, 1993).

For the HCW system, a force reduction factor of $R = 6$ has been specified according to FEMA-450 (2003). Although FBD offers a simple procedure for seismic design, the CR of the coupled-wall system is not explicitly specified as a design requirement. Therefore, FBD can lead to CR values outside of the range specified by the various researchers. Moreover, force reduction factors have not been specified for all CW structural systems, e.g. CLT-CW system or RCW system. Therefore, performance-based design approaches, explicitly accounting for the performance objectives for the specific structural system, are preferred.

The PBD emerged two decades ago as consequence of the extensive damage observed during the Northridge (1994) and Kobe (1995) earthquakes (Cornell and Krawinkler, 2000; Porter, 2003). PBD involves number of response objectives corresponding to different hazard levels and advocates use of nonlinear analysis procedures. Direct-displacement based design (DDBD) (Priestley et al., 2007) have been proposed as a viable PBD. In DDBD, nonlinear properties are more directly accounted for through use of effective linear stiffness and damping properties of SDOF approximation of the

building. Furthermore, the use of displacement as design response parameter is more compatible with PBD, where displacement-related engineering demand parameters (EDP) are most commonly considered to assess seismic performance.

1.3 Project scope

For the CLT-CW systems, the proposed tasks are:

- CW system (10-, 15- and 20-storey timber core buildings, Figure 1.3) will be considered using CLT balloon shear-walls and with energy dissipator coupling beams.

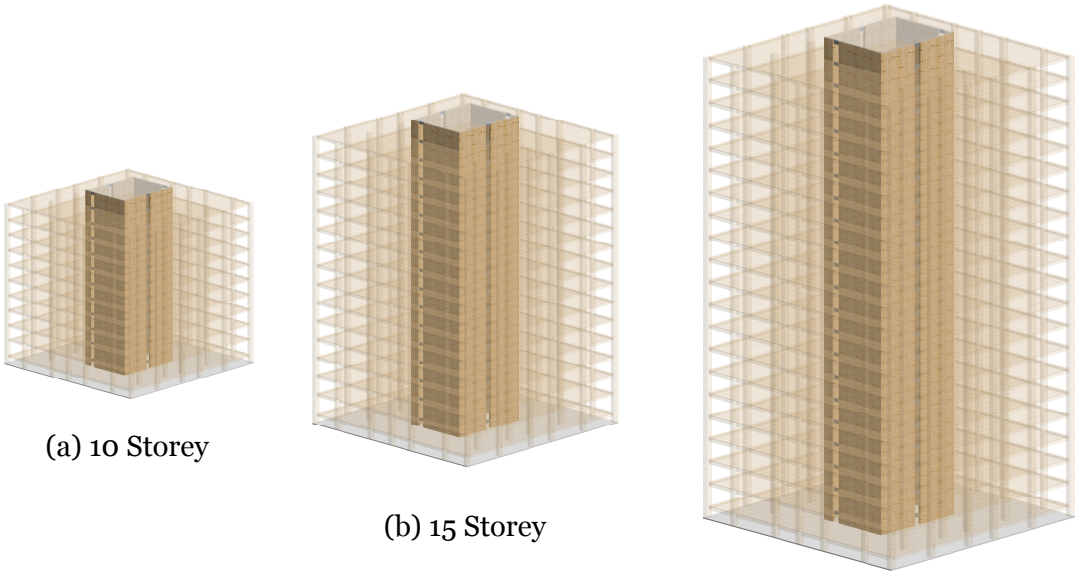

(a) 10 Storey

(b) 15 Storey

(c) 20 Storey

Figure 1.3: 3D View of high-rise-mass-timber building with CW system

- To reduce the demand of ductility on the coupling beams, the external damper (friction damper) is introduced in the hybrid coupled system.
- Fifteen different conditions are considered to examine the behavior of the CLT-CW system under different coupling ratio (CR) values (10%, 20%, 30%, 40%, and 50%) and combined seismic modification factors ($R_o R_d$) of 3, 4.5, and 6.
- Once the structural design are optimized, the over-strength and ductility factors, in congruence with NBC 2015, will be developed using FEMA P695 procedure.

1.4 Organization of report

This report contains 8 chapters. Details of each chapter are:

- **Chapter 1** introduces the general motivation and overview of the different tall-mass-timber structures. Moreover, the chapter highlights the general purpose of CW systems and the different seismic design methods that can be applied.
- **Chapter 2** presents a thorough literature review including the background for the evolution of CW systems, their structural behaviour, and the different analysis models that exists in literature. The chapter also reviews the different CW system types and coupling beam materials that exist in literature.
- **Chapter 3** provides the detail model parameters including the plan and 3D view of the prototype structure. Moreover, this chapter provides the general load cases, combination and model analysis of the structures. Besides, the OpenSees numerical modeling parameters for CLT panels, shear-links and hold-down types are provided. The selected ground motions and building site seismic behavior are also briefed under this chapter.
- **Chapter 4** presents the general procedure for the seismic design of the CW system. After introducing the concept of continuous medium method, the analysis and design of CLT-CW system is presented. A numerical example that shows the complete procedure is provided.
- In **Chapter 5**, the result for the nonlinear static and dynamic analysis is discussed. The result for maximum inter-storey drift ratio, residual inter-storey drift ratio, and hold-down and coupling beam force-displacement responses are given in this chapter.
- **Chapter 6** discusses the performance evaluation of the seismic modification factors, that are used to design the CLT-CW systems, using the procedures outlined by FEMA P695.
- Finally, in **Chapter 7**, the PBD procedure for seismic design of the CW system is presented. After defining the different performance objectives, a step-by-step preliminary proportioning of the fundamental geometries of the CW systems is provided. Results obtained from the performed nonlinear static and dynamic analysis are discussed. Finally, **Chapter 8** synthesizes the results of the

previous chapters and provides the conclusions and future research perspectives of this report. Supplementary information on parametric analysis and design of experiment are provided as appendices of this report.

Chapter 2

Literature Review

2.1 Introduction

Traditionally, buildings were built at lower heights with rigid moment resisting frames that comprises simple vertical and horizontal structural elements. Nonetheless, with the continuous rise in population and technological advancement of construction industry, the construction of tall buildings of ever-growing heights have been continuously taking place worldwide (Ali and Moon, 2018). Conceptually, as buildings are built taller and slender, the provision of seismic and wind resistance becomes a critical design consideration. As a result, many innovations in structural systems or lateral load resisting systems (LLRSs) have emerged. CW system is one of the classical and efficient types of LLRSs used in modern tall building designs. The concept of CW system was introduced as early as the late 1940s (Chitty, 1947) when continuous medium theory was used to analyze cantilever beams coupled using cross-bars. With this method, the cross-bars were replaced into an equivalent continuous medium that can transmit actions of the same type as the discrete cross-bars. The same concept was then applied to predict stresses in tall buildings (Chitty, 1947) and allow a rapid assessment of horizontal deflections in coupled-shear wall structures subject to lateral loads (Coull and Choudhury, 1967b; Smith et al., 1981; Smith and Coull, 1991). Based on the material and behavior of coupling beams, the value of coupling ratio, and the shear-walls type, there are various classification of CW system. Moreover, CW system can be modelled in different ways. The detail classification, modeling and analysis type of CW system are dealt in the subsequent sections of this chapter.

2.2 Coupled wall behavior

In CW systems, part of the base moment in the individual walls is converted to wall axial forces by means of shear forces developed in the coupling beams (Figure 2.1). The degree of coupling (amount of converted moment) provided by the coupling beams has a major impact in the structural performance of the CW system (Coull and Choudhury, 1967a; El-Tawil et al., 2010; Smith and Coull, 1991). The parameter that measures the induced degree of coupling and controls the behavior of the CW system is called coupling ratio (CR). For a two-wall system, the CR is defined as (El-Tawil et al., 2010):

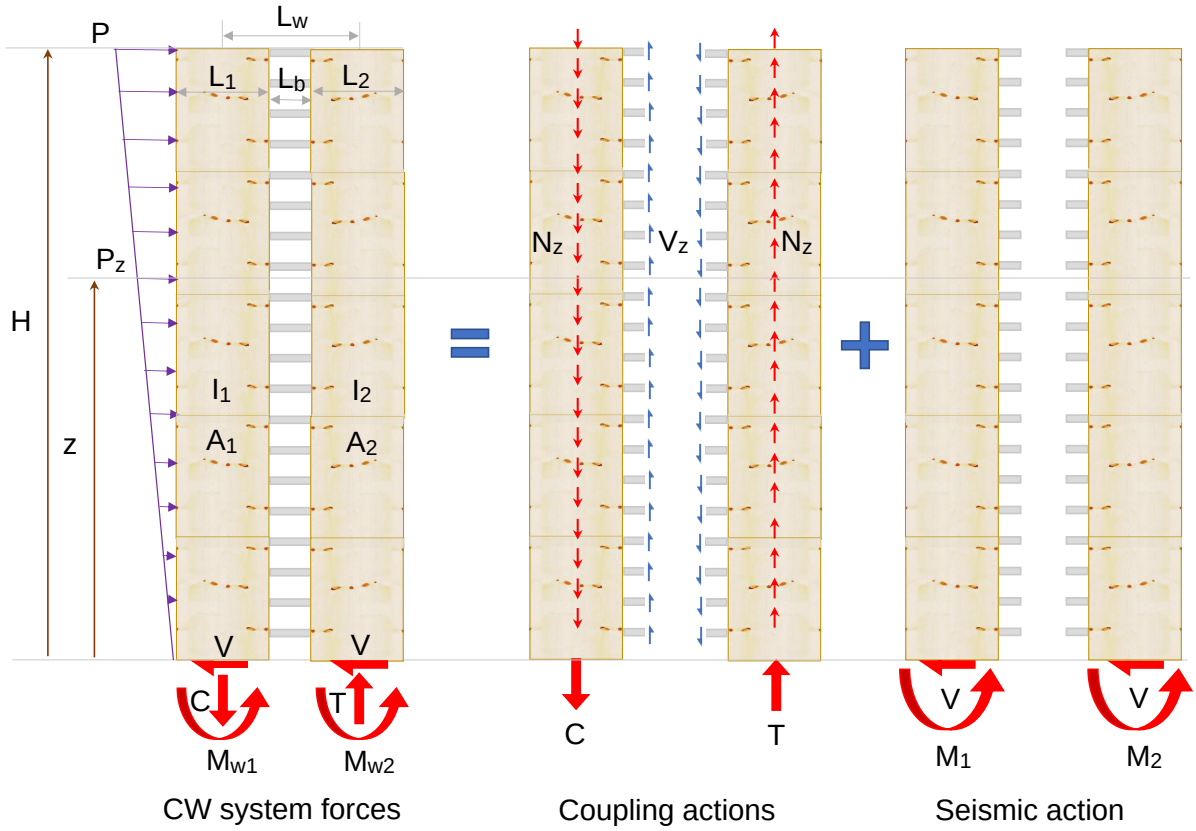

Figure 2.1: The development of coupling system

$$CR = \frac{TL_w}{M_{max}} = \frac{TL_w}{TL_w + \sum M_{wall}} = \frac{L_w \sum V_{z,i}}{TL_w + \sum M_{wall}}, \tag{2.1}$$

where $M_{max} = M_1 + M_2$ = total overturning moment due to lateral forces, $T = C$ =axial load induced by the shear forces of the coupling beams, L_w = distance between the centroid of the two walls, M_{wall} = reduced base moment of the individual walls ($M_{w1} = M_{w2}$ for symmetrical walls), and $\sum V_{z,i}$ = accumulation of coupling beam

shears acting at the edge of all piers.

Different values of CR, depending on the type and uniformity of the CW structure, have been recommended in the literature. El-Tawil et al. (2002) recommended CR range values from 30% to 45% based on a study conducted for 12-storey hybrid CW (HCW) structure with uniform coupling beams distributed throughout the height of the building. Xuan et al. (2006) used a CR = 80% and designed a 15-storey efficient reinforced concrete or conventional CW (CCW) structure by providing and distributing three groups of coupling beams. Harries and McNiece (2006) designed two 30-storey CCW system with CR values of 67% and 78%. This latter study was conducted by reducing the wall capacities three times over the wall height and changing the stiffness of the coupling beams in proportion to the shear demands.

Canadian Concrete Standard (CSA 2014) and Chaallal et al. (1996) have also classified the behaviour of CCW as partial (for CR value $< 66\%$) and full coupling (for CR value >= 66%), and low, intermediate and high coupling, respectively. The low coupling behavior indicates that coupling beams develop almost no or little coupling moments (the beams are pinned links), the intermediate coupling indicates that coupling action is activated and resisted some percentage of the imposed overturning moments, while the high coupling (such as pierced walls) exhibits a stiff behavior in which the wall piers effectively behave as a single pier (Chaallal et al., 1996; El-Tawil et al., 2010). Figure 2.2 illustrates the structural behavior of three CW systems under different degrees of CR.

Among these three classes of CW systems, an intermediate coupling whose CR in the range of 30% to 45% are the most optimal in the sense that the wall piers will neither experience highest base wall rotations, story drifts, shear distortions and deflections due to high overturning moment (in the case of lower CR values) nor suffer from early crushing due to high axial force induced by the coupling action (in the case of higher CR values) (El-Tawil et al., 2010). This recommendation works well for CCW and HCW systems. However, unlike the reinforced concrete and hybrid structures, the behavior of coupling action in mass-timber structures with CLT wall pier is relatively a new area of research and there has been no recommendation placed for it. What we knew with this type of structures is that with the relatively low axial strength the CLT have (compared to RC walls), the optimal coupling ratio can not go as high as that of its alternate reinforce or hybrid systems. Therefore, in this paper, different CR values

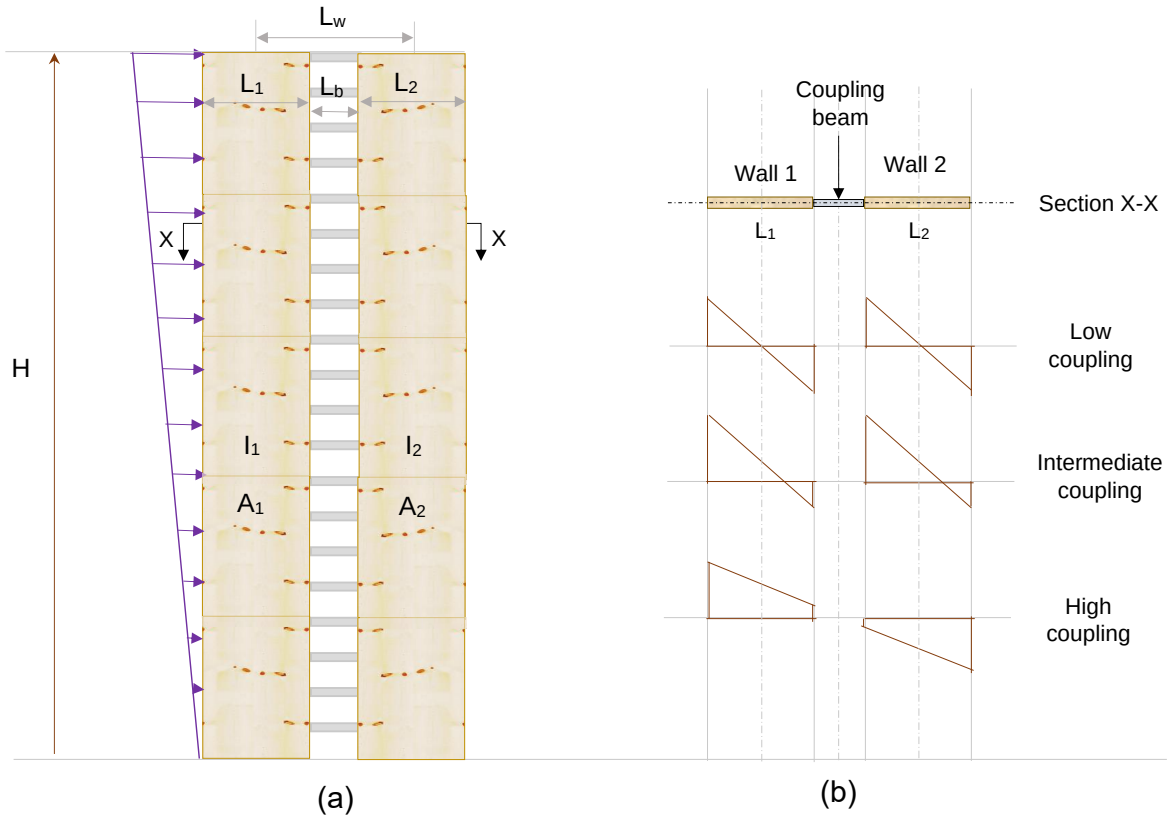

Figure 2.2: Behavior of CW system with different degree of CR: a) Response of CW; b) Strain Distribution

(10% to 50%) are investigated as a parametric study in the performed analyses.

2.3 Analysis model types

Different linear and nonlinear analysis models have been used to analysis the complex behavior of CW systems (El-Tawil et al., 2010). The models used can be grouped as: continuous medium method (CMM), equivalent frame method (EFM), multi-spring model (MSM), and finite element method (FEM). The CMM is an elastic method of analysis that provides a good approximation for preliminary designs and should be accompanied by a more accurate nonlinear analysis method in order to evaluate the preliminary design. Even though helpful information about the behaviour of CW can be obtained by EFM and MSM, their results seems to be more of qualitative. Nevertheless, they are computationally efficient and have been adopted in the inelastic dynamic analyses of CW systems (Spacone and El-Tawil, 2004). On the other hand, FEM are relatively the most accurate, complex and cumbersome method that can be used to study the detail nonlinear response of structures (El-Tawil et al., 2010).

It's worth-mentioning that although the existing CW system studies were conducted on CCW structures, the general behavior and mechanics are the same for all CW systems (El-Tawil et al., 2010). Accordingly, in this report, the CMM and FEM are used to design the preliminary CLT-CW geometrical parameter and study the nonlinear responses of the structure under the action of different ground motions, respectively.

2.3.1 Continuous medium method

Continuous Medium Method (CMM) allows to study the behaviour of CW structures and understand the relative influence of the wall piers and coupling beams (Smith and Coull, 1991). The method has been termed with various names in the literature such as "continuous connection method", "continuum method", "shear connection method", and "laminar analysis" (Eljadei and Harries, 2014; Smith and Coull, 1991). First used to solve the 'dowelled cantilever' problem, CMM has been applied in the study of tall buildings under the action of wind load (Chitty, 1947). This method reduces the high statically indeterminacy of CW into a problem modeled as single fourth-order differential equation. CMM results in closed-form solutions for the internal forces and displacements of various types of CW structures, e.g. (Coull and Choudhury, 1967a; Ha and Tan, 1999; Smith and Coull, 1991). The derivation of the internal forces and displacements are based on the plane CW structure, where the coupling beams are modeled as a continuous connecting medium whose bending and shear properties are equivalent to those of the connecting beams (Harries et al., 2004). The internal shear forces (in terms of flow or laminar) determined in the continuum are then integrated over the storey heights to yield a concentrated shear force for each coupling beam. As CMM is an approximate method of analysis, its applicability is limited for uniform or quasi-uniform structures (Smith and Coull, 1991). The detail derivation and resulting closed-form solutions depends on the type of lateral loads (concentrated, uniform, triangular, etc) and the CW system. Derivation and solutions for CW systems with different lateral load patterns are presented in chapter 10 and Appendix A of Smith and Coull (1991). The relevant closed-form solutions and their applicability's are discussed in detail in Chapter 4 of this report.

2.3.2 Equivalent frame method

Equivalent Frame Method (EFM) is more accurate and sophisticated method than CMM, which can be used to analyse irregular CW systems (Smith and Coull, 1991). This equivalent wide-column beam frame analogy is referred as a very versatile and economic approach that accommodates both linear and nonlinear analysis necessary for PBD approaches (El-Tawil et al., 2010; Smith and Coull, 1991). In the simplest EFM, the coupled walls are modeled as series of frame members, where each of the wall piers are represented by wide-columns located at the wall's centers. The horizontal frame members consist of two different sections, the rigid or stiff arms and connecting or coupling beams. The stiff arms span between the wall-beam connection and the effective column, and thus incorporate the condition that plane sections remain plane, and ensure the correct rotations and vertical displacements at the faces of the walls (Eljadei and Harries, 2014; Smith and Coull, 1991). While modeling the column, the axial (EA) and flexural (EI) rigidity of the walls must be assigned to the columns. Similarly, connecting beams should be assigned with the actual axial, flexural and shear rigidity, specifically for $ld < 5$ (Smith and Coull, 1991).

2.3.3 Multi-spring model

The one-dimensional idealization of wall piers in equivalent column-beam model, discussed in section 2.3.2, has several shortcomings. One important limitation is that it assumes rotations to occur around points lying on the central axis of the wall piers and does not account the fluctuation of the wall N.A. (Colotti, 1993; Spacone and El-Tawil, 2004). As a result, multi-spring model has been used based on the macro-elements model which was originally proposed to investigate the behavior of a cantilever shear wall by Kabeyasawa (1982) and later on by Colotti (1993), Cheng et al., (1993), and Shahrooz et al., (1993). This macro-elements model is a transition between the frame analogy method and the more complex microscopic finite-element modelling approaches (Eljadei and Harries, 2014). The model consists of number of series/ parallel nonlinear springs that are connected to rigid beams at their top and bottom extremes. The vertical springs represent the inelastic axial and and strength of the wall piers, while the horizontal and rotational springs simulate the shear strength, and flexural stiffness of the wall web respectively. Moreover, the top and bottom rigid elements represent the physical dimension of the wall piers (El-Tawil et al., 2010;

Eljadei and Harries, 2014).

2.3.4 Finite element method

In this method, the wall piers are divided into finite mesh elements or polygon surfaces and the connecting beams are modeled as line elements. The size of the FE meshes has an effect in the accuracy and computational time of the analysis. Generally, the smaller the mesh size is the accurate the analysis will be until mesh independent resolution or convergence is reached. Depending on the shape of the elements, stiffness matrices are created and solved to give nodal displacements and associated forces (Smith and Coull, 1991). The application of this method were limited for the cases when the structural wall piers have flange sections, notably irregular openings and complex support conditions (Smith and Coull, 1991). Advances in structural analysis software, during the last couple of decades, has solved its notable shortcomings (e.g: speed, cost) and is becoming structural engineer's choice to elastically analyze structural walls (El-Tawil et al., 2010).

2.4 Types of coupled-wall buildings

2.4.1 Conventional coupled-Wall system

The conventional coupled-wall (CCW) system refers to RC walls coupled with RC beams. Cast in-place RC coupling beams have been traditionally considered. Depending on the depth-to-length ratio of the RC coupling beams, they can primarily a moment or shear resistance. The later types (high shear-strength diagonal deep RC beams) have a significant shear component due to the small clear span between the walls and, therefore, they must be detailed to yield and dissipate energy in shear. This detailing in conjunction with a large required beam depth (El-Tawil et al., 2009), have led to the consideration of other alternatives, such as hybrid coupled wall (HCW) systems (El-Tawil and Kuenzli, 2002; El-Tawil et al., 2010; Harries et al., 1997).

2.4.2 Hybrid coupled-Wall system

As alternative to RC coupling beams, other types of coupling elements can be used. An example is steel beams in HCW system (El-Tawil and Kuenzli, 2002; Harries

et al., 1997). The steel beams are embedded into the RC walls for the purpose of forming moment-resisting connections. However, the fixity of steel beams to RC walls is not perfect and the effective fixed point has been assessed at one third of the embedment length (El-Tawil et al., 2009). Moreover, special detailing is required at the embedment region, in order to ensure the integrity of the moment-resisting connection. Shahrooz et al. (1993) and Park and Yun (2005) described the mechanics of the steel beam, embedment region and concrete wall interaction. Furthermore, Lu et al. (2018) carried out shaking table tests and numerical analyses for the HCW system. To improve the earthquake resilience of buildings, however, the use of reparable or replaceable structural components in locations where the system is liable to damage are preferable. This leads to the evolution of replaceable CW system.

2.4.3 Replaceable coupled-Wall system

In replaceable coupled wall (RCW) system, the coupling elements added between walls act as energy-dissipating elements (dampers). That is, after a major seismic event, these coupling beam elements can be replaced. A plethora of structural elements and devices have been proposed for coupling elements in RCW systems. Christopoulos and Montgomery (2013) proposed a viscoelastic beam element that functions in shear, and it is therefore appropriate for short spans between the walls. Shen (2002) and Kurama (2004) introduced a novel post-tensioned HCW system for providing with self-centering capability to the HCW system. Li et al. (2020) studied the seismic performance assessment of the HCW system equipped with novel self-centering steel truss coupling beams.

Ji and Hutt (2020) proposed a design procedure, member sizing, connection detailing and modelling recommendations for a novel HCW system. This system comprised a shear link in the middle of each coupling beam element, for the purpose of ensuring the ductile response of the steel element in shear. Furthermore, Ji et al. (2018) went on to conduct seismic performance evaluation of this system. Zona et al. (2016) introduced an innovative HCW system, wherein the columns participate in lateral system response through coupling beams.

Yang et al. (2020) has also proposed an innovative self-centering conical friction damper that utilizes conical surfaces (male and female to slide one over the other) and post-tensioning tendons to provide high compression forces between the casing plates.

The proposed system has the ability to resist loads applied in all directions (axial, shear, and moment) and dissipate high energy.

2.5 CLT coupled Wall (CLT-CW) system

Mass timber buildings have recently gained momentum due to the environmentally-friendly property of wood and the enhanced mechanical properties of engineered wood products such as CLT (Brandner et al., 2016). CLT is an engineered panel-like wood product that can be used as structural wall or floor element. In CLT buildings, energy dissipation is attained through inelastic deformations of the connections between CLT walls and CLT floors or between contiguous CLT wall panels (Gavric et al., 2015). These connections are usually dowel-type steel connections and the energy dissipation is from yielding of the steel dowels in shear and from crushing of the surrounding wood material, giving rise to a pinched hysteretic response. Significant research has gone to enhance the energy dissipation capacity of CLT buildings by using alternative energy-dissipating connections instead of conventional ones (e.g. (Blomgren et al., 2019; Loo et al., 2016)). For example, Iqbal et al. (2015) examined laminated veneer lumber (LVL) walls coupled with UFP dissipaters.

Use of coupling beams to connect CLT walls could be a means of enhancing system stiffness, strength and energy-dissipation capacity. The CLT-CW system was examined by Pei et al. (2017) by using the CLT floors as coupling elements. The CLT floors, however, are not ductile elements and provide limited energy dissipation capacity for use in high-seismicity areas. Liu and Lam (2014) investigated the seismic behaviour of a six story CLT-CW prototype. The coupling beams were made of 175 mm thick 5-layer CLT panels and steel plates with dowels were used to transfer the lateral loads, and connect the walls and coupling beams. Tesfamariam et al. (2021) utilized the RC coupling beam, and developed corresponding seismic modification factors. Dowden and Tatar (2019) examined CLT-CW system with replaceable structural fuses provided at the two ends of steel coupling beam. The system limits the damage to the replaceable structural fuses and provide excellent energy dissipation. However, the CLT-CW system examined in this paper was kept at a high level and the conclusions were merely based on nonlinear pushover analyses. The studies made by Pei et al. (2017) and Tesfamariam et al. (2021) were based on platform types of CLT systems. Tesfamariam et al. (2021) highlighted that, with the platform type system, the energy

dissipation and kinematics is not efficient for the CW system. A balloon type CLT walls, (e.g. (Chen and Popovski, 2020)) is ideal to engage the CLT wall and energy dissipator coupling beams. Hence, the contribution of this project paper is to propose and develop the design guideline for balloon type CLT-CW structure. Moreover, this study has examined the behavior of the CLT-CW system under different coupling ratio (CR) and combined seismic modification factors ($R_o R_d$) conditions.

Chapter 3

Case study building and modeling

3.1 Building type and prototype definitions

Three building heights, 10-, 15-, and 20-storey, CLT-CW systems are investigated. Details of the 20-storey CLT-CW is shown in Figure 1.2. The structural model comprises glulam beams and columns, CLT floor panels, CLT core shear-walls, and steel coupling beams with replaceable shear-links. The glulam beams and columns are gravity-load carrying structural elements that do not have any contribution in resisting the lateral loads. The seismic force resisting system layout consists of CLT shear-walls connected with coupling beams that have the ability to reduce the base moment induced in the system and dissipate the seismic energy. Two types of energy dissipation mechanisms exist in the CLT-CW system. The primary and secondary energy dissipation mechanisms are achieved through the yielding of the shear links or coupling beams and hold-downs, respectively. The shear-links act as a fuse system to protect the CLT wall assemblies. Once the shear-links degrade under a cyclic load, the hold-downs start to yield. Moreover, the CLT shear-walls exhibit flexural responses.

3.2 Load cases and combinations

Four load combination cases (Table 3.1) are considered to design the building following NBC (2015). The load considered are dead load (D), live load due to use and occupancy (L), load due to snow and rain (S) and earthquake load (E). The building is located

Vancouver, British Columbia (BC), and the corresponding snow and seismic loads are determined based on the provisions of NBC (2015). The members are then designed against the maximum load obtained from the combination of the above-mentioned load cases. Table 3.2 summarize the design loads (for the considered building at the specified site location) and load combinations used in the study, respectively.

Table 3.1: Load combinations for ultimate limit state

Case	Load Combination
1	1.4 D
2	1.25 D + 1.5 L + 1.0 S
3	1.25 D + 1.0 L + 1.5 S
4	1.0 D + 1.0 E + 0.5 L + 0.25 S

3.3 Gravity-load design

Douglas Fir-Larch Glued-Laminated (DF Glulam) timber product are used for the design of frame elements (beams and columns). Similarly, CLT Grade E1 multi-layer wood products are used for floor and shear-walls panels. CLT floor panels, with dimensions shown in Figure 3.1, are designed as a one-way slab using a 5-ply CLT Grade E1 per ANSI/APA PRG 320 (ANSI, 2012) and CSA 086-14 (2016). Gravity-load analysis of the CLT-CW system is performed using assumed geometric sections in ETABS software. Results are extracted and the glulam columns, beams, and CLT wall piers are designed following the CSA 086-14 (2016) standard. Iterations were performed to achieve the appropriate geometric section of the system. The gravity load design and details are summarized in Tesfamariam and Das (2021).

3.4 Modeling and modal analysis

3.4.1 OpenSees modeling

A nonlinear model was developed for a 2D frame of the building (at the location of the CLT shear walls) in both the north-south (strongest) and east-west (weakest) directions. As can be seen from Figure 3.2 (a), the two 2D CLT-CW systems that resist lateral force in the Y direction are symmetric, each comprising two equal CLT

Table 3.2: Design load cases

Structural Design Loading - Gravity Loads:		
Snow load	$S = I_s[S_s(C_bC_wC_sC_a) + S_r]$ where:	
	S_s = Ground snow load	1.8 kPa
	S_r = Rain load	0.2 kPa
	C_b = Basic roof snow factor	0.8
	C_w = Wind exposure factor (for normal condition)	1.0
	C_s = Roof slope factor (for $\alpha \leq 30^o$)	1.0
	C_a = Accumulation factor	1.0
	I_s = Importance factor	1.0
	For strength:	
	S = $1.0 \times [1.8 \times 0.8 \times 1.0 \times 1.0 \times 1.0 + 0.2]$ =	**1.64 kPa**
	For serviceability:	
	S = $0.9 \times [1.8 \times 0.8 \times 1.0 \times 1.0 \times 1.0 + 0.2]$ =	**1.48 kPa**
Live load		**2.0 kPa**
Superimposed dead load		**0.95 kPa**
Self weight of member		Based on assumed section
Structural Design Loading - Lateral Loads:		
Earthquake	S_a (0.2) = 0.8480	
	S_a (0.5) = 0.7510	
	S_a (1.0) = 0.4250	
	S_a (2.0) = 0.2570	

shear-wall panels of lengths 6 m. Where as, the 2D CLT-CW systems in the X direction are unsymmetrical (Figure 3.2 (b)), each comprising two CLT shear-wall panels of lengths 5.75 m and 2.25 m. The nonlinear finite element for the 2D models was developed in Open System for Earthquake Engineering Simulation (OpenSees) (Mazzoni et al., 2006). In this finite element framework, numerical model of single elements and connections, and CLT shear wall system is formulated. Moreover, the global system is formed by assembling the model components: BRB hold-downs, CLT wall 2D elements, and coupling beams. The following subsections illustrates both the component and system level modeling and calibration procedures.

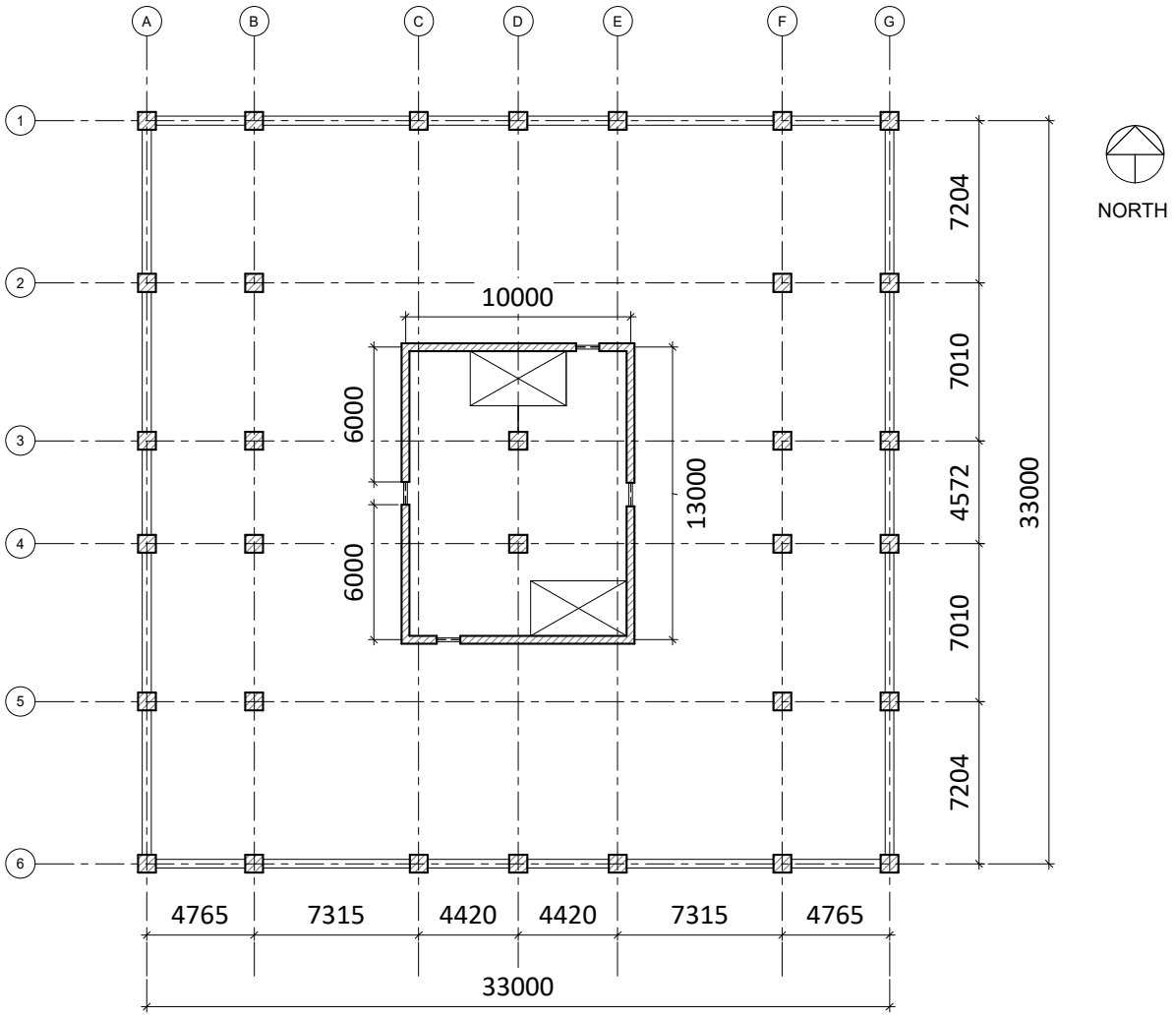

Figure 3.1: Building plan view (Dimensions in mm).

CLT shear-wall panels

The CLT shear-wall panel possesses high elastic stiffness, and it essentially behaves as a rigid body during in-plane response. Consequently, the CLT wall panels are modelled as linear elastic *quad* elements. *ElasticIsotropic* OpenSees material model is utilized, with effective Young's modulus and Poisson's ratio values. For example, for the 20 storey building model with overall CLT panel thickness of 245 mm is modeled with an equivalent Young's modulus (E_m) of 10.54 GPa as proposed by (Rinaldin and Fragiacomo, 2016) and Poisson's ratio of 0.3.

The OpenSees command used for the CLT shear-wall material is:

nDMaterial *ElasticIsotropic $matTag $E $v <$rho>*

where:

Table 3.3: Gravity-load design results

CLT-CW system	Structural element	Design section	Remark
20 storey	CLT shear-walls	9-ply (315 mm)	E-W (x) direction
	CLT shear-walls	7-ply (245 mm)	N-S (y) direction
	Glulam beams	215 mm × 342 mm	all beams
	Glulam columns	365 mm × 1064 mm	all columns
15 storey	CLT shear-walls	7-ply (245 mm)	E-W (x) direction
	CLT shear-walls	5-ply (175 mm)	N-S (y) direction
	Glulam beams	175 mm × 304 mm	all beams
	Glulam columns	315 mm × 1064 mm	all columns
10 storey	CLT shear-walls	7-ply (245 mm)	E-W (x) direction
	CLT shear-walls	5-ply (175 mm)	N-S (y) direction
	Glulam beams	175 mm × 304 mm	all beams
	Glulam columns	315 mm × 1026 mm	all columns

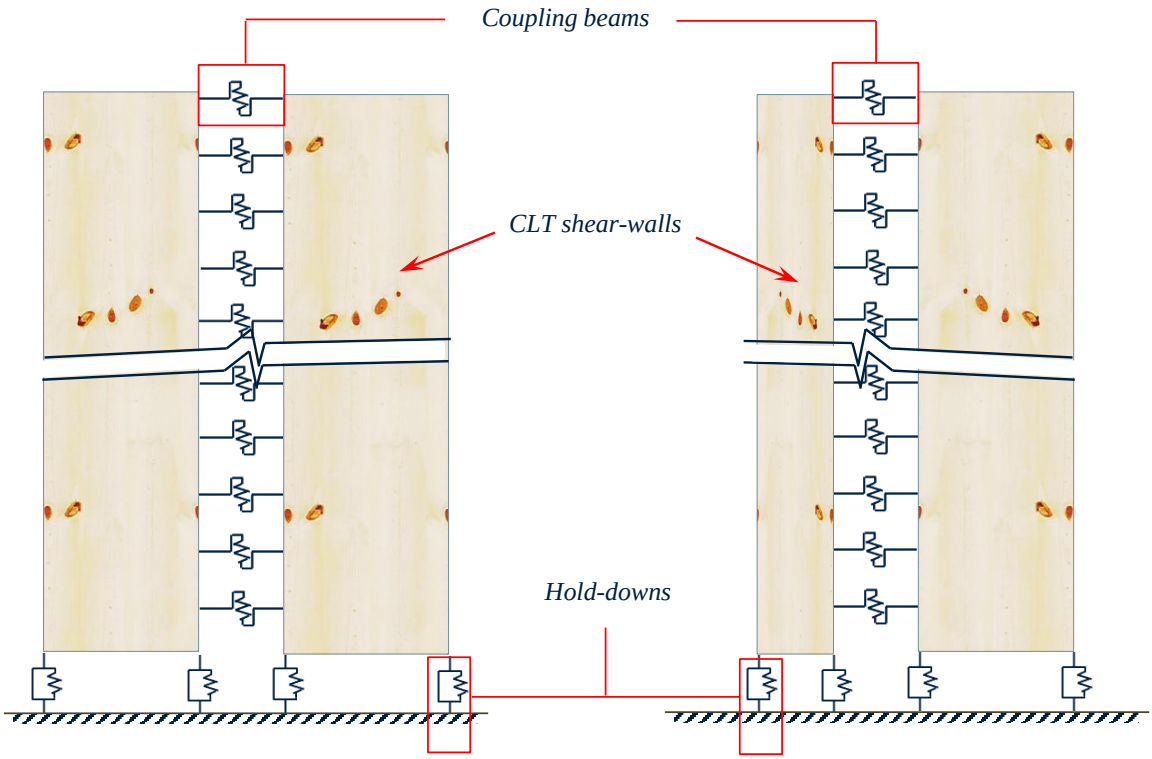

Figure 3.2: Nonlinear finite element model of the CLT-CW system in OpenSees: (a) along Y or strongest direction; and (b) along X or weakest direction

The OpenSees command used for the CLT shear-wall element is:

$matTag	integer tag identifying material
$E	elastic Modulus
$v	Poisson's ratio
$rho	mass density (optional, default = 0.0)

element quad *$eleTag $iNode $jNode $kNode $lNode $thick $type $matTag <$pressure $rho $b1 $b2>*

where:

$eleTag	unique element object tag
$iNode $jNode $kNode $lNode	four nodes defining element boundaries, input in counter-clockwise order around the element.
$thick	element thickness
$type	string representing material behavior. The type parameter can be either "PlaneStrain" or "PlaneStress."
$matTag	tag of nDMaterial
$pressure	surface pressure (optional, default = 0.0).
$rho	element mass density (per unit volume) from which a lumped element mass matrix is computed (optional, default=0.0)
$b1 $b2	constant body forces defined in the iso-parametric domain (optional, default=0.0)."

Coupling beams

The two rigid ends of the coupling beams are modelled using OpenSees *Steel01 UniaxialMaterial* materials and *elasticBeamColumn* elements. A *zeroLength* nonlinear vertical spring (as in Christopoulos and Montegomery (2013)) is utilized to model the central "fuse" component of the coupling beam (Figure 3.3). Summarized below are the OpenSees material and element commands used to model the coupling beams.

uniaxialMaterial Steel01 *$matTag $Fy $E0 $b <$a1 $a2 $a3 $a4>*

where:

element elasticBeamColumn *$eleTag $iNode $jNode $A $E $Iz $transfTag <-mass $massDens> <-cMass>*

where:

element zeroLength *$eleTag $iNode $jNode -mat $matTag1 $matTag2 ... -dir $dir1 $dir2 ...<-doRayleigh $rFlag> <-orient $x1 $x2 $x3 $yp1 $yp2 $yp3>*

where:

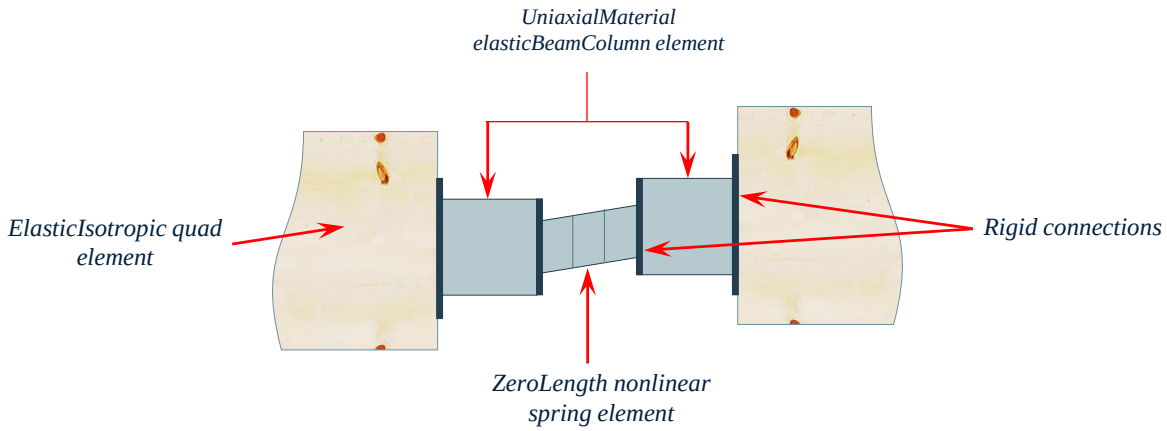

Figure 3.3: Replaceable coupling beam modeling elements

$matTag	integer tag identifying material
$Fy	yield strength
$E0	initial elastic tangent
$b	strain-hardening ratio (ratio between post-yield tangent and initial elastic tangent)
$a1	isotropic hardening parameter, increase of compression yield envelope as proporti--on of yield strength after a plastic strain of $a2*($Fy/E0). (optional)
$a2	isotropic hardening parameter (see explanation under $a1) (optional).
$a3	isotropic hardening parameter, increase of tension yield envelope as proportion of yield strength after a plastic strain of $a4*($Fy/E0) (optional).
$a4	isotropic hardening parameter (see explanation under $a3) (optional).

$eleTag	unique element object tag
$iNode $jNode	end nodes
$A	cross-sectional area of element
$E	Young's Modulus
$Iz	second moment of area about the local z-axis
$transfTag	identifier for previously-defined coordinate-transformation object
$massDens	element mass per unit length (optional, default = 0.0)
-cMass	to form consistent mass matrix (optional, default = lumped mass matrix)

$eleTag	unique element object tag
$iNode $jNode	end nodes
$matTag1 $matTag2 ...	tags associated with previously-defined UniaxialMaterials
$dir1 $dir2 ...	material directions: 1,2,3 - translation along local x,y,z axes, respectively; 4,5,6 - rotation about local x,y,z axes, respectively
$x1 $x2 $x3	vector components in global coordinates defining local x-axis (optional)
$yp1 $yp2 $yp3	vector components in global coordinates defining vector yp which lies in the local x-y plane for the element. (optional)
$rFlag	optional, default = 0 rFlag = 0 no rayleigh damping (default) rFlag = 1 include rayleigh damping

Figure 3.4 illustrates the hysteretic response of the modelled coupling beam under the action of cyclic loading. The initial elastic stiffness E_0 (kN/mm) of the coupling beams

is considered to be half of the value of the yield strength F_y (kN) (Ji and Hutt, 2020; Zona et al., 2018) with a strain-hardening ratio b = 0.01 (Figure 3.4).

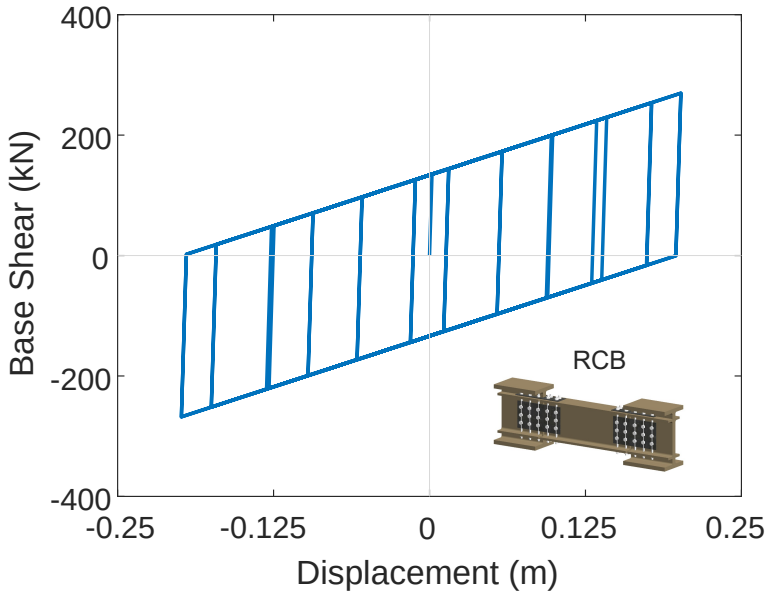

Figure 3.4: Hysteretic response of coupling beams (Replaceable shearlink)

hold-downs

To satisfy the high axial demand, BRB hold-down (Tesfamariam et al., 2021) is modeled using OpenSees *Steel01 uniaxialMaterial*. The contact between the CLT wall and the base is modeled as a parallel system by introducing OpenSees *uniaxial elastic no-tension (ENT)* material (Figure 3.3). To capture the contact between the CLT wall and the base, a large elastic stiffness value is assigned to the ENT spring under compression. Command below is used in introducing the ENT material object.

uniaxialMaterial ENT *$matTag $E*

where:

$matTag	integer tag identifying material
$E	tangent

The parallel spring formulation is implemented in OpenSees with the following command:

uniaxialMaterial Parallel *$matTag $tag1 $tag2 ... <-factors $fact1 $fact2 ...>*

where:

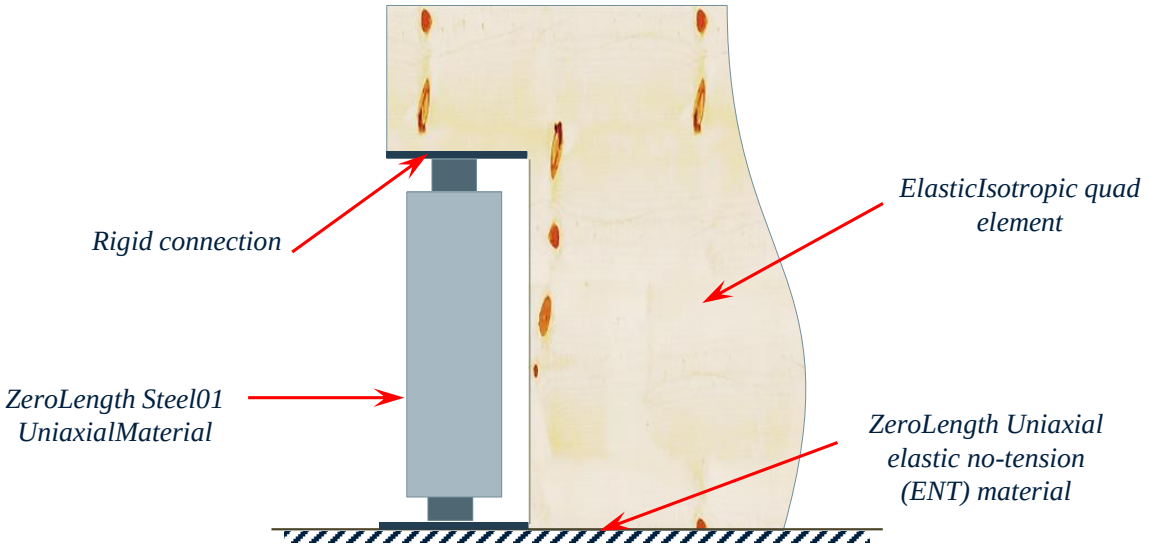

Figure 3.5: BRB hold-down modeling elements

$matTag	integer tag identifying material
$tag1 $tag2 ...	identification tags of materials making up the material model
$fact1 $fact2 ...	factors to create a linear combination of the specified materials. Factors can be negative to subtract one material from an other. (optional, default = 1.0)

Figure 3.6 illustrates the parallel system along with the response of the BRB hold-down. The initial elastic stiffness E_0 (kN/mm) of the BRB hold-downs is considered to be equivalent with the value of the yield strength F_y (kN) (Tesfamariam et al., 2021) with a strain-hardening ratio b = 0.01.

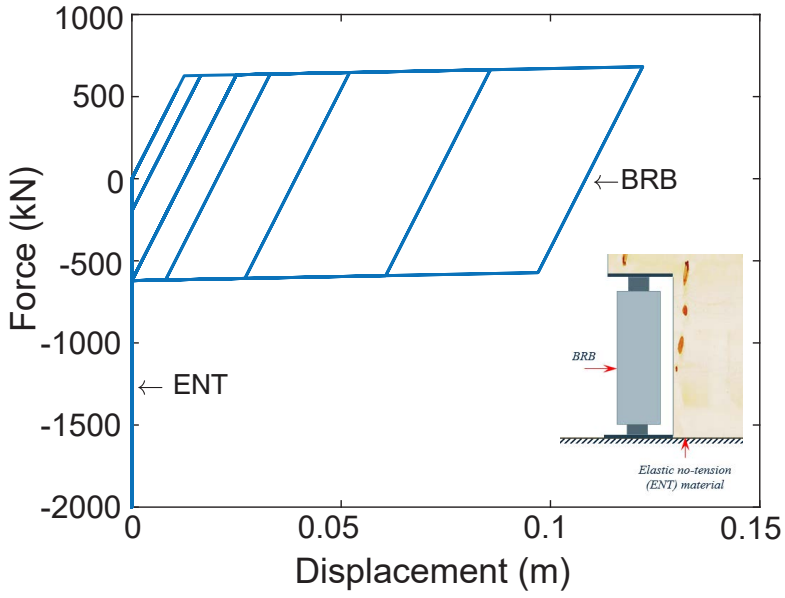

Figure 3.6: Hysteric response of BRB hold-down connection

P-Delta effect

As the P-Delta effect is important for tall-storey building, its effect is modelled by using a leaning column. OpenSees *elasticBeamColumn* and *truss* elements are used to model the leaning column and truss elements, respectively (Figure 3.7).

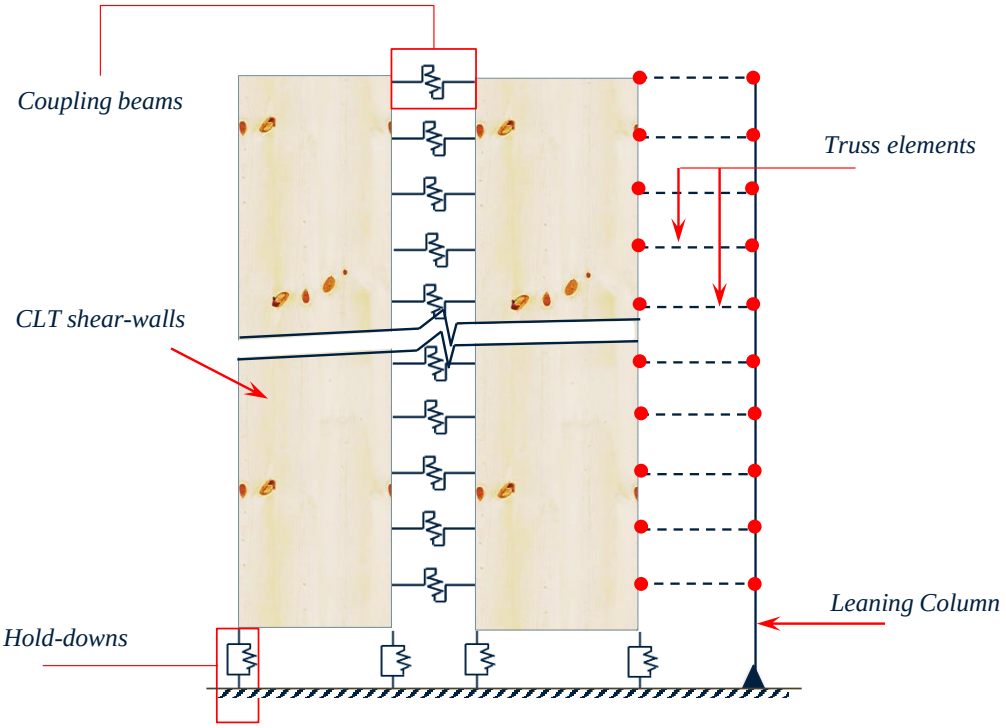

Figure 3.7: Numerical model for P-Delta effect

Chapter 4

Seismic Design

4.1 General

Linear and nonlinear analysis models can be used to analyse CW systems (El-Tawil et al., 2010). In this report, elastic analyses methods, continuous medium method (CMM) and equivalent lateral force analysis (ELFA), are used to determine the preliminary CLT-CW geometry and seismic demand. Moreover, nonlinear time history analysis (NLTHA) is utilized to evaluate the structural performance of the CLT-CW system.

As discussed in Chapter 3, a total of three building heights (10, 15, and 20 storeys) are considered. The prototype structures were located at Vancouver (City Hall), BC - Canada. The plan and elevation views of the prototype buildings is given in Chapter 3, Figures 3.1 and 1.2, respectively. Seismic design of the CLT-CW system is performed considering different values of CR, and over-strength R_o and ductility-related modification R_d factors, R_oR_d. A 2D CW systems (Figure 4.1), both the X (weakest) and Y (strongest) directions are considered. In this chapter, detail seismic analysis and design of the CW system for the 20 storey building in the Y direction is presented. Figure 4.1 shows the force parameter and geometrical notation for the selected CW system.

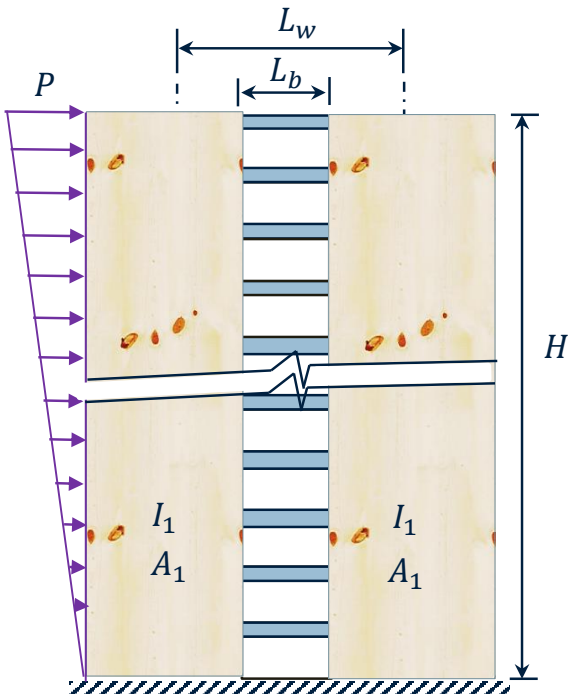

Figure 4.1: Symmetrical two wall CW system

4.2 Continuous medium method

CMM is a simplified (approximate) elastic method that can be used to analyse and design the preliminary geometries of CW systems for a uniform or quasi-uniform structures. The method reduces the statically indeterminate CW system into a problem modeled as single fourth-order differential equation, and provides a closed-form solutions depends on the type of lateral loads (Smith and Coull, 1991). These closed-form solutions are derived by assuming that, under the action of lateral loads, the inflection point of the coupling beams occurs at their mid span without experiencing any axial deformation. The governing differential equations, in terms of the axial force, N, and drift or lateral deformation, y, and corresponding height, z, are given by Smith and Coull (1991):

$$\frac{d^2}{\mathrm{d}z^2}N - (k\,\alpha)^2\,N = -\frac{\alpha^2}{I}M \tag{4.1}$$

$$\frac{d^4}{\mathrm{d}z^4}y - (k\,\alpha)^2\,\frac{d^2}{\mathrm{d}z^2}y = \frac{1}{\mathrm{EI}}\left(\frac{d^2}{\mathrm{d}z^2}M - (k\,\alpha)^2\,\frac{k^2-1}{k^2}M\right) \tag{4.2}$$

The parameters α and k, in the above Equations 4.1 and 4.2, measure the relative

flexibility of the coupling beams and the wall piers, and the relative flexural to axial stiffness of the wall piers, respectively, and are defined as:

$$\alpha = \sqrt{\frac{12\ I_c\ (L_w)^2}{L_b^3\ h\ I}} \tag{4.3}$$

$$k = \sqrt{1 + \frac{A\ I}{A_1\ A_2\ (L_w)^2}} \tag{4.4}$$

where I = total moments of inertia of the wall piers ($I = I_1 + I_2$); L_w = distance between wall centroids $\left(L = \frac{L_1+L_2}{2} + L_b\right)$; L_1 and L_2 = length of each wall piers; L_b = length of coupling beam; h = story height; A = total areas of the wall piers ($A = A_1 + A_2$); and I_c = effective moment of inertia of the coupling beam accounting for shear deformations (equation 4.5).

$$I_c = \frac{I_b}{1 + \left(\frac{12\ E_b\ I_b}{L_b^2\ G_b\ A_b}\ \lambda\right)} \tag{4.5}$$

where I_b and A_b = gross moment of inertia and area of the coupling beam, respectively; E_b and G_b = Young's and shear modulus of the coupling beam, respectively; and λ = shape factor, defined as the ratio of the plastic to elastic section moduli, $\frac{Z_x}{S_x}$.

Low value of α implies a relatively flexible CW system where the coupling beams develop little end moments and its behavior is governed by the flexural response of the individual walls (El-Tawil et al., 2010). For CCW and HCW, values of k varies between 1.0 to 1.2, where $k = 1.0$ (lower limit), indicates axially rigid wall piers. For structurally and architecturally practical CW systems, the values of k ranges between 1.0 to 1.1 (El-Tawil et al., 2010; Harries et al., 2004).

Multiplying k and α parameters with H (the total height of the building), $(k\alpha H)$, provides additional meaningful parameter called stiffness parameter. The stiffness parameter measures the stiffness of the coupling beams and is used to determine the elastic coupling ratio, CR, as (Chaallal and Nollet, 1997):

$$CR = \frac{3}{k^2(k\alpha H)^2}\left[\frac{(k\alpha H)^2}{3} - \cosh(k\alpha H) + \frac{\sinh(k\alpha H) - \frac{k\alpha H}{2} + \frac{1}{k\alpha H}}{\cosh(k\alpha H)}\sinh(k\alpha H)\right] \tag{4.6}$$

Moreover, the axial load (N_z), shear flow (q_z) and lateral deformation (y_H) at each storey are function of $k\alpha H$, and relative height parameter, $\frac{z}{H}$ (for only N_z and q_z). The closed-form solutions for N_z, q_z and y_H, considering a triangular lateral load condition, are given by Smith and Coull (1991):

$$N_z = \frac{PH^2}{k^2\ L_w}F_1\left(\frac{z}{H}, k\alpha H\right) \tag{4.7}$$

$$q_z = \frac{\mathrm{PH}}{k^2\ L_w}F_2\left(\frac{z}{H}, k\alpha H\right) \tag{4.8}$$

$$y_H = \frac{11PH^4}{120\ \mathrm{EI}}F_3(k\alpha H) \tag{4.9}$$

where P = triangular lateral load, EI = flexural stiffness, and parameters F_1, F_2, and F_3 are defined as:

$$\begin{aligned} F_1 = {} & \frac{\sinh(k\alpha H) - \frac{k\alpha H}{2} + \frac{1}{k\alpha H}}{(k\alpha H)^2\cosh(k\alpha H)}\sinh(k\alpha(H-z)) - \frac{\cosh(k\alpha(H-z))}{(k\alpha H)^2} \\ & + \frac{1}{2}\left(1-\frac{z}{H}\right)^2 - \frac{1}{6}\left(1-\frac{z}{H}\right)^3 + \frac{1}{(k\alpha H)^2}\left(\frac{z}{H}\right) \end{aligned} \tag{4.10}$$

$$\begin{aligned} F_2 = {} & \frac{\sinh(k\alpha H) - \frac{k\alpha H}{2} + \frac{1}{k\alpha H}}{(k\alpha H)\cosh(k\alpha H)}\cosh(k\alpha(H-z)) - \frac{\sinh(k\alpha(H-z))}{(k\alpha H)} \\ & + \left(1-\frac{z}{H}\right) - \frac{1}{2}\left(1-\frac{z}{H}\right)^2 - \frac{1}{(k\alpha H)^2} \end{aligned} \tag{4.11}$$

$$F_3 = 1 - \frac{1}{k^2} + \frac{120}{11}\frac{1}{k^2(k\alpha H)^2}\left[\frac{1}{3} - \frac{1 + \left(\frac{k\alpha H}{2} - \frac{1}{k\alpha H}\right)\sinh(k\alpha H)}{(k\alpha H)^2\cosh(k\alpha H)}\right] \tag{4.12}$$

4.3 Seismic design of CLT-CW systems

The steps followed to determine the seismic forces and CLT-CW system design is summarized in Figure 4.2. The steps followed in this reported is adopted from the HCW's prescriptive design method provided in Eldaei (2012). A parametric study is undertaken for R_oR_d = 3, 4.5, and 6, and CR = 10% to 50% that results in 15 different combinations (Table 4.1). For the different parametric studies, the CLT-CW system is designed and its performance is investigated. A step-by-step numerical example is provided for $R_oR_d = 3$ and $CR = 30\%$.

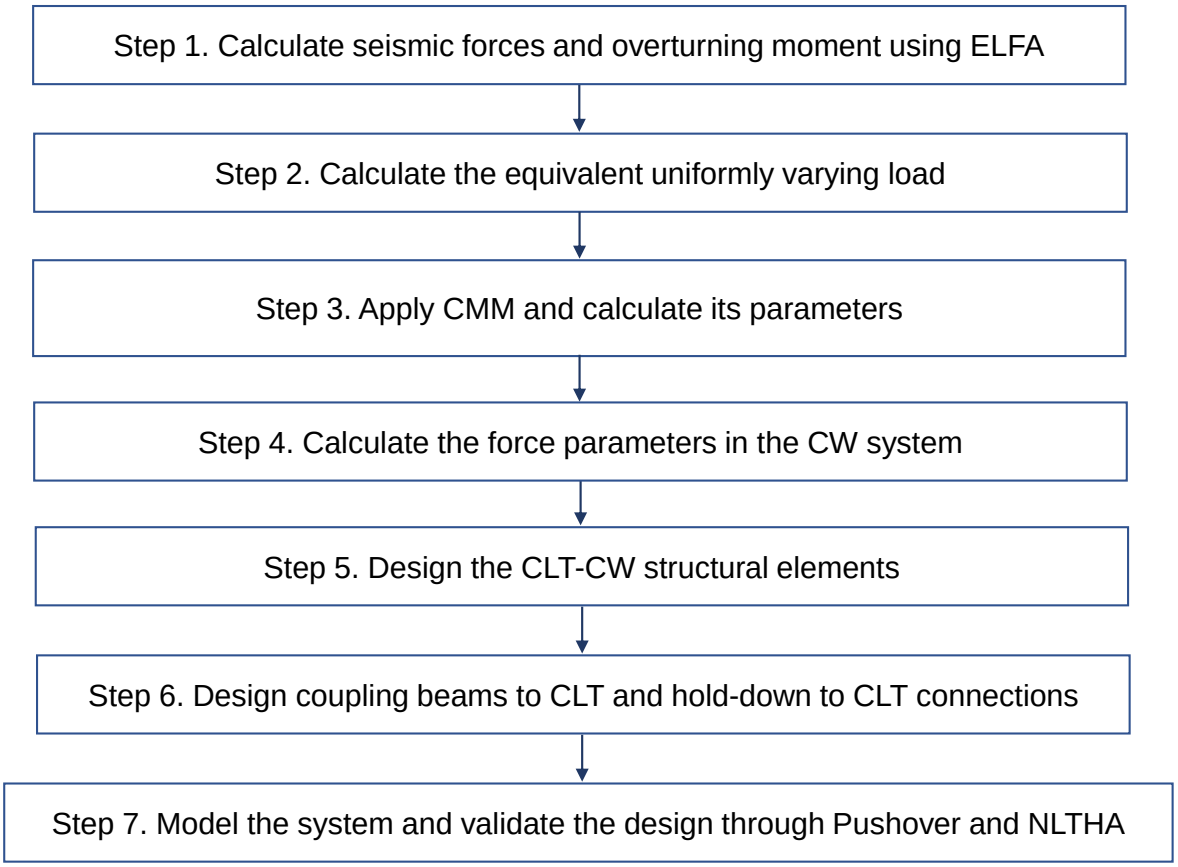

Figure 4.2: Seismic design framework for CLT-CW system

Step 1. Calculate seismic forces and overturning moment using ELFA:

- Check the applicability of the structure for ELFA procedure.
- Calculate the base shear, lateral seismic forces, cumulative base shears and moments as per the code standards.

The total lateral seismic force, V is calculated as per the NBC (2015).

Table 4.1: Natural periods of the 20 storey CLT-CW system.

No.	R_oR_d	CR (%)	T_1 (s)	T_2 (s)	T_3 (s)
1	3	10	2.341	0.529	0.224
2	3	20	2.181	0.486	0.210
3	3	30	2.108	0.460	0.200
4	3	40	2.069	0.443	0.194
5	3	50	2.044	0.432	0.189
6	4.5	10	2.475	0.555	0.231
7	4.5	20	2.270	0.512	0.219
8	4.5	30	2.178	0.485	0.210
9	4.5	40	2.127	0.467	0.203
10	4.5	50	2.093	0.454	0.198
11	6	10	2.579	0.572	0.235
12	6	20	2.352	0.531	0.225
13	6	30	2.241	0.504	0.216
14	6	40	2.180	0.486	0.210
15	6	50	2.139	0.472	0.205

$$V = \frac{S(T_a)\ M_v\ I_e\ W}{R_d R_o} \tag{4.13}$$

where $S(T_a)$ = the design spectral response acceleration taken at the fundamental period T_a, M_v = higher mode effects factor on the base shear, I_e = importance factor, W = total seismic weight of the structure (the dead load plus 25% of the design snow load plus 60% of the storage load), and R_oR_d = combined ductility-overstrength factors (Mitchell et al., 2003; NBC, 2015).

For structures with shear walls, the preliminary fundamental period of vibration can be computed as (NBC, 2015):

$$T_a = 0.05\ {h_n}^{0.75} \tag{4.14}$$

where h_n = total height of the building (m). Alternatively, the fundamental period

of vibration from modal analysis can be used, provided that the value is not be taken greater than 2.0 times that determined in equation 4.14 (Clause 4.1.8.11, NBC (2015)).

The design base shear at each story level, F_x, is determined as (NBC, 2015):

$$F_x = \frac{(V - F_t)\, W_x h_x}{(\sum_{i=x}^{n} W_i h_i)} \tag{4.15}$$

where V = total lateral seismic force, F_t = portion of V assumed to be concentrated at the top of the building which is defined by equation 4.16, W_x = weight of the building at each storey, and h_x = height of storey x (m).

$$F_t = \begin{cases} 0 & \text{for } T_a < 0.7 \\ 0.07\, T_a\, V & \text{for } T_a \geq 0.7 \end{cases} \tag{4.16}$$

where F_t need not exceed $0.25\, V$.

Similarly, the overturning moment at each story level, M_x, is given by (NBC, 2015):

$$M_x = J_x \sum_{i=x}^{n} F_i\, (h_i - h_x) \tag{4.17}$$

where J_x = base overturning moment reduction factor at story level x and is defined as:

$$J_x = \begin{cases} 1.0 & \text{for } h_x \geq 0.6\, h_n, \text{and} \\ J + (1 - J)\left(\frac{h_x}{0.6\, h_n}\right) & \text{for } h_x < 0.6\, h_n \end{cases} \tag{4.18}$$

where J = base overturning moment reduction factor (Table 4.1.8.11. of NBC (2015)).

For $R_o R_d = 3$ and $CR = 30\%$, the ELFA parameters and the calculated seismic forces and overturning moment are summarized in Tables 4.2 and 4.3.

Step 4. Calculate the equivalent uniformly varying load:

- Determine the equivalent or approximate triangular lateral load for the lateral

Table 4.2: Equivalent lateral force analysis parameters.

T_a	: $2.108\ s$ ($\leq 2 \times (0.05 \times 60^{0.75})$)
$S(T_a)$	: $0.255\ g$
M_v	: 1
I_E	: 1
$R_o R_d$	: 3
n (number of storeys)	: 20
h_x (height at storey x)	: $3\ m$
h_n (total height, H)	: $60\ m$
w_x (weight at each storey x)	: $1,100\ kN$
W (total weight)	: $22,000\ kN$
F_t	: $261.90\ kN$
V (total base shear)	: $1,870.73\ kN$

seismic forces obtained in Step 2.

The equivalent triangular lateral load, P, is calculated to be $62.5kN/m$ using equation 4.19.

$$P = 2 \times \frac{V}{H} \tag{4.19}$$

Step 3. Apply CMM and calculate its parameters:

- Given the CLT-CW geometric parameters, calculate the parameter k (from equation 4.4).
- For predefined value of CR and calculated value of k, determine the corresponding value of $(k\alpha H)$ from equation 4.6.
- Calculate the values of F_1, F_2, and F_3 (using equations 4.10, 4.11, and 4.12, respectively) at storey height z.
- Determine the axial load developed at each story of wall piers and shear flow on the continuous medium at each story using equations 4.7 and 4.8, respectively.

Table 4.3: The distribution of seismic forces on the 20-storey CLT-CW system.

Storey, n	Height, H (m)	$w_x h_x$ (kNm)	F_x (kN)	V_x (kN)	J_x	M_x (kNm)
20	60	65,846	413	0	1	0
19	57	62,601	144	413	1	1,239
18	54	59,356	136	557	1	2,910
17	51	56,111	129	693	1	4,990
16	48	52,866	121	822	1	7,457
15	45	49,621	114	944	1	10,288
14	42	46,376	107	1,058	1	13,461
13	39	43,131	99	1,164	1	16,953
12	36	39,886	92	1,263	1	20,743
11	33	36,641	84	1,355	1	24,611
10	30	33,396	77	1,439	1	28,641
9	27	30,151	69	1,516	1	32,820
8	24	26,906	62	1,585	1	37,121
7	21	23,661	54	1,647	1	41,517
6	18	20,416	47	1,701	1	45,982
5	15	17,171	39	1,748	1	50,490
4	12	13,926	32	1,787	1	55,017
3	9	10,681	25	1,819	1	59,540
2	6	7,436	17	1,844	1	64,035
1	3	4,191	10	1,861	1	68,481

For CLT Grade E1 panel ($E_0 = 11.7\ GPa$, and $E_{90} = 9\ GPa$) with length L and thickness t, the axial area and moment of inertia of the CLT panel can be calculated using equations 4.20 and 4.21, respectively.

$$A_1 = A_2 = 4t \tag{4.20}$$

$$I_{eff} = \frac{EI_{eff}}{E_0} = \frac{\sum_{i=1}^{n} E_i \cdot t_i \cdot \frac{L_i^3}{12} + \sum_{i=1}^{n} E_i \cdot t_i \cdot L_i \cdot z_i^2}{E_0} \tag{4.21}$$

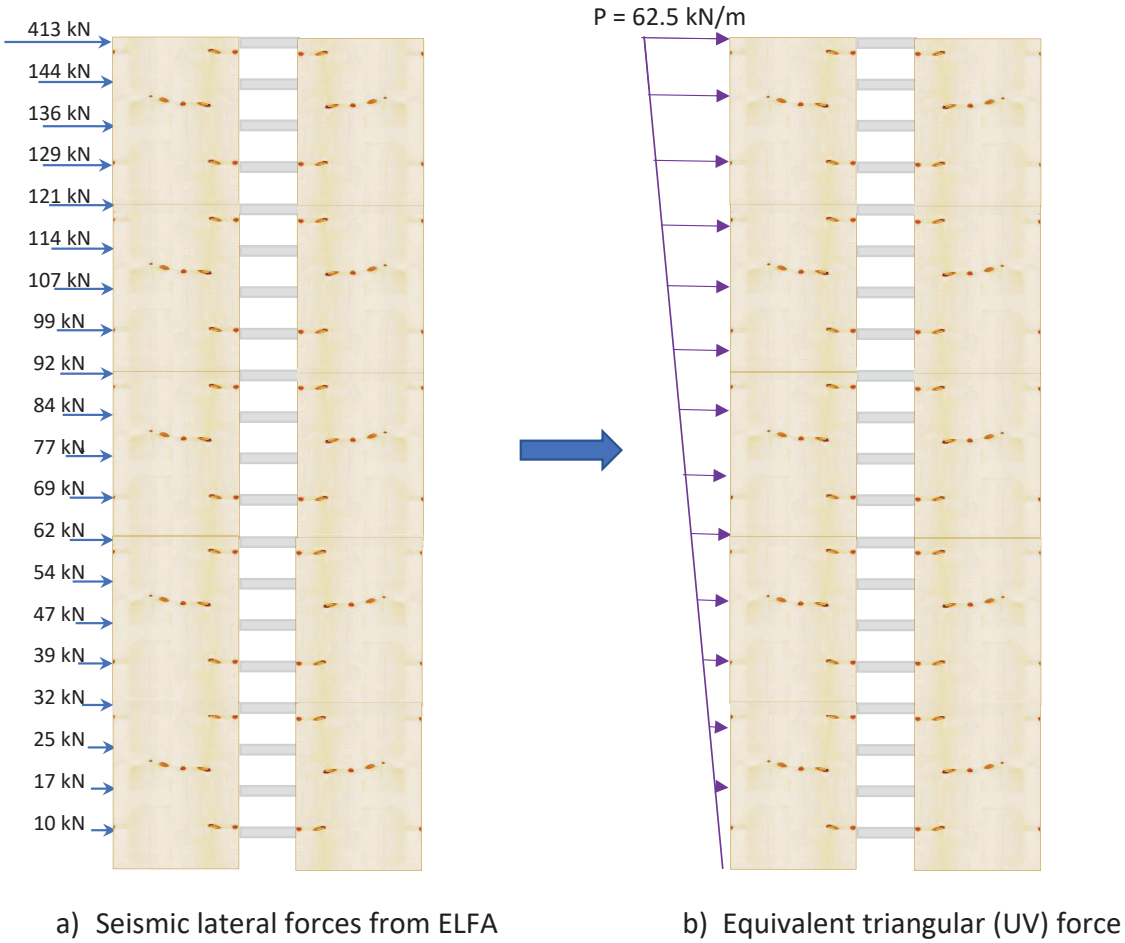

Figure 4.3: ELF and its equivalent lateral load distribution

For symmetrical CW system, where: $A_2 = A_1$ and $I = 2I_1$, equation 4.4 can be simplified to the form:

$$k = \sqrt{1 + \frac{4\ I_1}{A_1\ L_w^2}}. \tag{4.22}$$

A 7-ply CLT Grade E1 panel with $L_1 = L_2 = 6.0\ m$ and $t = 35\ mm$ (per layer), the effective axial stiffness of the CLT layers (considering the longitudinal layers only) is calculated to be $A = A_1 = A_2 = 0.84\ m^2$. Similarly, its effective flexural stiffness, $I = I_1 = I_2 = 3.97\ m^4$. Substituting the values of $A_1 = 0.84\ m^2$ and $I_1 = 3.97\ m^4$, and considering $L_w = 6+1 = 7\ m$, the parameter K becomes 1.177. Accordingly, the values of F_1, N, F_2, V_z, F_3, y, and DR are summarized in Table 4.4. Note that the shear force induced on each of the coupling beams (V_z in Table 4.4) is calculated by integrating equation 4.8 over the building height, and is given by:

$$V_z = q_z h \tag{4.23}$$

Distributions of drift, axial and shear forces are summarized in Table 4.4 for $R_o R_d = 3$ and $CR = 30\%$. The same procedure can be followed for the rest of the combinations (Table 4.1). The distribution of the axial force, shear force, and deformation throughout the height of the building is illustrated in Figure 4.4.

Table 4.4: Summary for the distributions of drift, axial and shear forces.

n	z (m)	z/H	F_1	N_z (kN)	F_2	V_z (kN)	F_3	y (m)	DR (%)
20	60	1	0	0	0.16	182	0.588	0.469	0.782
19	57	0.95	0.008	186	0.161	183	0.588	0.363	0.637
18	54	0.9	0.016	373	0.162	185	0.588	0.277	0.513
17	51	0.85	0.024	562	0.164	187	0.588	0.208	0.408
16	48	0.8	0.033	754	0.167	190	0.588	0.154	0.32
15	45	0.75	0.041	949	0.169	193	0.588	0.111	0.248
14	42	0.7	0.049	1,146	0.171	195	0.588	0.079	0.188
13	39	0.65	0.058	1,345	0.172	196	0.588	0.054	0.14
12	36	0.6	0.067	1,545	0.172	197	0.588	0.037	0.101
11	33	0.55	0.075	1,745	0.171	195	0.588	0.024	0.072
10	30	0.5	0.084	1,942	0.168	192	0.588	0.015	0.049
9	27	0.45	0.092	2,135	0.164	187	0.588	0.009	0.032
8	24	0.4	0.1	2,321	0.157	179	0.588	0.005	0.02
7	21	0.35	0.108	2,498	0.148	169	0.588	0.002	0.012
6	18	0.3	0.115	2,664	0.137	156	0.588	0.001	0.006
5	15	0.25	0.121	2,815	0.123	140	0.588	0	0.003
4	12	0.2	0.127	2,947	0.105	120	0.588	0	0.001
3	9	0.15	0.132	3,057	0.084	96	0.588	0	0
2	6	0.1	0.135	3,141	0.06	69	0.588	0	0
1	3	0.05	0.138	3,195	0.032	47	0.588	0	0
0	0	0	0.139	3,214	0	0	0.588	0	0

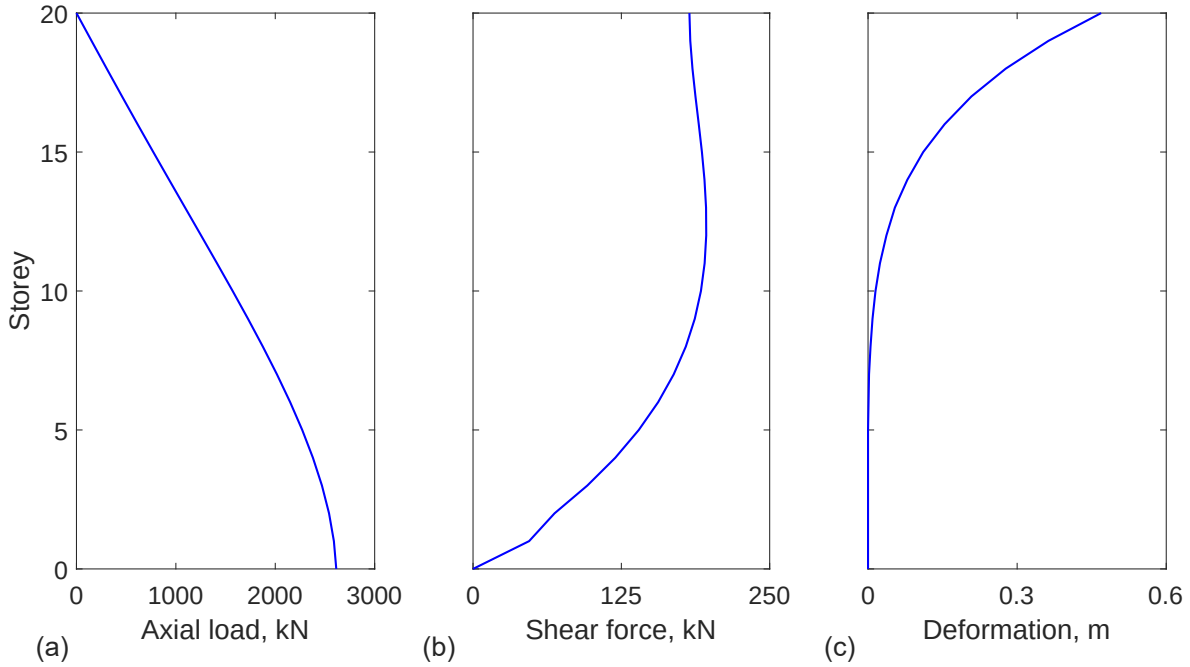

Figure 4.4: Continuum method results: (a) Axial load in kN; (b) Shear force in kN; and (c) Deformation in m.

Step 4. Calculate the force parameters in the CW system:

- From the force parameters obtained in step 4, determine the resistance moment gained from the coupling action and reduce the base overturning moment obtained in Step 3 by this amount.
- Knowing the reduced moment and determined axial loads from Step 4, calculate the resultant axial actions at the extreme faces of the wall piers (hold-down locations).

The resistance moment M_c developed by the coupling action is given by:

$$M_c = T \times L_W = N_{total} \times L_W \tag{4.24}$$

where

$$N_{total} = \sum_{i=1}^{n} N_i \tag{4.25}$$

N_i is the axial load at storey "i" and thus, the reduced moment in each of the wall piers is given by:

$$M_w = M_1 = M_2 = \frac{M_{\max} - M_R}{2} \tag{4.26}$$

The coupling and reduced moment (in the wall piers) are summarized in the Table 4.5 and Figure 4.5.

Table 4.5: Coupled-wall force parameters.

n	z (m)	N (kN)	M_{max} (kNm)	M_c (kNm)	M_w (kNm)
20	60	0	0	0	0
19	57	186	1,245	1,300	-27
18	54	373	2,927	2,609	159
17	51	562	5,023	3,934	544
16	48	754	7,510	5,279	1,116
15	45	949	10,364	6,643	1,861
14	42	1,146	13,563	8,024	2,770
13	39	1,345	17,084	9,418	3,833
12	36	1,545	20,903	10,817	5,043
11	33	1,745	24,778	12,212	6,283
10	30	1,942	28,828	13,592	7,618
9	27	2,135	33,025	14,942	9,042
8	24	2,321	37,341	16,247	10,547
7	21	2,498	41,749	17,489	12,130
6	18	2,664	46,221	18,648	13,787
5	15	2,815	50,731	19,702	15,515
4	12	2,947	55,256	20,628	17,314
3	9	3,057	59,769	21,400	19,185
2	6	3,141	64,250	21,990	21,130
1	3	3,195	68,673	22,368	23,153
0	0	3,214	73,019	22,501	25,259

Step 5. Design the CLT-CW structural elements:

- Having the design force parameters for both the coupling beams (shear force and bending moment) and the axial loads at the extreme faces of the wall piers, perform the preliminary design for the coupling beam and CLT-CW, respectively.

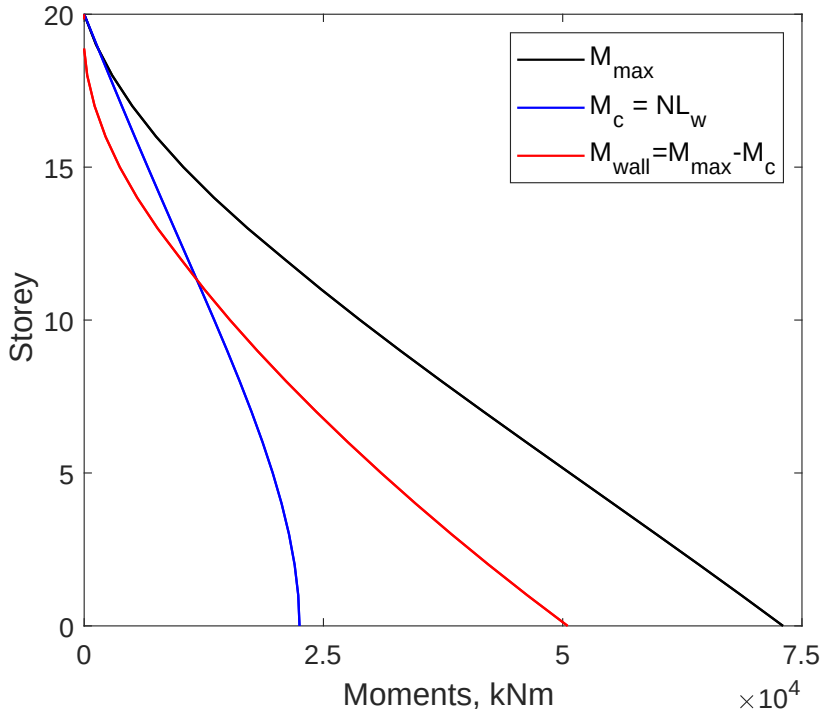

Figure 4.5: Distribution of moment over the height of the building

- Determine the required connection between the coupling beams and CLT-CW, and the CLT wall hold-downs based on the design force parameters.

The forces on the coupling beams are shear force and end moment. As can be seen in Figure 4.4 (b), the shear induced in the coupling beams is not uniform. For an efficient design, CSA (2014), and Harries and McNeice (2006) recommend up to 20% vertical redistribution of shear forces between coupling beams. However, the total demand provided should not be less than the total required (El-Tawil et al., 2010; Harries and McNeice, 2006). Based on these recommendations, the design strength of the coupling beams (V_{des}) is provided as:

$$V_{des} = max\ (0.8\ V_{max},\ V_{ave}) \tag{4.27}$$

where V_{max} and V_{ave} = maximum and average shear forces, respectively. The values $0.8V_{max}$, V_{ave}, and V_{des} are $158\ kN$, $163\ kN$, and $163\ kN$, respectively.

The force parameters developed at the base of the CLT shear walls are concentrated at extreme ends of the wall, assuming the shear walls will exhibit rocking action under the action of seismic load. Hence, the demand in the hold-down is calculated as the

maximum design tensile force (F_{des}) developed in the base and is given by the static equilibrium equation:

$$F_{des} = \frac{M_{wall}}{L_1} + \frac{T}{2} = \frac{M_{wall}}{L_1} + \frac{\sum V_{z,i}}{2} \tag{4.28}$$

Applying equation 4.28, the value of F_{des} becomes $4,317\ kN$.

Step 6. Design coupling beam to CLT and hold-down to CLT connections

The proposed connections, for both the coupling beams and BRB hold-downs, use steel bolts with steel side plates, as shown in Figure 4.6. Accordingly, the design guideline provided on CSA O86-19 section 12.4 (CSA, 2019) for bolts is used. The proposed connection for the coupling beam will be subjected to combined shear and moment actions (Figure 4.6 (a)). The moment is changed in to an equivalent force system and distributed to the bolts, as per given in Porteous and Kermani (2013). The shear and moment (equivalent force) demand in each bolt are given by Equations 4.29 and 4.30, respectively.

$$F_{v,i} = \frac{V_{des}}{n_F} \tag{4.29}$$

$$F_{m,i} = \frac{M_{des}\sqrt{x_i^2 + y_i^2}}{\sum x_i^2 + \sum y_i^2} \tag{4.30}$$

where $F_{v,i}$ and $F_{m,i}$ = shear and moment demand in bolt i, respectively; V_{des} = total design shear force; n_F = number of bolts, x_i and y_i = distances from centre of connection to bolt i, respectively; and M_{des} = design moment, which is calculated as:

$$M_{des} = V_{des}\ (\frac{L_b}{2} + x_c) \tag{4.31}$$

where x_c = distance from the edge of the wall to the centroid of the bolts (”OA” in Figure 4.6 (a)). x_c for this particular connection is = 120 + 1.5*90 = 255 mm.

Table 4.6 summarizes the values of the above parameters and resultant force acting in each of the bolts, for the rectangular arrangement of bolts. It should be noted that only

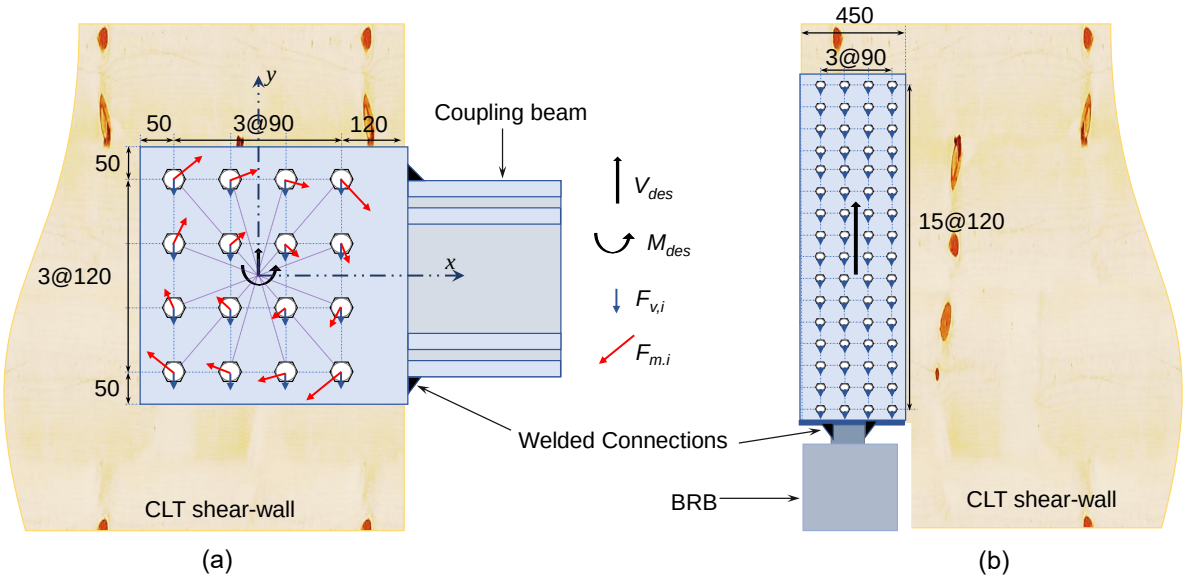

Figure 4.6: Connection details (in mm): (a) Coupling beam to CLT connections and (b) Hold-down to CLT connections.

effect of the induced shear forces (by the coupling action) is considered and that axial loads and direct transversal loads are neglected.

The steel side plates are provided in both faces of the CLT walls and hence, the problem has two shear planes. The lateral strength resistance for each of the four modes of failure (”a”, ”c”, ”d”, and ”g”) are examined as given by CSA O86-19 (CSA, 2019). The unit lateral strength resistance (n_u) is taken as the smallest value of the lateral strength resistance for the considered four modes of failures. The factored lateral strength resistance (N_r) for each bolt in the CLT wall is obtained as (CSA, 2019):

$$n_{u,a} = f_1 d_F t_1 \tag{4.32}$$

$$n_{u,c} = \frac{1}{2} f_2 d_F t_2 \tag{4.33}$$

$$n_{u,d} = f_1 d_F^2 \left(\sqrt{\frac{1}{6} \frac{f_2}{(f_1 + f_2)} \frac{f_y}{f_1}} + \frac{1}{5} \frac{t_1}{d_F} \right) \tag{4.34}$$

$$n_{u,g} = f_1 d_F^2 \left(\sqrt{\frac{2}{3} \frac{f_2}{(f_1 + f_2)} \frac{f_y}{f_1}} \right) \tag{4.35}$$

Table 4.6: Shear, moment and resultant forces on coupling beam to CLT connections.

i	$x(mm)$	$x^2(mm^2)$	$y(m)$	$y^2(mm^2)$	$F_{m,i}$ (kN)	$F_{v,i}$ (kN)	θ	F_R (kN)
1	-135	18225	180	32400	61.53	10.19	126.87	56.02
2	-45	2025	180	32400	50.74	10.19	104.04	49.27
3	45	2025	180	32400	50.74	10.19	75.96	54.12
4	135	18225	180	32400	61.53	10.19	53.13	68.13
5	-135	18225	60	3600	40.4	10.19	156.04	31.37
6	-45	2025	60	3600	20.51	10.19	126.87	16.54
7	45	2025	60	3600	20.51	10.19	53.13	27.84
8	135	18225	60	3600	40.4	10.19	23.96	49.88
9	-135	18225	-60	3600	40.4	10.19	203.96	31.37
10	-45	2025	-60	3600	20.51	10.19	233.13	16.54
11	45	2025	-60	3600	20.51	10.19	306.87	27.84
12	135	18225	-60	3600	40.4	10.19	336.04	49.88
13	-135	18225	-180	32400	61.53	10.19	233.13	56.02
14	-45	2025	-180	32400	50.74	10.19	255.96	49.27
15	45	2025	-180	32400	50.74	10.19	284.04	54.12
16	135	18225	-180	32400	61.53	10.19	306.87	68.13

The unit lateral strength resistance (n_u) is taken as the smallest value of the above equations 4.32 to 4.35. The factored lateral strength resistance (N_r) for each bolt in the CLT wall is obtained as (CSA, 2019):

$$N_r = \phi n_u K_D K_{st} K_T n_s \tag{4.36}$$

where f_1 and f_2 are embedment strength of members 1 (steel plate) and 2 (CLT), t_1 and t_2 are thicknesses of members 1 and 2, d_F is the diameter of bolt, f_y is the yield strength of bolts in bending, n_s is the number of shear planes, ϕ is the resistance factor, and K_D, K_{st}, and K_T are load duration, service condition, and treatment factors respectively.

Considering a $28.575\ mm$ ($1 - 1/8$") diameter ASTM A307 bolts with $f_y = 310\ MPa$, steel plate thickness of $6\ mm$ with $f_u = 335\ MPa$, and 7 layer grade E CLT shear-

wall panels; the lateral strength resistance for modes of failure ”a”, ”c”, ”d”, and ”g”, are calculated (in terms of kN/ shear plane/ bolt) as 172.31, 49.35, 60.65, and 43.77 respectively. Mode failure ”g” governs and the factored lateral strength resistance (N_r) for each bolt = $87.53\ kN$.

Only tensile force is considered for the hold-down, hence the demand in each bolt is determined by Equations 4.29. Same bolt diameters and steel plate thicknesses are adopted, and for the design axial load of $4,317\ kN$, a minimum of 50 bolts are required in the proposed rectangular arrangement of bolts (Figure 4.6 (b)). Welded connections are used to connect the steel plates with both the coupling beams and the BRB hold-downs.

Step 7. Model the system and validate the design through Pushover and NLTHA

The proposed method of analyzing the CLT-CW, CMM, is an elastic method of analysis that provides a good approximation for preliminary designs (El-Tawil et al., 2010; Smith and Coull, 1991). To fully understand the behaviour of CW systems and evaluate its preliminary designed components, a more accurate method (nonlinear analysis) should be accompanied (Smith and Coull, 1991). Accordingly, the CLT-CW system is further examined by nonlinear static and dynamic analyses, and are discussed in the subsequent chapter.

Chapter 5

Nonlinear Static and Dynamic Analyses

Structures are designed to yield and dissipate energy under seismic excitation. Nonlinear performance or response of structures is examined through nonlinear static and nonlinear dynamic analyses (NBC, 2015). This chapter presents the nonlinear response analysis of the CLT-CW systems designed in Chapter 4. Results for the nonlinear static and dynamic analyses along with the energy dissipation capacities of the ductile elements of the system are provided. Moreover, effects of the initially assumed seismic modification factors and coupling ratio values are discussed.

5.1 Nonlinear static (pushover) analysis

Both static and cyclic pushover analyses are performed to study the behavior of CLT-CW system up to collapse. The collapse is considered to occur either at model instability or 5% drift ratio (Deng et al., 2019; Tesfamariam et al., 2021; van de Lindt et al., 2020).

5.1.1 Static pushover analysis

Figures 5.1 and 5.2 depict the nonlinear response of the CLT-CW systems under the action of monolithically increased loads.

Figure 5.1 shows the pushover curve for the 20 storey CLT-CW system along the Y (strongest) direction. The figure clearly shows the response the structural system

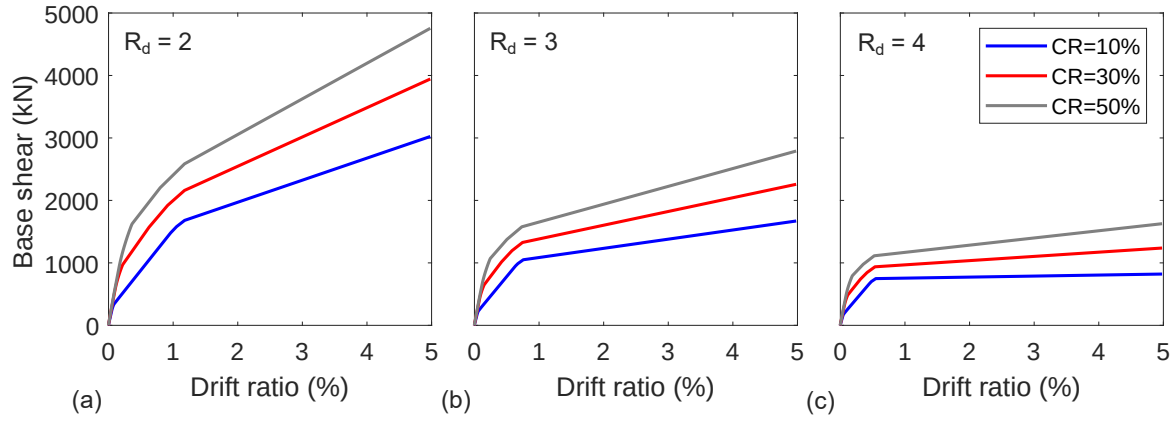

Figure 5.1: Pushover analysis for the 20-storey CLT-CW building along Y (strongest) direction

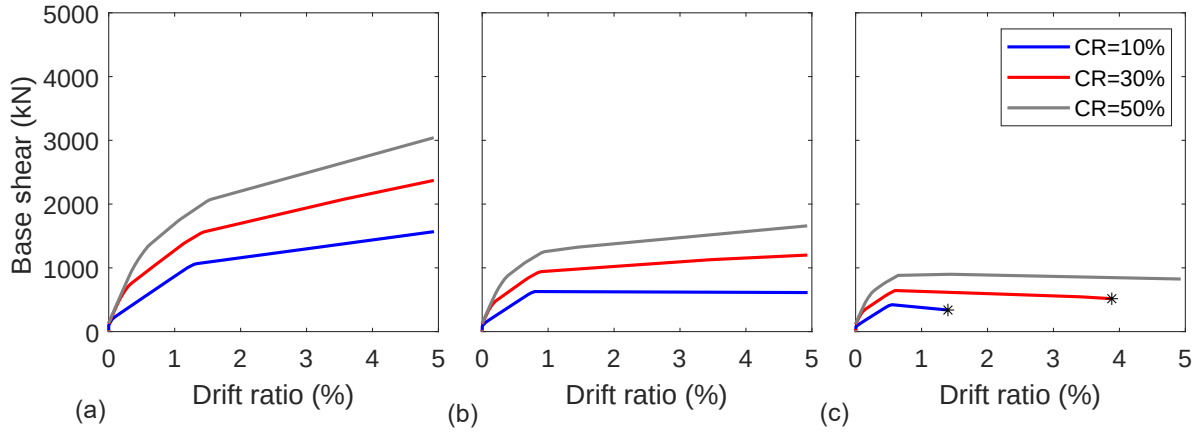

Figure 5.2: Pushover analysis for the 20-storey CLT-CW building along X (weakest) direction

under the action of different combinations of CR (10%, 30%, 50%) and R_d (2, 3, 4) values. Significant increase in strength and stiffness of the system is demonstrated for the CLT-CW system designed with R_d = 2 (Figure 5.1 (a)) compared to those designed with R_d = 3 (Figure 5.1 (b)) and 4 (Figure 5.1 (c)). An increase in strength of the system is also observed when using higher values of CR. Similar observation can be inferred from Figure 5.1 for the response of the system in the X (weakest) direction. However, the strength in the X direction, as expected, is relatively weaker than the strength in the Y direction. Moreover, as can be seen from Figure 5.2 (c) and CR = 10% and 20%, the system exhibits strength deterioration and collapses before it reaches a drift ratio of 5%. The asterisk in Figure 5.2 (c) shows the failure point at which the structure is deformed up to a displacement which is characterised by a 20% base shear reduction (Panagiotakos and Fardis, 2001; Petrone et al., 2017).

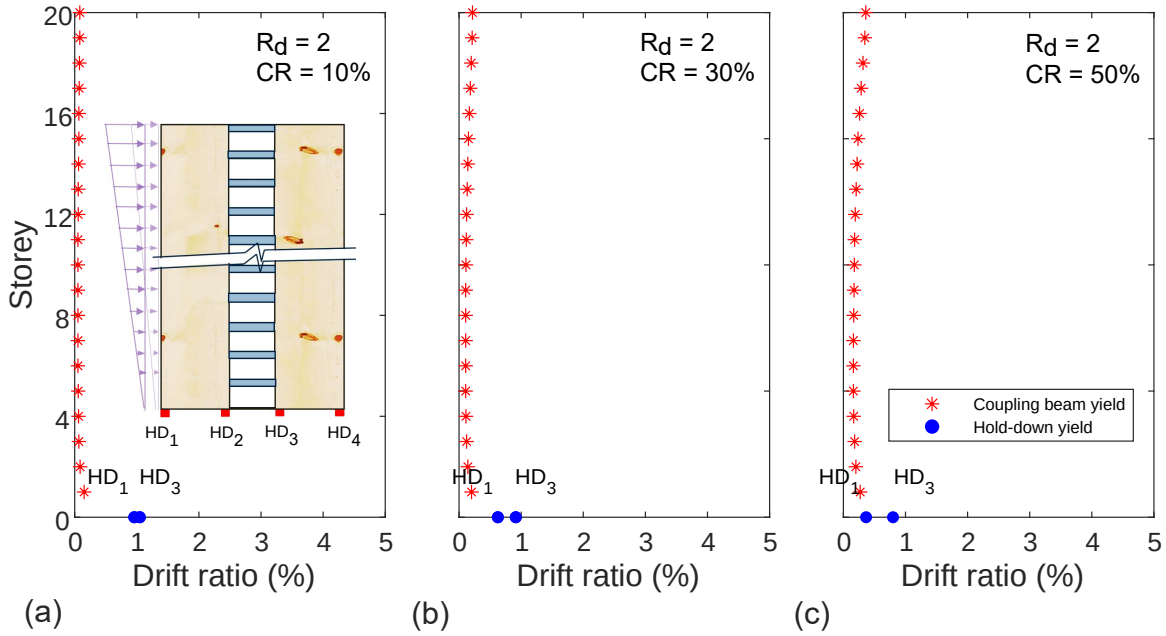

Figure 5.3: Sequence of coupling beam and hold-down yielding for $R_d = 2$ in Y direction

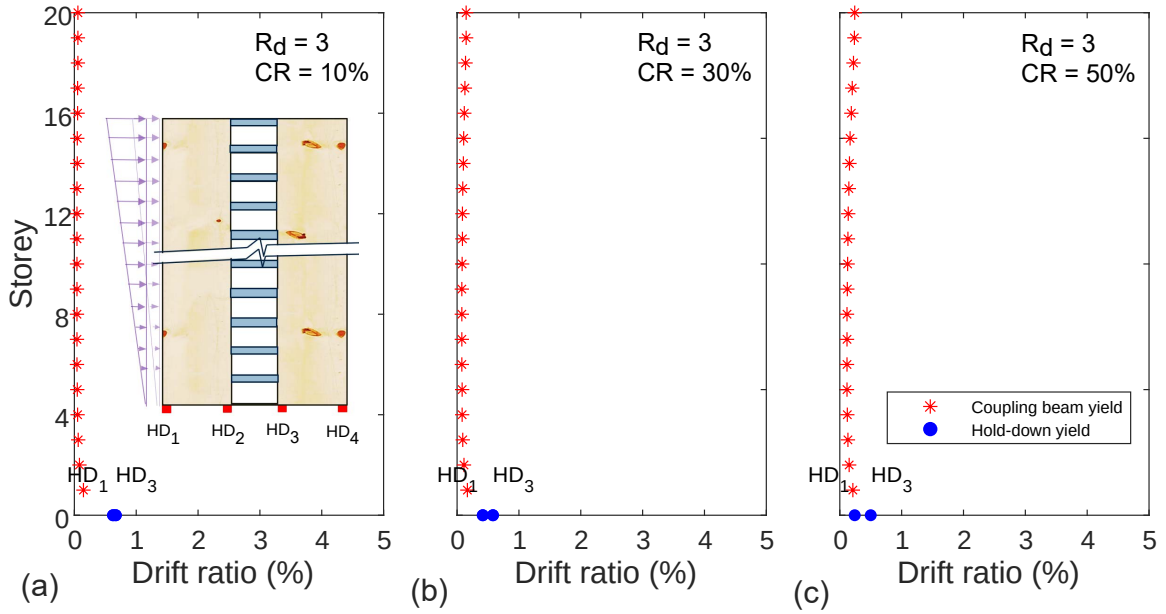

Figure 5.4: Sequence of coupling beam and hold-down yielding for $R_d = 3$ in Y direction

Figures 5.3 and 5.4 show the yielding sequence of coupling beam and hold-downs as with respect to drift ratio. The figures illustrate a fairly consistent sequence of yielding between the coupling beams and hold-downs. In all cases, the coupling beams yield prior to the hold-downs and this is in agreement with the preferred sequence of yielding in CW systems (El-Tawil et al., 2010). The hold-down yielding is more delayed for

cases with CR = 10% (Figures 5.3 (a), 5.4 (a)) comparing with those designed with CR = 30% and 50%. For R_d = 2 and CR = 10% (Figure 5.3 (a)), the coupling beams yield almost simultaneously with the exception at the first two - three storey where the yielding sequence is delayed. This is mainly due to the provision of uniform strength coupling beams considered in the design, even when the demand at these location was minimum. The CLT-CW systems designed with R_d = 2 and CR = 50% (Figure 5.3 (c)) is another extreme case, where the coupling beams relatively yield at different drift ratio values. Coupling beam yielding is initiated at floor levels 5 to 8 and progressed both upwards and downwards. The sequence of the yielding almost matches with the actual demand and provided strength of the coupling beams, in which the beams within the middle $2/3$ of the building were provided with smaller strength and hence, yielded prior to the top and bottom level coupling beams.

5.1.2 Cyclic pushover analysis

Conventional or monolithic pushover curve is obtained by applying a monotonic lateral load distribution and the response obtained by this procedure does not consider the effect of cyclic loading effects. This method neglects the cumulative damage due to repeated cyclic loading, as that of the seismic excitation. Consequently, this overestimate the strength and stiffness of the system. However, stiffness degradation and strength deterioration are one of the important characteristics of structures. Cyclic pushover procedure overcomes this limitation and captures the cumulative damage of structural components under the action of cyclic loading. Therefore, this method can provide a good approximation to the seismic response of structures comparable with that of nonlinear dynamic analysis. Accordingly, the cyclic pushover analysis is performed for the CLT-CW systems.

Results similar to the conventional pushover curves are illustrated in Figures 5.5 and 5.6 for Y and X directions, respectively. The CLT-CW systems designed with R_d = 2 exhibit significant increase in strength and stiffness of the system compared to those designed with R_d = 3 and 4. Similarly, an increase in strength of the system is also observed when using higher values of CR. The cyclic pushover curve for CLT-CW systems designed along the X direction, (in Figure 5.6 R_d = 4) demonstrates a rapid stiffness degradation and strength deterioration of the system along the weakest direction. As can be seen from the figure, the system exhibits an immediate strength

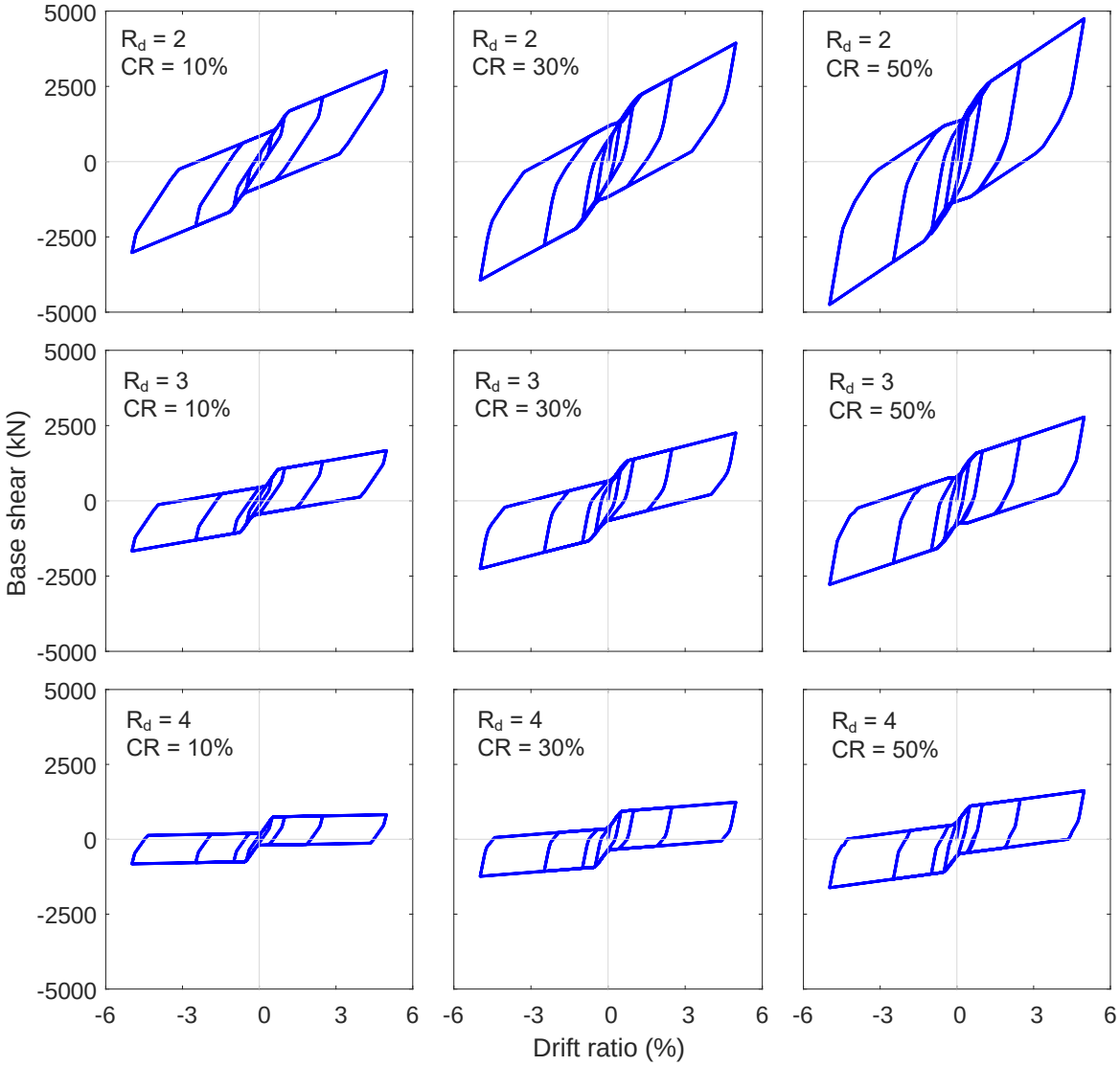

Figure 5.5: Cyclic pushover analysis for the 20-storey CLT-CW building along Y direction

deterioration once it reaches the maximum strength. Similar observation was made in the monolithic pushover curve as well. Hence, CLT-CW systems designed with $R_d = 4$ show a lesser performance and ultimately fails at the point indicated by asterisk, the point at which the structure is deformed up to a displacement which is characterised by a 20% base shear reduction.

5.2 Seismic hazard and ground motion selection

Ground motion (GM) selection is carried out by matching the response spectra of the selected records to a target response spectrum at the site of interest. The ground

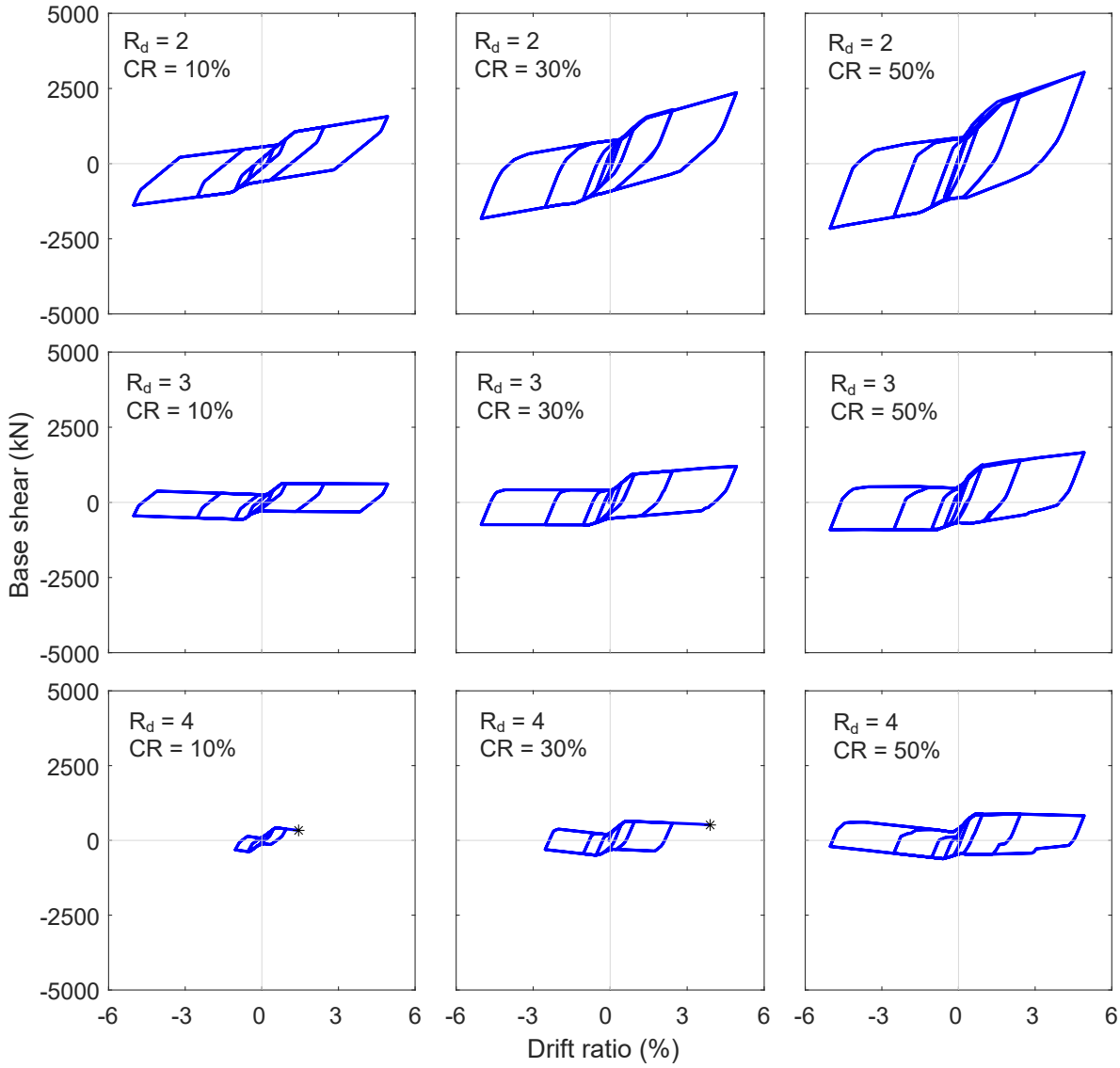

Figure 5.6: Cyclic pushover analysis for the 20-storey CLT-CW building along X direction

motion selection is reported in Tesfamariam et al. (2019b; 2021).

A probabilistic seismic hazard analysis (PSHA) tool is used based on Monte Carlo simulations (Atkinson and Goda, 2011) by implementing all major components of the national seismic hazard model (Halchuk et al., 2014). A set of records based on regional seismic hazard characteristics, using multiple-conditional mean spectrum-based record selection method (Goda, 2019), at the anchor period of TA = 2.0 s, 30 records (bi directional) are selected, i.e. 60 unidirectional records. Lower and upper limit vibration periods, T_{min} = 0.1 s and T_{max} = 4.0 s, are considered for the ground motion selection. Figure 5.7 compares the response spectra of the selected ground motion records with the target spectrum. The match is satisfactory over a wide range

of vibration periods from 0.1 s to 4.0 s (Tesfamariam et al., 2021).

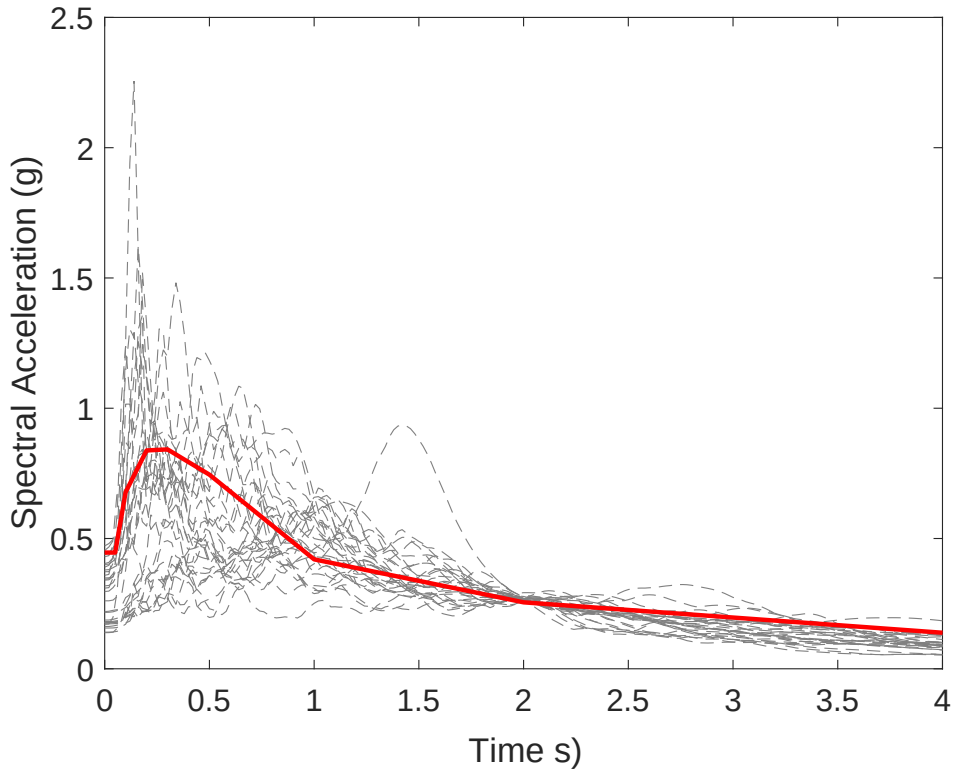

Figure 5.7: Spectral acceleration for Vancouver - BC

5.3 Nonlinear time history analysis

Nonlinear time history analysis (NLTHA) is used to asses the nonlinear response of the systems under the action of seismic excitation. The analysis is carried out using the 30 GM records shown in Figure 5.7.

5.3.1 Peak responses of the CLT-CW system

Maximum inter-story drift ratio (MaxISDR), residual inter-story drift ratio (ResISDR), and horizontal peak floor acceleration (PFA) are computed to access the performance of the CLT-CW systems. Figures 5.8 and 5.9) are provided to show the ISDR and floor acceleration time series for GM #1 and #24 in the Y and X directions, respectively.

Maximum inter-storey drift ratio

One of the key indicators of the structural performance of buildings under the action of lateral forces is the value of MaxISDR. As per NBC (NBC, 2015)), the MaxISDR for

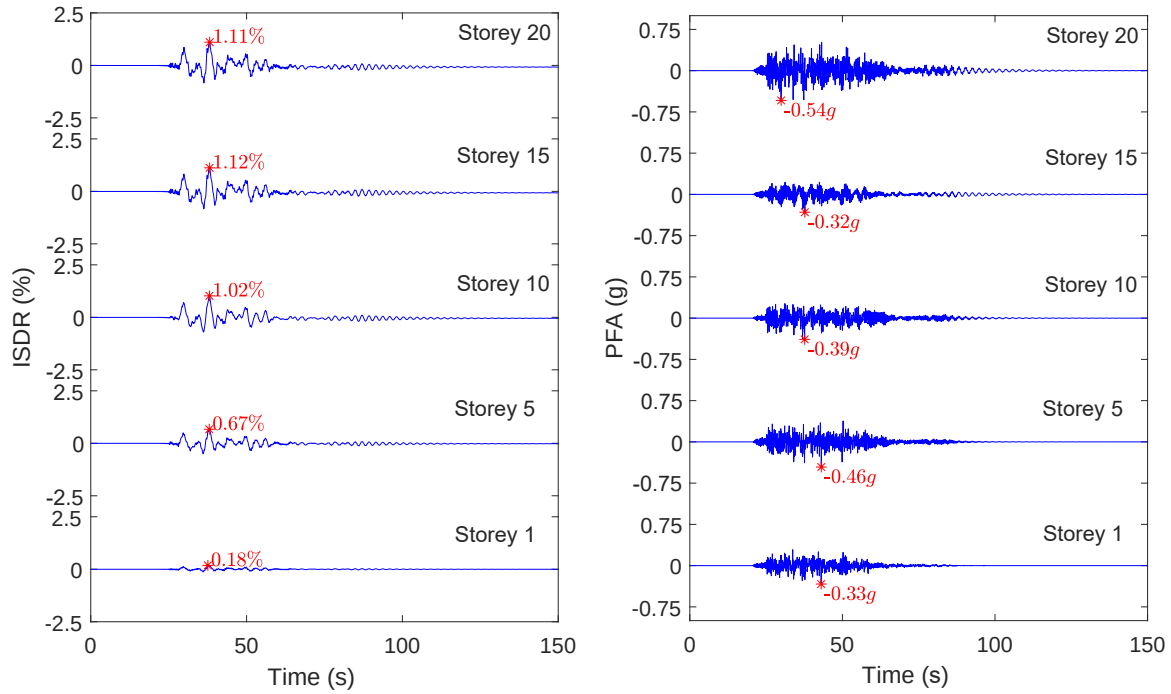

(a) Inter-storey drift ratio (%)

(b) Floor acceleration (g)

Figure 5.8: ISDR and floor acceleration time series results for R_d = 2, CR = 30%, and GM #1 in Y direction.

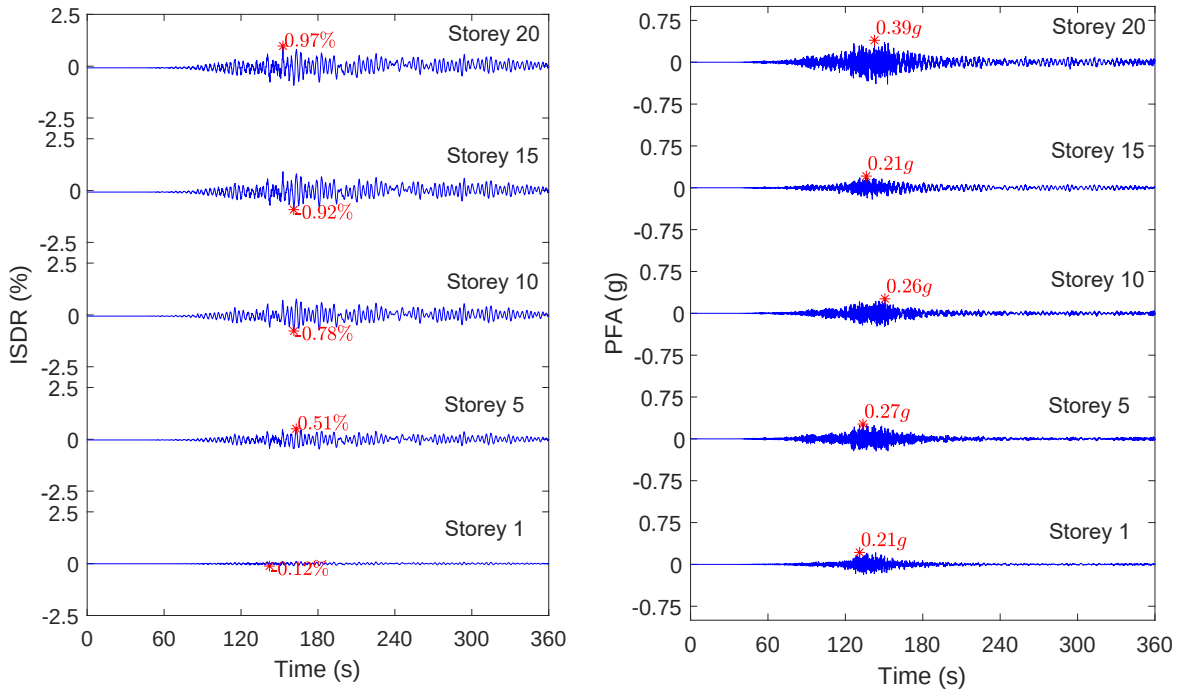

(a) Inter-storey drift ratio (%)

(b) Floor acceleration (g)

Figure 5.9: ISDR and floor acceleration time series results for R_d = 2, CR = 30%, and GM #24 in X direction.

2% PE in 50 years and collapse prevention limit state is 2.5%.

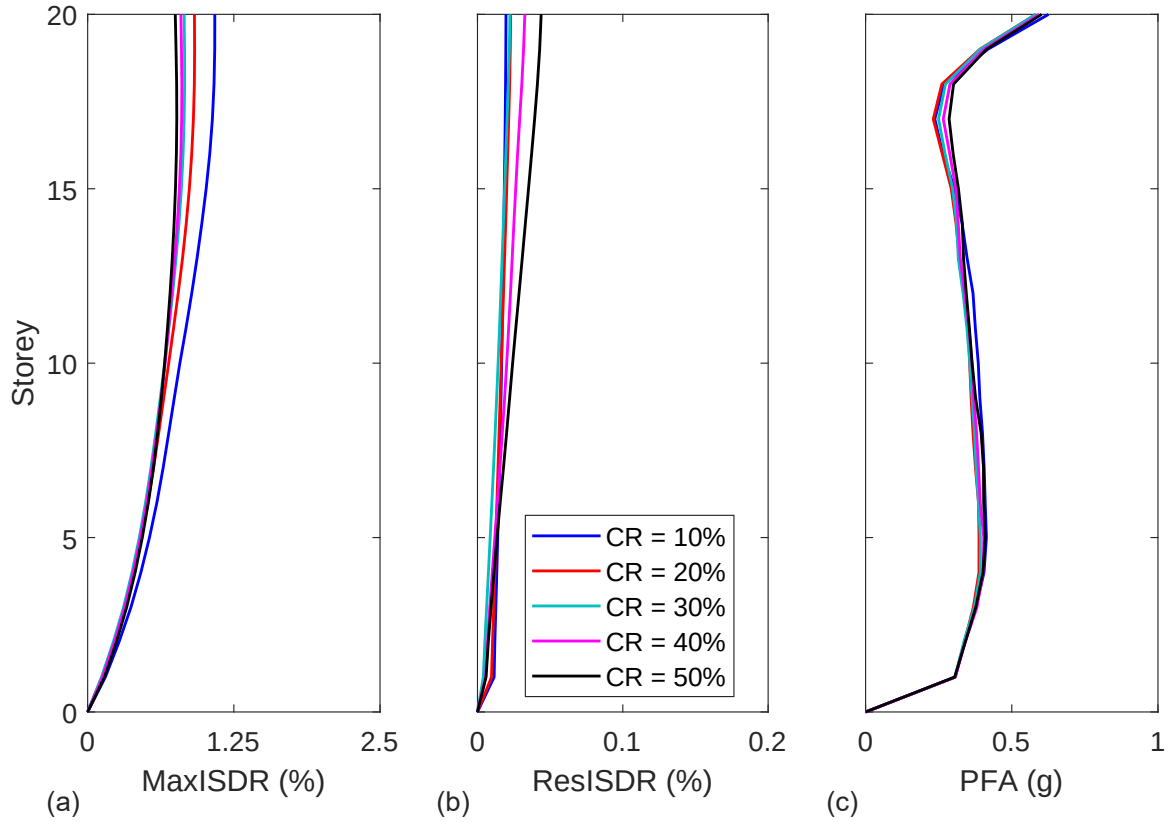

Figure 5.10: Results of nonlinear time history analysis for R_d = 2 in the Y direction: (a) MaxISDR; (b) ResISDR; and (c) PFA.

Figures 5.10 and 5.11 illustrate, for R_d = 2 and five different values of CR (10%, 20%, 30%, 40%, and 50%), the mean values (results of the 60 GMs) of MaxISDR, ResISDR and PFA along the height of the building in the Y and X directions, respectively. From the figures, it is evident that the mean MaxISDR values ranges 1% to 1.35% that is well below the NBC limit of 2.5%. Moreover, in all cases, the average MaxISDR is relatively higher for smaller CR values. The primary reason for this that the strength demand (from the CMM analysis) of the coupling beams at smaller CR values is small and hence, exhibit large nonlinear displacement. As expected, the mean MaxISDR in the weakest direction (Figure 5.10 (a)) of the CLT-CW system is larger compared to the response in the strongest direction (Figure 5.11 (a)). Generally, the mean MaxISDR is maximum at higher storeys (Figures 5.10 (a), 5.11 (a), 5.8a, and 5.8b). The reason for this is the CLT walls exhibit larger drift coupled with large deformation of the coupling beams at those higher storeys. Similar trend is observed for CLT-CW system designed with R_d = 3 and 4.

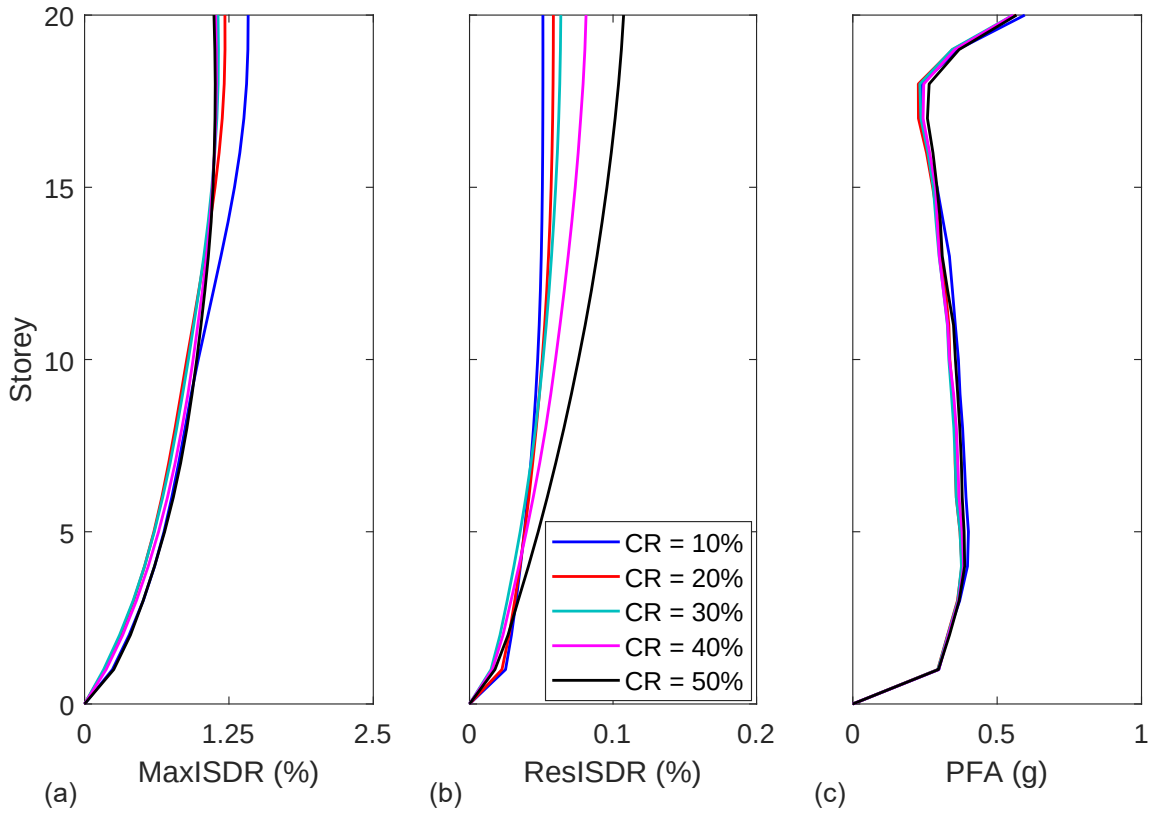

Figure 5.11: Results of nonlinear time history analysis for R_d = 2 in the X direction: (a) MaxISDR; (b) ResISDR; and (c) PFA.

Residual inter-storey drift ratio

Another important structural performance indicator is the ResISDR. This parameter measures the permanent or non-reversible deformation of the building at the end of the applied GM. Figures 5.10 (b) and 5.11 (b) illustrate the values of the ResISDR throughout the height of the building in the Y and X directions, respectively. As can be seen from the figures, the values of ResISDR are below 0.2%. Values of the ResISDR are within the intended limit of 1%, a value provided by TBI (2017) to protect excessive post-earthquake deformations that likely will cause condemnations or excessive downtime repairs of buildings. Moreover, ResISDR increase with the increase in the height of the structure. Besides, CLT-CW systems with higher CR exhibit larger ResISDR values.

Peak floor acceleration

Figures 5.10 (c) and 5.11 (c) demonstrate the distribution of the PFA throughout the height of the building, in terms of gravitational acceleration (g) units, in the Y and

X directions, respectively. As can be seen from the figures, the PFA values remain less than 0.5g for storeys 1 to 18, and achieves their maximum value at the top storey levels. No significant difference is observed between CLT-CW systems in the Y and X directions. The value of CR also appears to have no effect on PFA.

5.3.2 Effect of different values of R_d

In this section, the effect of R_d on MaxISDR and ResISDR, for all CR and building height is summarized. The over-strength factor of R_o = 1.5, as in CSA 086-14 (CSA, 2016; NBC, 2015), is adopted and three seismic modification factors, R_d = 2, 3, and 4, are examined.

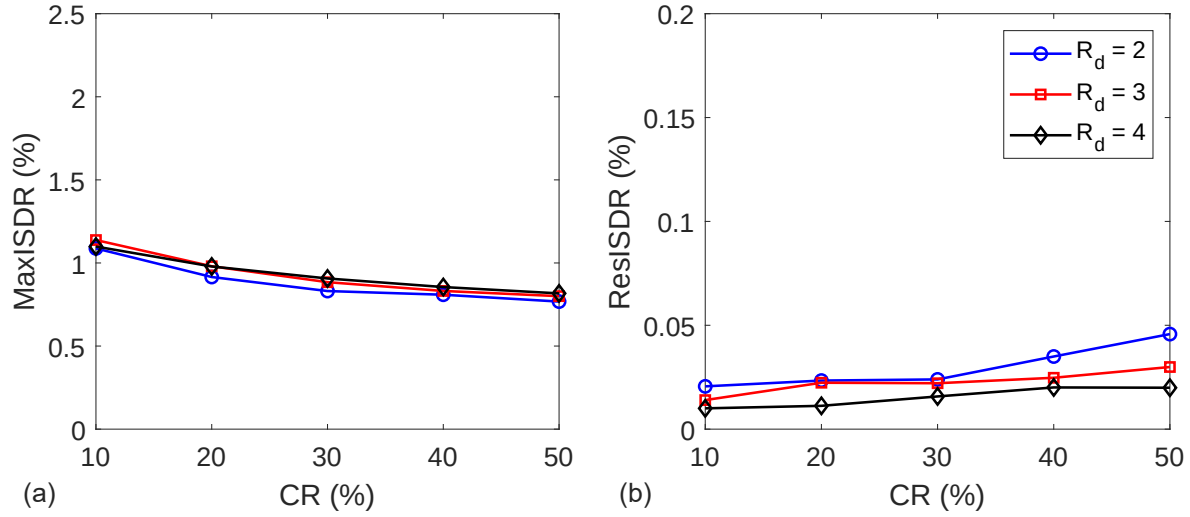

Figure 5.12: Nonlinear time history analysis result for 20 storey CLT-CW system (along Y direction): a) MaxISDR; and b) ResISDR.

Figures 5.12, 5.14, and 5.16 illustrate the summary for the MaxISDR and ResISDR for the 20, 15, and 10 storey CLT-CW buildings, respectively, in the Y direction. Similarly, Figures 5.13, 5.15, and 5.17 illustrate the summary for the MaxISDR and ResISDR for the 20, 15, and 10 storey CLT-CW buildings, respectively, in the X direction. As expected, higher MaxISDR are observed for CLT-CW system designed with R_d = 4 (in all Figures 5.12 (a) to 5.17 (a)). The reason for this is that CLT-CW designed with R_d = 4 experienced high seismic reduction that led the system to have lower capacity. The elements of the system are then allowed to yield and deform largely.

The behavior of the coupling beams and hold-downs will be discussed in the subsequent sections. The most important observation is that the 20 storey CLT-CW system designed with R_d = 4 (CR values 10%, 20%, 30%, and 40%) failed in the X

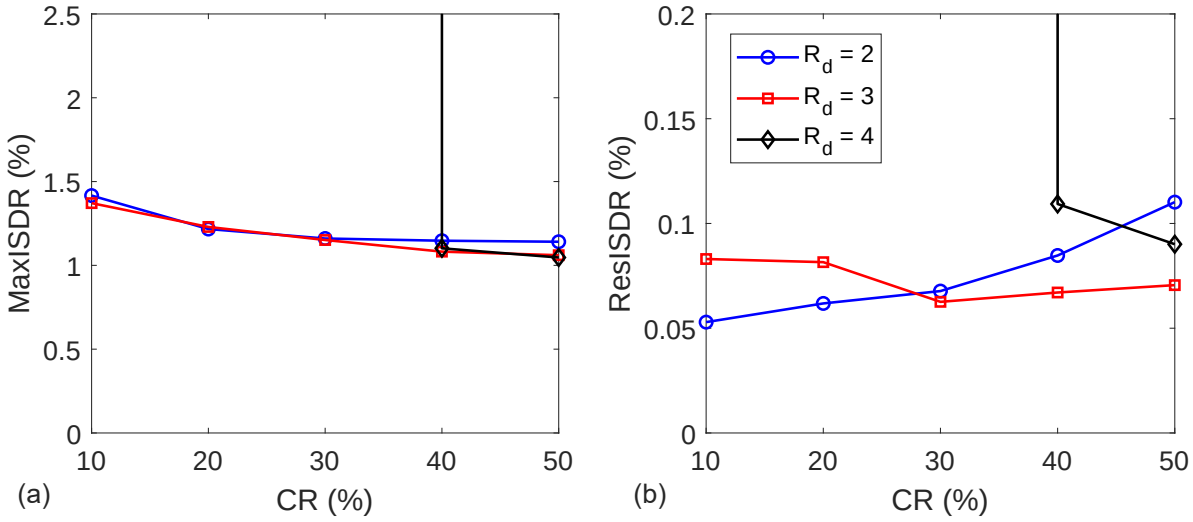

Figure 5.13: Nonlinear time history analysis result for 20 storey CLT-CW system (along X direction): a) MaxISDR; and b) ResISDR.

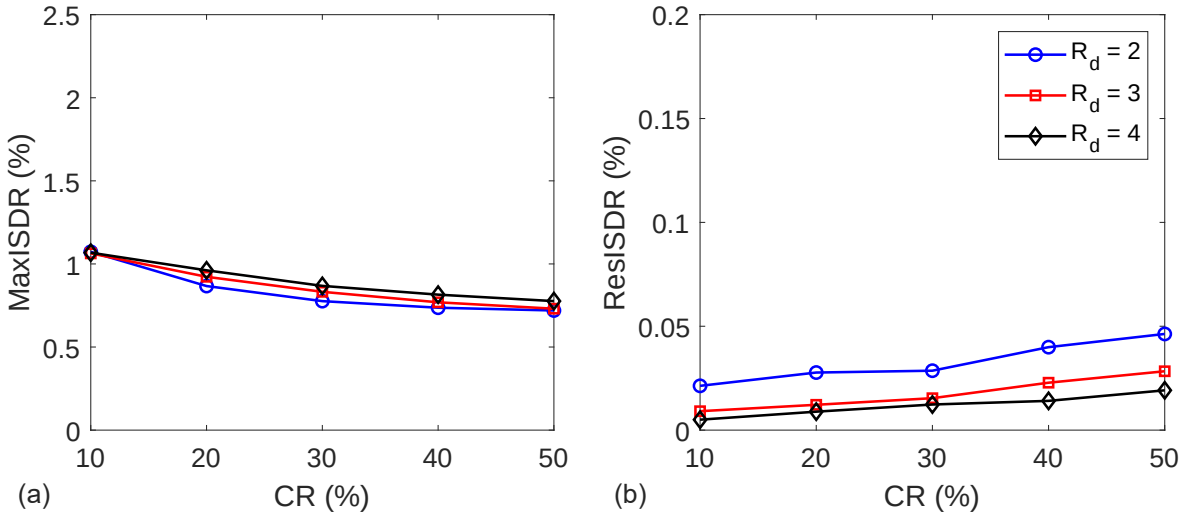

Figure 5.14: Nonlinear time history analysis result for 15 storey CLT-CW system (along Y direction): a) MaxISDR; and b) ResISDR.

direction (Figure 5.13). The same was observed in the nonlinear static analyses as well. CLT-CW system designed with R_d = 4 does not satisfy the required performance and hence, discussion in the upcoming sections will be limited to CLT-CW systems with R_d values of 2 and 3.

5.3.3 Effect of different values of CR

The behaviour of the CLT-CW system is examined under five CR = 10%, 20%, 30%, 40%, and 50%. From Figures 5.12 (a) to 5.17 (a), systems with higher CR value reveal

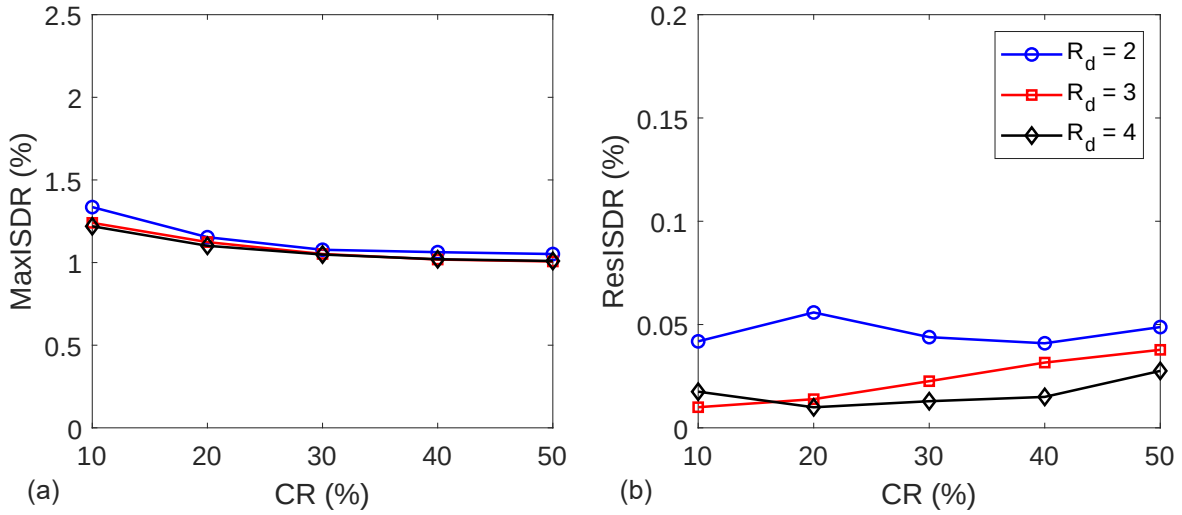

Figure 5.15: Nonlinear time history analysis result for 15 storey CLT-CW system (along X direction): a) MaxISDR; and b) ResISDR.

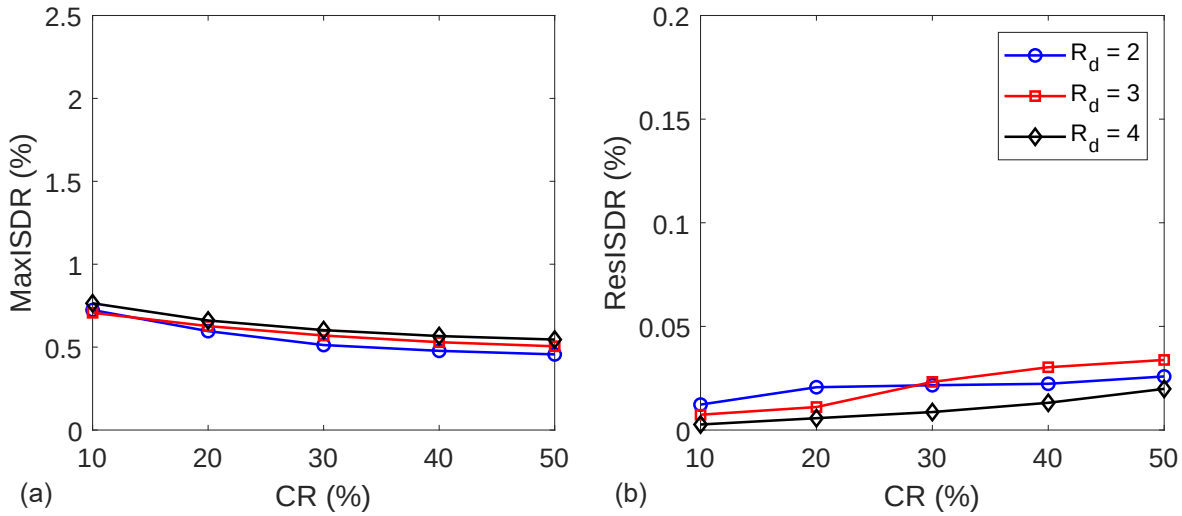

Figure 5.16: Nonlinear time history analysis result for 10 storey CLT-CW system (along Y direction): a) MaxISDR; and b) ResISDR.

less MaxISDR or displacement. This is due to the fact that CW systems with higher CR value have higher stiffness and strength. Thus, the values of MaxISDR significantly decreases with the increase in the value of CR. However, the values of ResISDR slightly increases with the increase in the value of CR (Figures 5.12 (b) to 5.17 (b)).

5.3.4 BRB Hold-down behavior

Figures 5.18 to 5.21 show the response of the BRB hold-downs, provided at the base of the CLT shear walls, for the 20 storey CLT-CW system at selected GMs. In all the

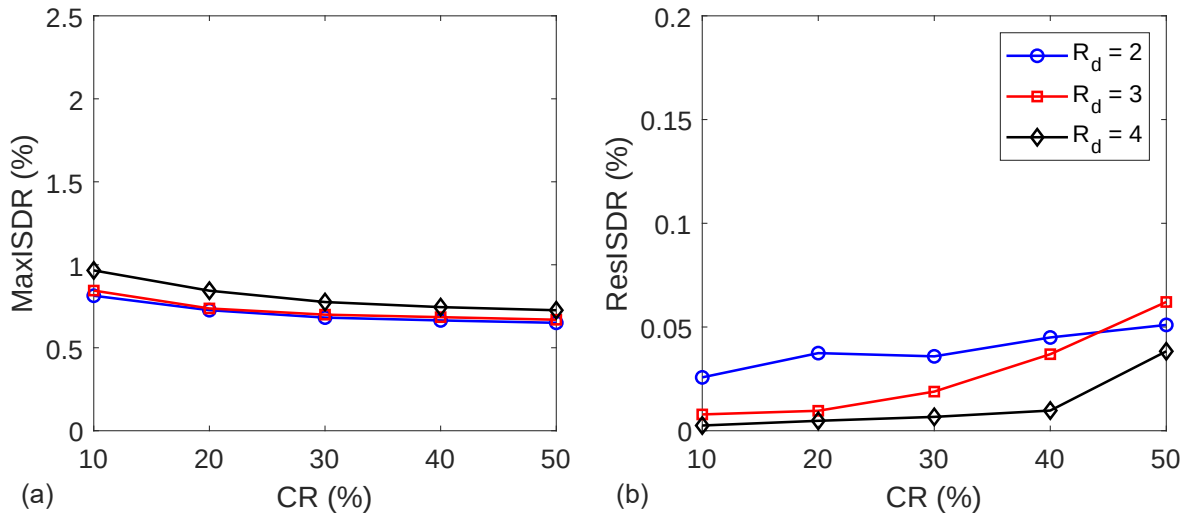

Figure 5.17: Nonlinear time history analysis result for 10 storey CLT-CW system (along X direction): a) MaxISDR; and b) ResISDR.

figures, (a), (b), (c), and (d) represents BRB hold-downs HD_1, HD_2, HD_3, and HD_4. Same capacity hold-downs were provided for both the outer and interior sides of the CLT walls in the Y (symmetrical wall) direction. Accordingly, Figures 5.18 and 5.19 illustrate symmetric hysteretic responses. In reality, the hold-downs at the outer sides of the CLT walls (HD_1 and HD_4) are subjected to higher axial action than these located at the inner sides (HD_2 and HD_3). However, as the provided strength are equal, the hold-downs at the outer sides of the CLT walls exhibit higher response than the inner ones.

In X (asymmetrical) direction, the dimensions of the two walls are not equal and the strength of the BRB hold-downs is proportioned based on the stiffness of their corresponding walls. As a result, Figures 5.20 and 5.21 illustrate different hold-down strengths. However, same strength is provided for hold-downs on the same wall (eg. HD_1 and HD_2 for the smaller CLT shear wall, and HD_3 and HD_4 for the bigger CLT shear wall). As can be seen from Figures 5.20 and 5.21, hold-downs located at the outer edge of the CLT shear walls ((a) and (d)) exhibit higher responses (similar to the response observed in the Y directions) than the inner ones ((b) and (c)).

For both the hold-downs in the X and Y directions, as the values of R_d increases from 2 (Figures 5.18 and 5.20) to 3 (Figures 5.19 and 5.21), the hysteresis curve for the hold-downs increases as the strength demand for large R_d value is small as dictated by the seismic analysis. Besides, when the values of CR increases from 10% to 50%, the hysteresis curve for the hold-downs decreases as the base moment demand decreases

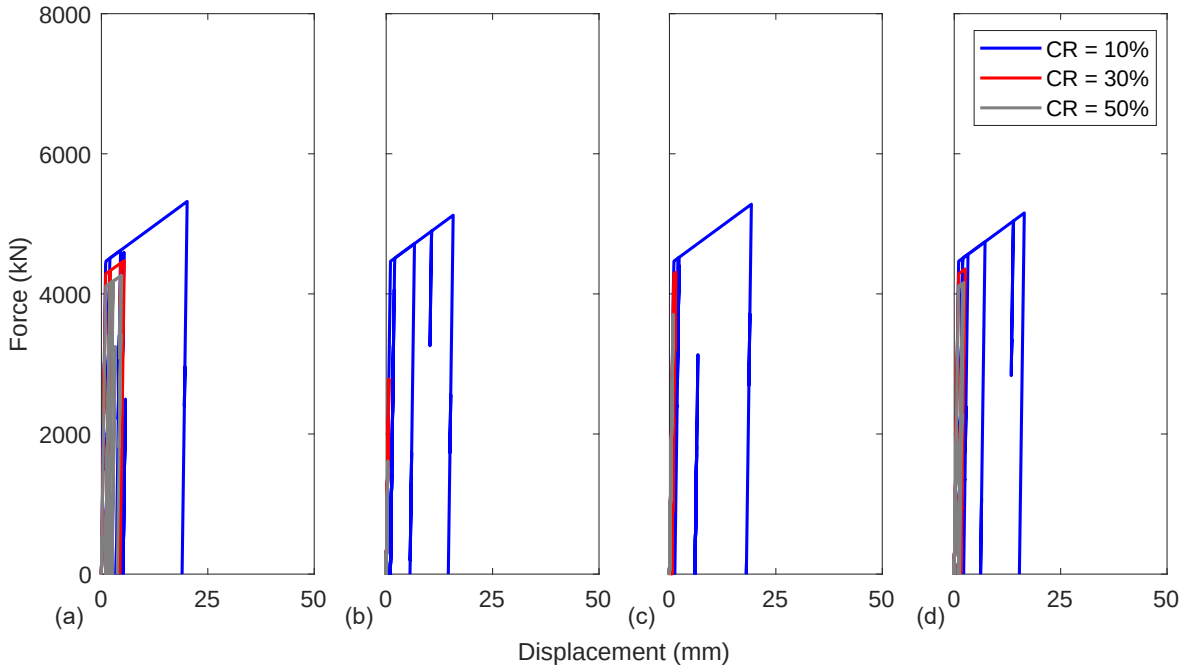

Figure 5.18: BRB Hold-down force-displacement curve for GM # 1 and R_d = 2 in Y direction: (a) HD_1; (b) HD_2; (c) HD_3; and (d) HD_4.

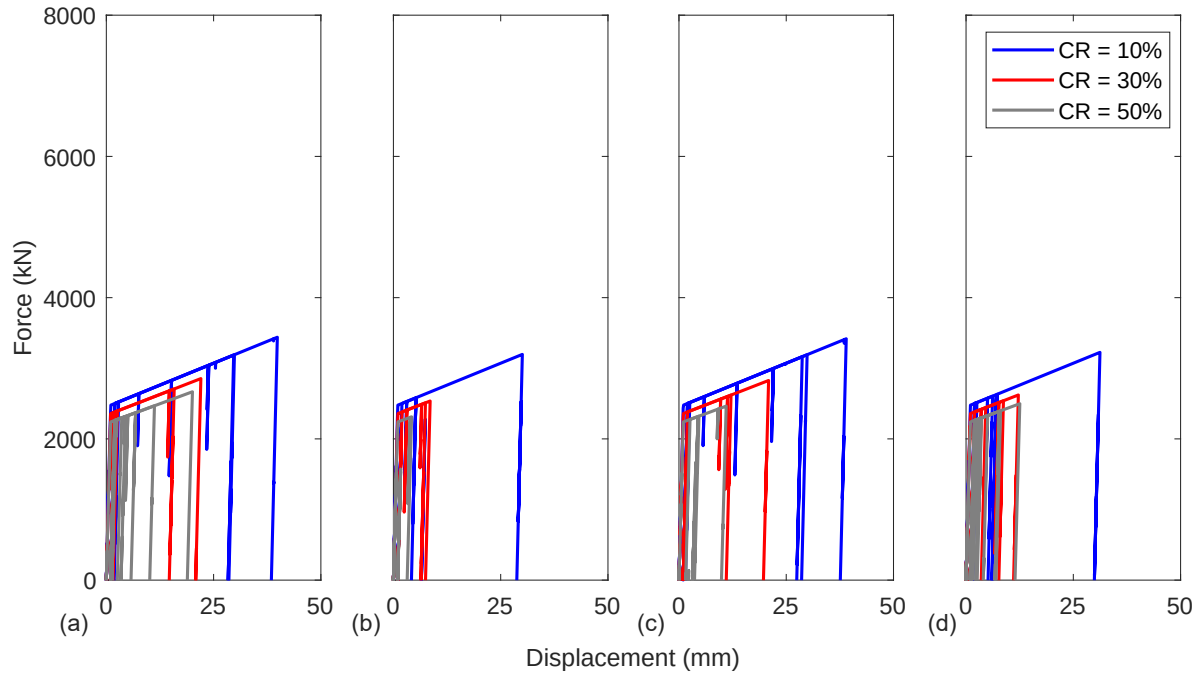

Figure 5.19: BRB Hold-down force-displacement curve for GM # 1 and R_d = 3 in Y direction: (a) HD_1; (b) HD_2; (c) HD_3; and (d) HD_4.

with an increase in the value of CR.

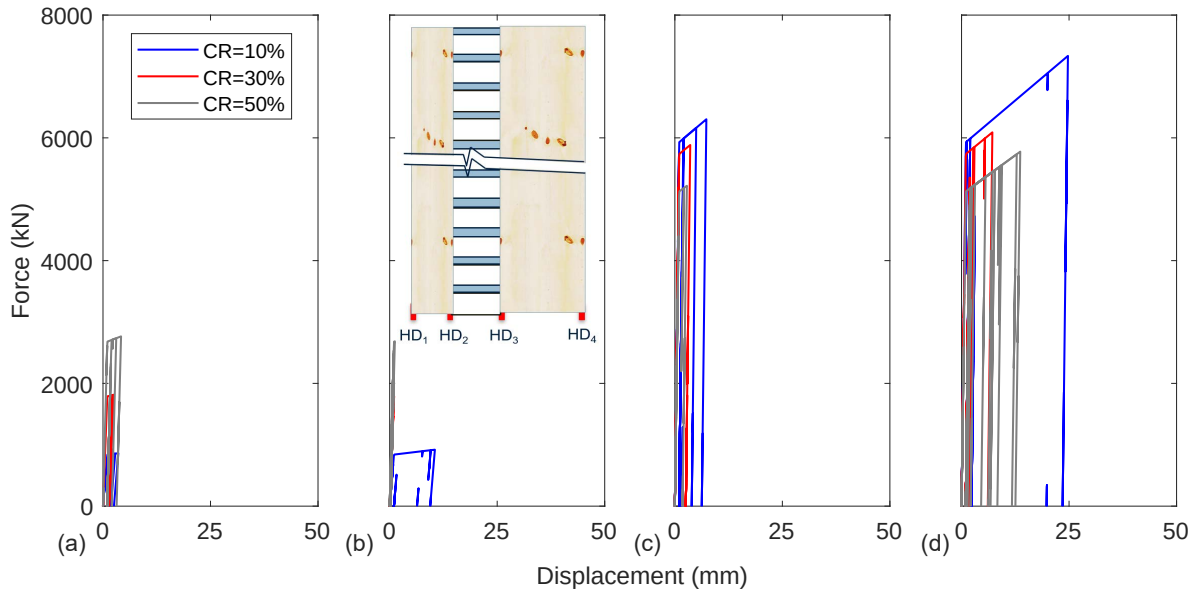

Figure 5.20: BRB Hold-down force-displacement curve for GM # 3 and R_d = 2 in X direction: (a) HD_1; (b) HD_2; (c) HD_3; and (d) HD_4.

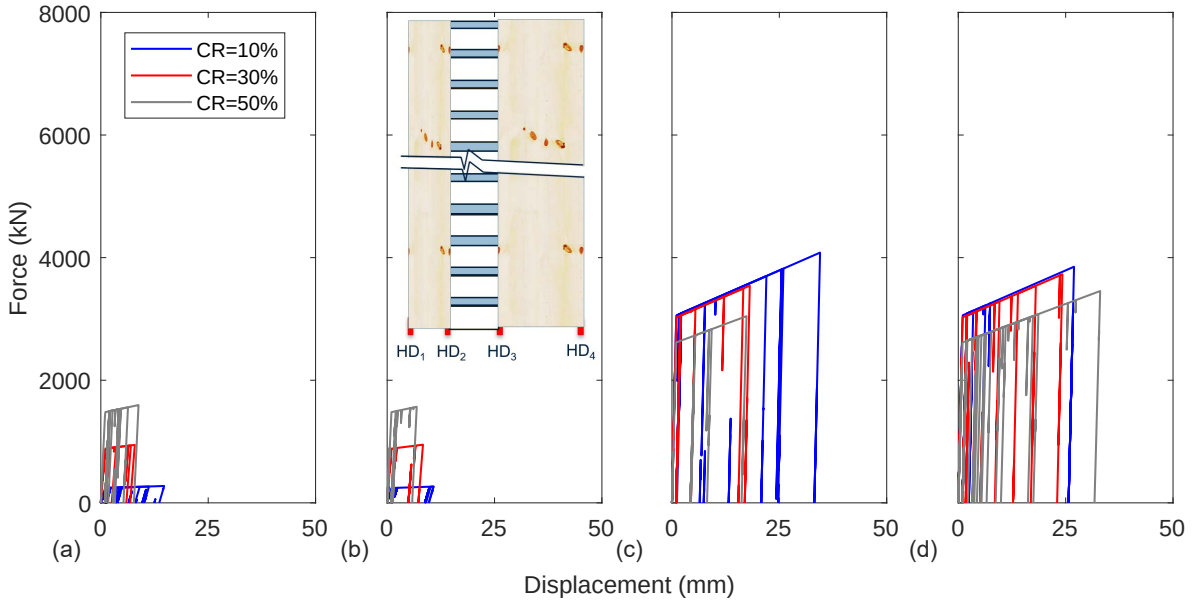

Figure 5.21: BRB Hold-down force-displacement curve for GM # 3 and R_d = 3 in X direction: (a) HD_1; (b) HD_2; (c) HD_3; and (d) HD_4.

5.3.5 Coupling beam behavior

The force-displacement response for all the coupling beams for the 20 storey CLT-CW system (over the height of the building) at selected GMs is shown in Figures 5.22 to 5.25. The response of the coupling beams is dictated by the shear force profile of the CMM analysis and the provided strength. Generally, the shear force profile (from the CMM analysis) increases with the increase in the height of the structure. As the

provided strength is an average of the actual demand, the response shown in Figures 5.22 to 5.25 increases with the increase in the height of the building.

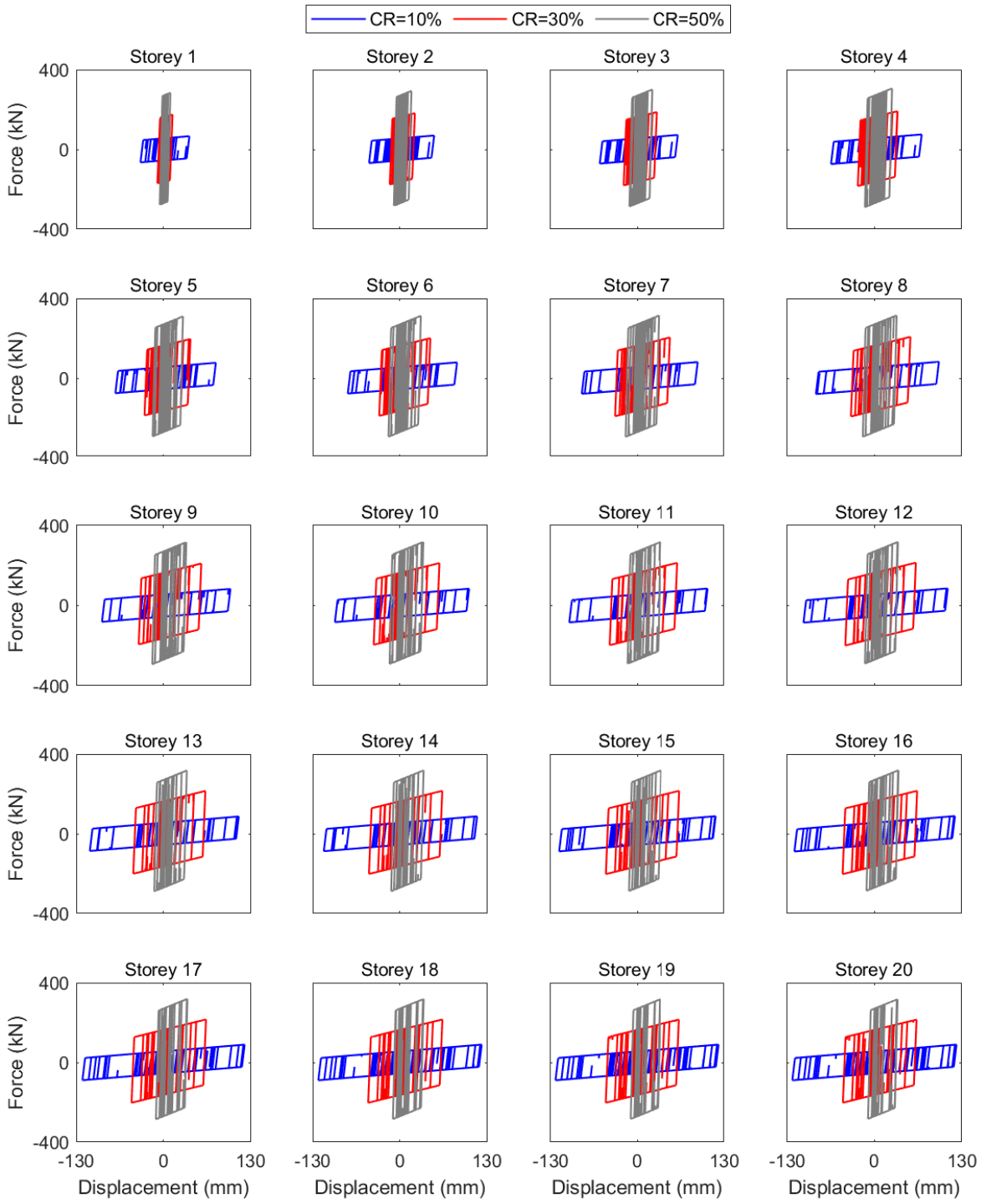

Figure 5.22: Coupling beam force-displacement curve for GM # 1 and R_d = 2 in the Y direction

Figures 5.22 and 5.23 illustrate that the hysteresis response for coupling beams in the symmetric (Y) direction for R_d = 2 and 3, respectively. As can be observed from the

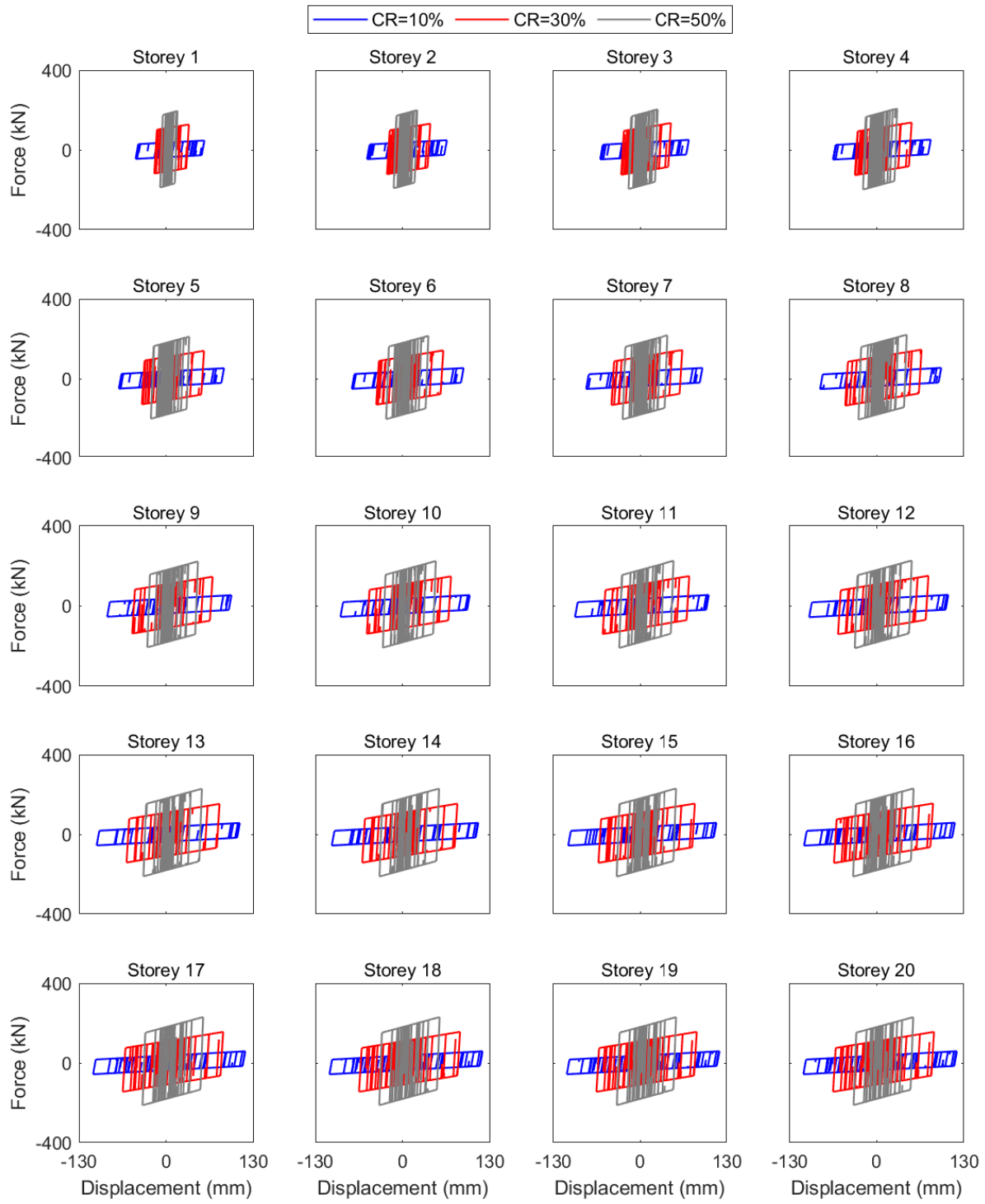

Figure 5.23: Coupling beam force-displacement curve for GM # 1 and R_d = 3 in the Y direction

figures, the response for the coupling beams designed with R_d = 3 is relatively higher than the corresponding response for the cases R_d = 2. The same reason as the hold-down response applies here, due to the fact that the provided strength for the coupling beam decrease with the increase in the ductility factors, R_d. Moreover, as the induced

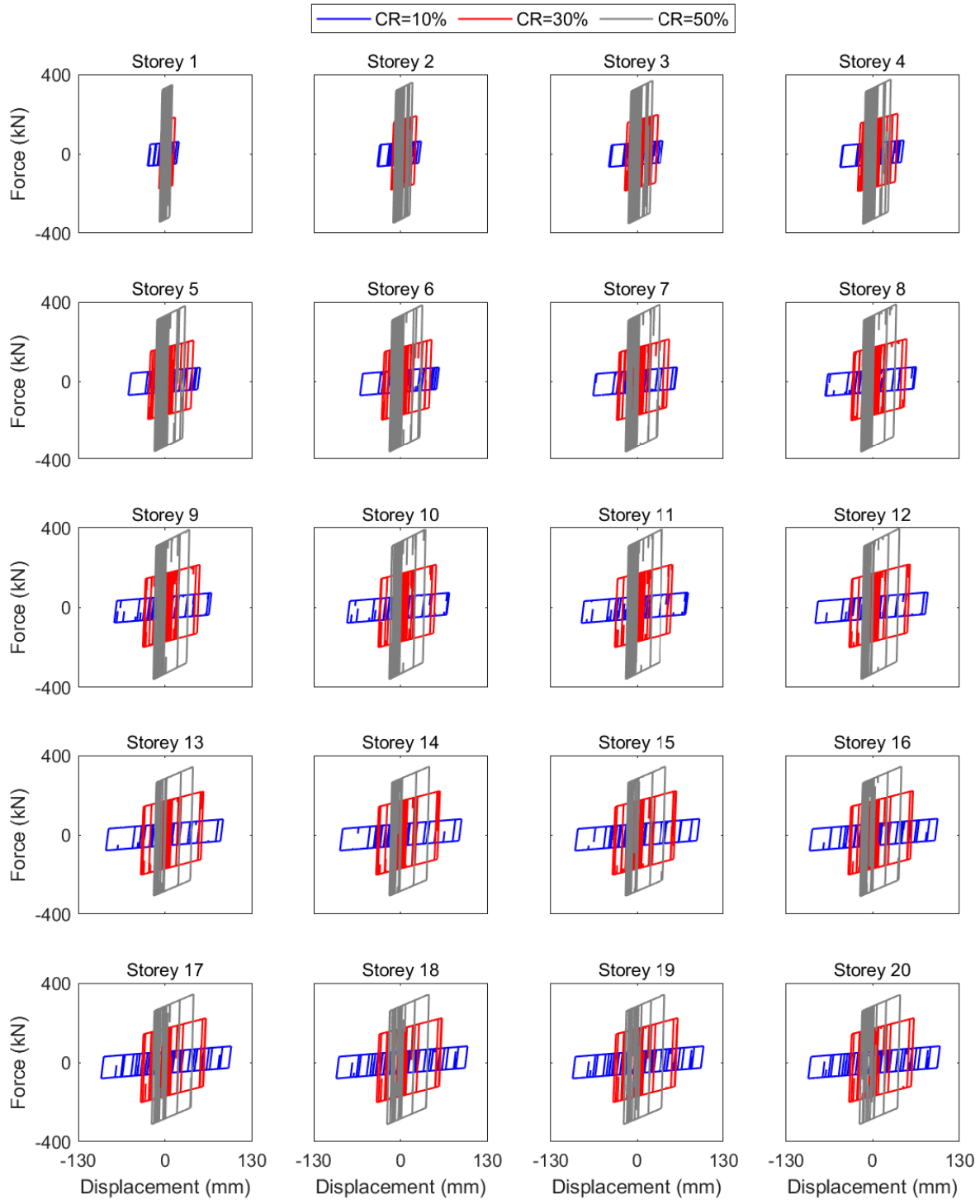

Figure 5.24: 20 storey coupling beam force-displacement curve for GM # 3 and R_d = 2 in the X direction

shear force in the coupling beam increases with the increase in the values of CR, the hysteresis response of the coupling beams decreases with the increase in the value of CR from 10% to 50%. Same conclusion can be made from Figures 5.24 and 5.25 that illustrate that the hysteresis response of coupling beams in the asymmetric (X)

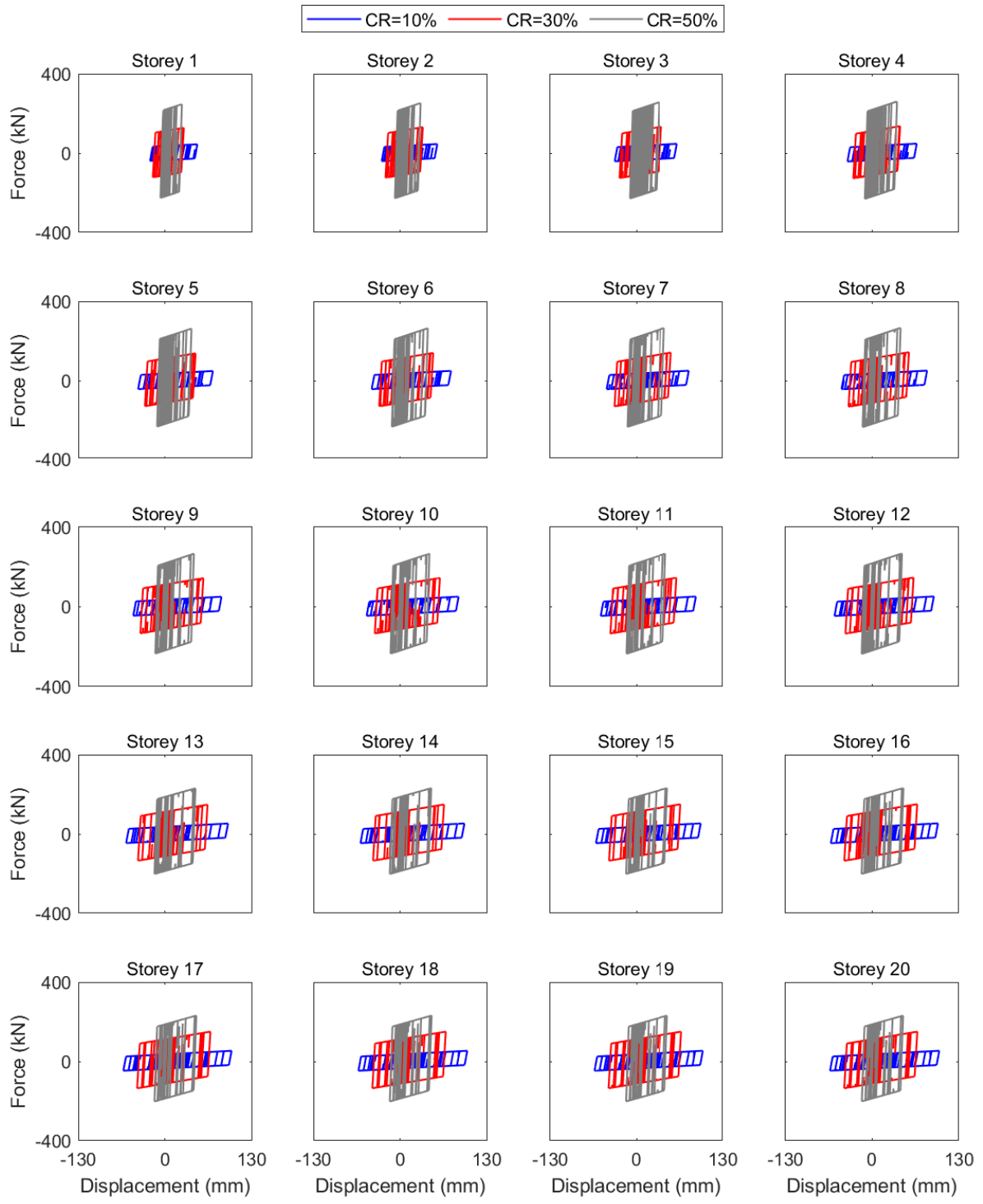

Figure 5.25: 20 storey coupling beam force-displacement curve for GM # 3 and R_d = 3 in the X direction

direction for R_d = 2 and 3, respectively.

Chapter 6

Over-strength and Ductility Modification Factors

The National Earthquake Hazards Reduction Program (FEMA, 2003) and NBC (2015) has defined seismic reduction factor as the factor that reduce the elastic design load of structures. This factor, first introduced in ATC-3-06 (ATC 1978) in late 1970s, accounts for both damping and ductility inherent in a structural system (Whittaker et al., 1999). As elastic lateral force analysis method is the cornerstone of seismic design practice, the need to estimate strength reduction factor for new and innovative lateral load resisting systems is important. For new structure, the FEMA P695 (2009) report provides a guideline to quantify an over-strength factor (Ω_o) and response modification factor (R). In fact, the NBC (2015) splits the response modification factor into over-strength factor (R_o) and ductility factor (R_d). These seismic performance evaluation factors (R_o and R_d) can be determined by performing the collapse risk assessment using Incremental Dynamic Analysis (IDA) (Vamvatsikos and Cornell, 2002). Accordingly, in this chapter, the seismic modification factors that were used to design the CLT-CW systems are evaluated using the procedures outlined in FEMA P695 (2009).

6.1 FEMA P695 performance evaluation criteria

To verify the acceptability of the trial value of the response modification factor R_d, FEMA P695 suggests the use of IDA to obtain collapse fragility and collapse margin ratio (CMR). The collapse fragility curves are modelled as a log-normal distribution, and defined by the median collapse intensity ($\widehat{S}_{CT}$) and standard deviation of natural

logarithm (β_{RTR}). Moreover, FEMA P695 (2009) defined β_{RTR} to be a dispersion of IDA results due to the variability within GM records. Due its insignificance on the final CMR, FEMA P695 (2009) suggests a constant value of $\beta_{RTR} = 0.4$ for structures with period based ductility ($\mu > 3$). The collapse margin ratio CMR is computed as:

$$CMR = \frac{\widehat{S}_{CT}}{S_{MT}} \tag{6.1}$$

where S_{MT} = spectral acceleration value at the fundamental period of the archetype structure under consideration. Once the CMR of each archetype is calculated, FEMA P695 (2009) adjusts this value to Adjusted Collapse Margin Ratio ($ACMR$) to account for the Spectral Shape Factor (SSF):

$$ACMR = SSF_i \times CMR_i \tag{6.2}$$

In this report, the GMs were selected and scaled for each archetype model based on their spectral acceleration values at the fundamental period of the considered archetype building. Therefore, SSF was set to 1, i.e. $ACMR_i = CMR_i$. In order to accurately calculate the safety against collapse, FEMA P695 (2009) considers more sources of uncertainties. The following set of bullets describes the considered system uncertainties.

- Design requirement uncertainty (DR): according to FEMA P695 (2009), this type of uncertainty is related to the robustness and completeness of design requirements of the archetype buildings. Table 6.1 summarizes quantitative the factors to consider to quantify the uncertainty as the log-normal standard deviation parameter (β_{DR}). This is assessment done qualitatively, based on completeness of the information and confidence in the basis of design requirement.

- Test data uncertainty (TD): uncertainty related to the quality of test data to calibrate and model the archetype buildings. Table 6.2 summarizes quantitative values of this uncertainty, as the log-normal standard deviation parameter (β_{TD}), based on the rating of quality of the test data. Table 6.2: Quality rating of test data from an experimental investigation program (FEMA, 2009).

- Modeling uncertainty (MDL): uncertainty related to the accuracy, robustness

Table 6.1: Quality rating of design requirements (FEMA, 2009).

Completeness and Robustness	Confidence in Basis of Design Requirements		
	High	Medium	Low
High: Extensive safeguards against unanticipated failure modes. All important design and quality assurance issues are addressed.	(A) Superior $\beta_{DR} = 0.1$	(B) Good $\beta_{DR} = 0.2$	(C) Fair $\beta_{DR} = 0.35$
Medium: Reasonable safeguards against unanticipated failure modes. Most of the important design and quality assurance issues are addressed.	(B) Good $\beta_{DR} = 0.2$	(C) Fair $\beta_{DR} = 0.35$	(D) Poor $\beta_{DR} = 0.5$
Low: Questionable safeguards against unanticipated failure modes. Many important design and quality assurance issues are not addressed.	(C) Fair $\beta_{DR} = 0.35$	(B) Poor $\beta_{DR} = 0.5$	-

Table 6.2: Quality rating of test data from an experimental investigation program (FEMA, 2009).

Completeness and Robustness	Confidence in Test Results		
	High	Medium	Low
High: Material, component, connection, assembly, and system behaviour well understood and accounted for all, or nearly all, important testing issues addressed.	(A) Superior $\beta_{TD} = 0.1$	(B) Good $\beta_{TD} = 0.2$	(C) Fair $\beta_{TD} = 0.35$
Medium: Material, component, connection, assembly, and system behaviour generally understood and accounted for most important testing issues addressed.	(B) Good $\beta_{TD} = 0.2$	(C) Fair $\beta_{TD} = 0.35$	(D) Poor $\beta_{TD} = 0.5$
Low: Material, component, connection, assembly, and system behaviour fairly understood and accounted for Several important testing issues not addressed.	(C) Fair $\beta_{TD} = 0.35$	(B) Poor $\beta_{TD} = 0.5$	-

and quality of the numerical models to capture seismic response and simulate the collapse mechanism of archetype buildings. Table 6.3 summarizes quantitative values of this uncertainty based on the rating of quality of the proposed numerical models as the log-normal standard deviation parameter (β_{MDL}). More information can be obtained from FEMA P695 (2009).

Based on the above sources of uncertainties, the total uncertainty for the performance evaluation process is obtained by combining RTR, DR, TD, and MDL. This total uncertainty is used to modify the interim fragility curves of each archetype building. The new collapse fragility curve is defined by a random variable (S_{CT}) as:

Table 6.3: Quality rating of index archetype models (FEMA, 2009).

Completeness and Robustness	Confidence in Modeling		
	High	Medium	Low
High: Index models capture the full range of the archetype design space and structural behavioral effects that contribute to collapse.	(A) Superior $\beta_{MDL} = 0.1$	(B) Good $\beta_{MDL} = 0.2$	(C) Fair $\beta_{MDL} = 0.35$
Medium: Index models are generally comprehensive and representative of the design space and behavioral effects that contribute to collapse.	(B) Good $\beta_{MDL} = 0.2$	(C) Fair $\beta_{MDL} = 0.35$	(D) Poor $\beta_{MDL} = 0.5$
Low: Significant aspects of the design space and/or collapse behaviour are not captured in the index models.	(C) Fair $\beta_{MDL} = 0.35$	(B) Poor $\beta_{MLR} = 0.5$	-

$$S_{CT} = \widehat{S}_{CT} \times \lambda_{TOT} \tag{6.3}$$

where S_CT = median collapse intensity from IDA and λ_{TOT} is the log-normally distributed random variable with a unit median and standard deviation of β_{TOT}. The λ_{TOT} is computed as (FEMA, 2009):

$$\lambda_{TOT} = \lambda_{RTR}\, \lambda_{DR}\, \lambda_{TD}\, \lambda_{MDL} \tag{6.4}$$

where λ_{RTR}, λ_{DR}, $\lambda_{TD,}$ λ_{MDL} are independent log-normal distributed random variables with medians of unity and standard deviation of RTR, DR, TD, MDL, respectively. At this point, it is to be noted that the above four random variables are statically independent (their joint probability distribution is the product of their marginal distribution), and the total collapse uncertainty parameter (β_{TOT}) can be calculated as (FEMA, 2009):

$$\beta_{TOT} = \sqrt{\beta_{RTR}^2 \times \beta_{DR}^2 \times \beta_{TD}^2 \times \beta_{MDL}^2} \tag{6.5}$$

For record-to-record uncertainty $\beta_{RTR} = 0.4$, FEMA P695 (2009) summarizes the values of β_{TOT}. Acceptable values of adjusted collapse margin ratio of each archetype buildings can be calculated based on the assumption that the collapse value of spectral intensity is a log-normal distributed random variable. This distribution has a median of S_{CT} and log-normal standard deviation of β_{TOT}. By considering β_{TOT} and

acceptable collapse probability as 10% and 20%, Table 8.4 summarizes the $ACMR_{10\%}$ and $ACMR_{20\%}$.

FEMA P695 (2009) proposed acceptability criteria to verify the adequacy of initially assumed force reduction factors is based on $ACMR_{10\%}$ and $ACMR_{20\%}$. The assumed R_d factors will be accepted if the calculated $ACMR$ ratios within the performance group and individually fulfill the following criterion:

- The calculated Average Adjusted Collapsed Margin Ratio ($\overline{ACMR}$) within the defined performance group is greater than $ACMR_{10\%}$.

$$\overline{ACMR} > ACMR_{10\%} \tag{6.6}$$

- The calculated individual Adjusted Collapsed Margin Ratio ($ACMR_i$) of each archetype building is greater than $ACMR_{20\%}$.

$$ACMR_i > ACMR_{20\%} \tag{6.7}$$

Evaluation of the over-strength factor was carried out based on the following recommendations from FEMA P695 (2009):

- The system over-strength factor should be greater than the calculated largest average value of over-strength among the considered performance groups.
- Maximum allowable over-strength factor of 3 is recommended in ASCE/SEI 7-05 due to practical design considerations.
- In NBC (2015), the maximum allowable over-strength factor is $R_o = 1.7$. For this study, following NBC (2015), the over-strength factor is set to 1.5.

6.2 Performance assessment of the proposed R_d factors using IDA

IDA (Vamvatsikos and Cornell, 2002) was used to compute the collapse risk. FEMA P695 (2009) suggests first to select the GMs for a 2% in 50 years uniform hazard spectrum. Subsequently dynamic analyses have been carried out by scaling the GM records up to the collapse spectral acceleration.

Table 6.4: Acceptable Values of Adjusted Collapse Margin Ratio ($ACMR_{10\%}$ and $ACMR_{20\%}$) (FEMA, 2009).

Total System Collapse Uncertainty	Collapse probability				
	5%	10%	15%	20%	25%
0.275	1.57	1.42	1.33	1.26	1.20
0.300	1.64	1.47	1.36	1.29	1.22
0.325	1.71	1.52	1.40	1.31	1.25
0.350	1.78	1.57	1.44	1.34	1.27
0.375	1.85	1.62	1.48	1.37	1.29
0.400	1.93	1.67	1.51	1.40	1.31
0.425	2.01	1.72	1.55	1.43	1.33
0.450	2.10	1.78	1.59	1.46	1.35
0.475	2.18	1.84	1.64	1.49	1.38
0.500	2.28	1.90	1.68	1.52	1.40
0.525	2.37	1.96	1.72	1.56	1.42
0.550	2.47	2.02	1.77	1.59	1.45
0.575	2.57	2.09	1.81	1.62	1.47
0.600	2.68	2.16	1.86	1.66	1.50
0.625	2.80	2.23	1.91	1.69	1.52
0.650	2.91	2.30	1.96	1.73	1.55
0.675	3.04	2.38	2.01	1.76	1.58
0.700	3.16	2.45	2.07	1.80	1.60
0.725	3.30	2.53	2.12	1.84	1.63
0.750	3.43	2.61	2.18	1.88	1.66
0.775	3.58	2.70	2.23	1.92	1.69
0.800	3.73	2.79	2.29	1.96	1.72
0.825	3.88	2.88	2.35	2.00	1.74
0.850	4.05	2.97	2.41	2.04	1.77
0.875	4.22	3.07	2.48	2.09	1.80
0.900	4.39	3.17	2.54	2.13	1.83
0.925	4.58	3.27	2.61	2.18	1.87
0.950	4.77	3.38	2.68	2.22	1.90

IDA results

Based on a preliminary assessment, the GMs were scaled up until a spectral acceleration value triggered the collapse of the building ($MaxISDR = 5\%$). In order to compute the collapse fragility curves and adjusted collapse margin ratio, the IDA was

performed using OpenSees software (Mazzoni et al., 2006).

In order to assess the median and the standard deviation of the collapse intensity and to approximate the fragility curve, the full IDA simulation was carried to get the collapse intensity values of all GMs. Figures 6.1 and 6.2 illustrate the IDA curves for the 15 cases reported in the previous chapter. The horizontal axis represents the maximum inter-story drift ratio ($MaxISDR$). The vertical axis gives the intensity measure which is defined as the spectral acceleration at the fundamental period of the building. The IDA results shown in Figures 6.1 and 6.2 are then used to obtain the collapse fragility curves, and are discussed in the next section.

Total system uncertainty

The total uncertainty (β_{TOT}) is determined with consideration of $\beta_{RTR},\ \beta_{DR},\ \beta_{MDL},$ and β_{TD}. Given its insignificant effect on the final $ACMR$ value, FEMA P695 sets $\beta_{RTR} = 0.4$. The design requirement uncertainty (β_{DR}) was determined to be fair (Table 6.1) with $\beta_{DR} = 0.35$. For this selection the confidence in the bases of design requirement is considered as medium. Moreover, considering CLT as a new construction material and the complexity in characterizing the structural behavior of wood, the completeness and robustness in the design method for this hybrid building was tagged as medium. Since the experimental tests on this hybrid structure are limited to its component level, the uncertainty related to test data was selected as fair (Table 6.2) with $\beta_{TD} = 0.35$. Uncertainty related to modeling was selected to be fair (Table 6.3) with $\beta_{MDL} = 0.35$. Finally, based on these selected values, the $\beta_{TOT} = 0.75$ is computed using Eq. 6.5.

Collapse fragility curves

The fragility curves reflect the probability of collapse of the hybrid buildings. These curves are cumulative distribution functions (CDF) developed by fitting a log-normal distribution through collapse intensity values for all GMs. The probability of these collapse points was determined by dividing the number of GM records that initiated the collapse of building to the total number of GM records. Median collapse intensity values and standard deviation of the collapse data were used as an input to define the CDF. The fragility curve was developed by the actual obtained log-normal standard deviation of collapse data points, and the "adjusted curve" was developed with the same

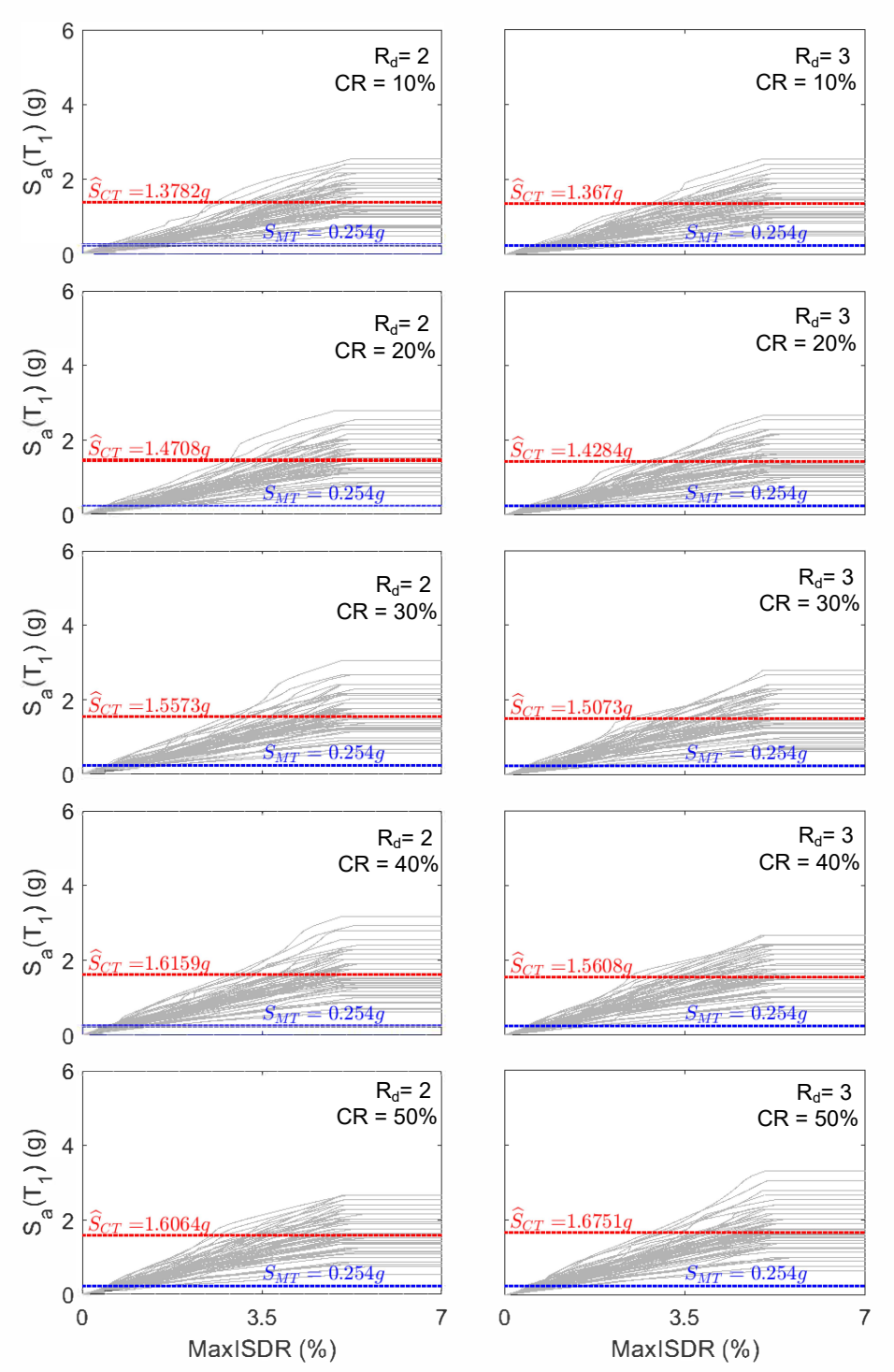

Figure 6.1: IDA curves for 20 storey CLT-CW system in the Y direction

median but a standard deviation of $\beta_{TOT} = 0.75$. For the considered cases, the collapse fragility curves are depicted in Figures 6.3 and 6.4.

FEMA P695 (2009) proposed acceptability criteria to verify the adequacy of initially assumed force reduction factors based on $ACMR_{10\%}$ and $ACMR_{20\%}$. The assumed R_d factors are accepted if the calculated $ACMR$ ratios were within the performance

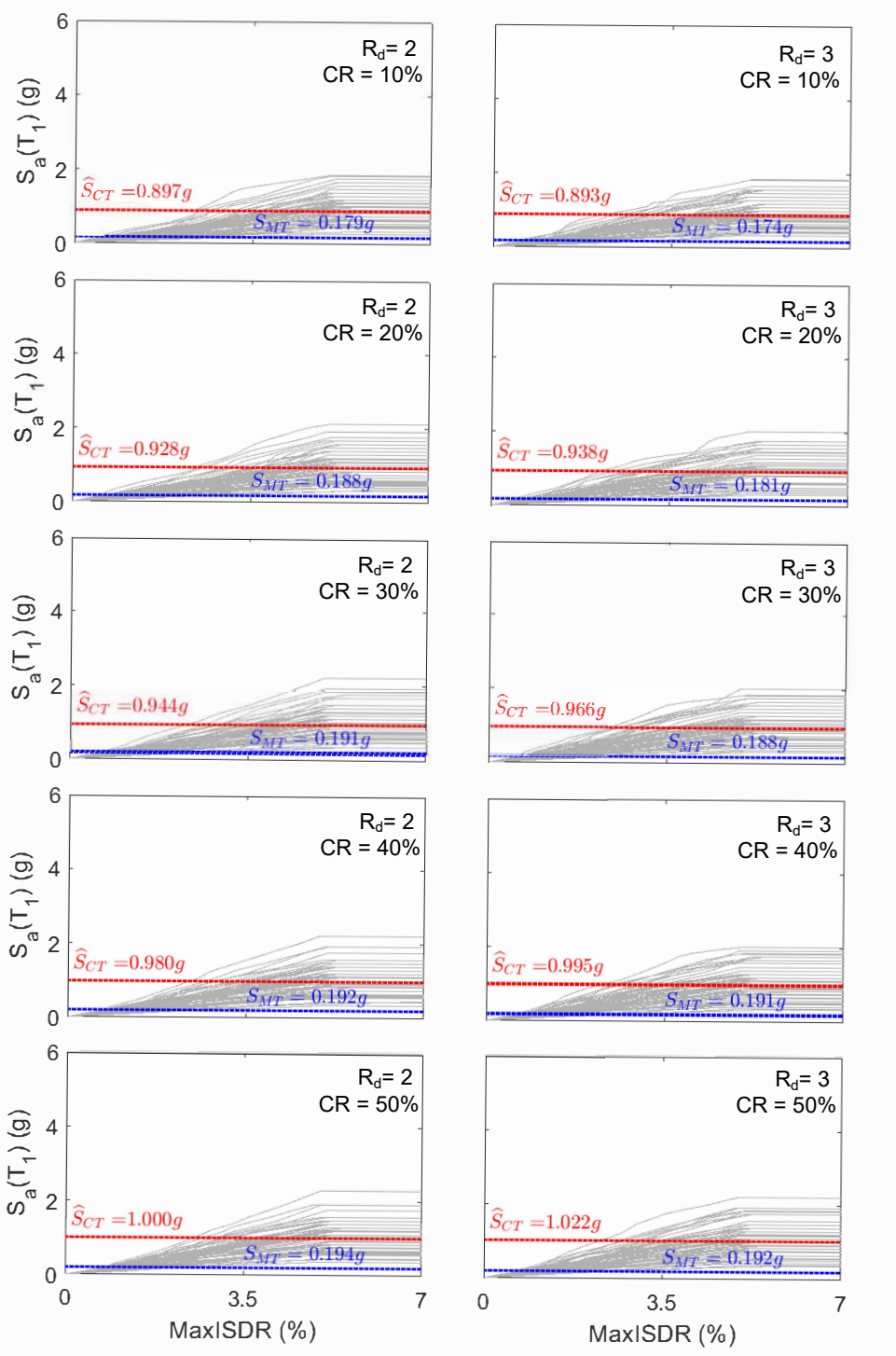

Figure 6.2: IDA curves for 20 storey CLT-CW system in the X direction

group and individually exceeded the values in Table 6.4. Accordingly, the proposed R_d factor are accepted if the calculated average $ACMR$ values within the performance group ($ACMR_{10\%}$) exceeds 2.61. Moreover, for individual criteria, the proposed factors were acceptable if the calculated $ACMR$ value ($ACMR_{20\%}$) exceeds 1.88. Since there exist one archetype per performance group, the $ACMR_{10\%} = 2.61$ was used for each

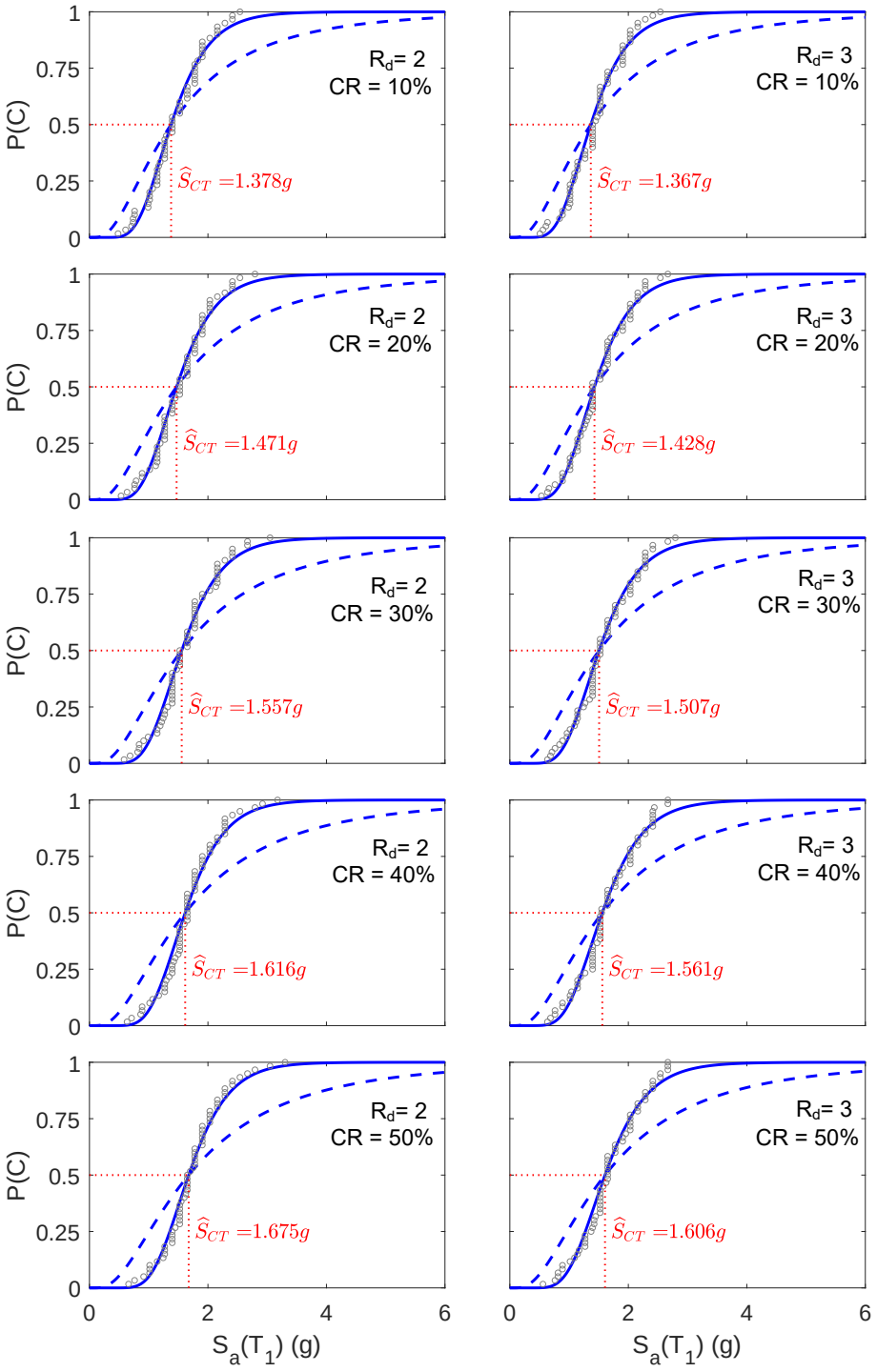

Figure 6.3: Collapse fragility curves for 20 storey CLT-CW system in the Y direction

archetype conservatively.

The ACMR results are summarized in Figures 6.5 to 6.7. From Table 6.4, for all the considered cases, the R_d values of 2 and 3 satisfies the $ACMR_{10\%} > 2.61$ criterion. As a result, they are selected as the appropriate R_d factors.

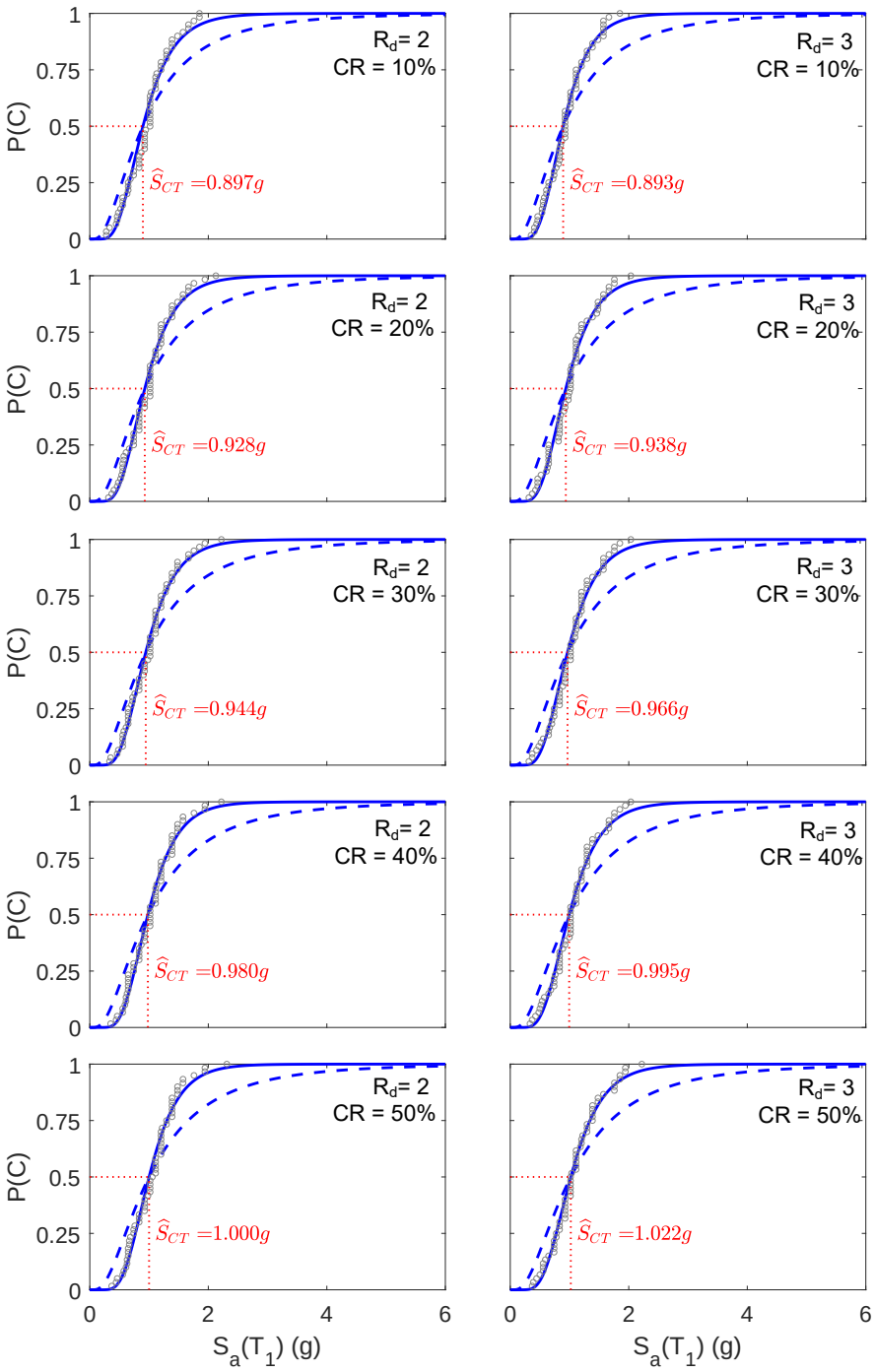

Figure 6.4: Collapse fragility curves for 20 storey CLT-CW system in the X direction

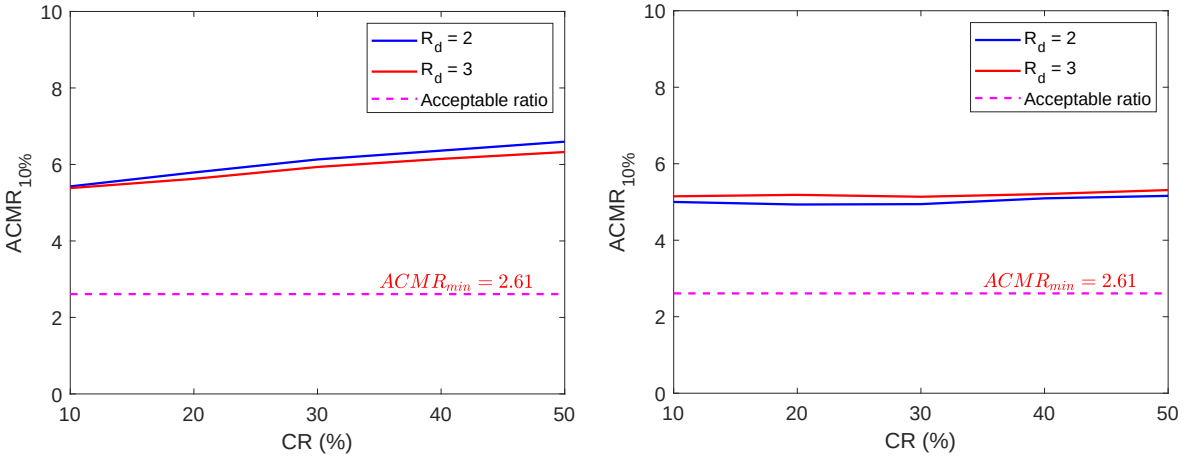

(a) Y direction (b) X direction

Figure 6.5: FEMA P695 acceptability evaluation for 20 Storey CLT-CW system.

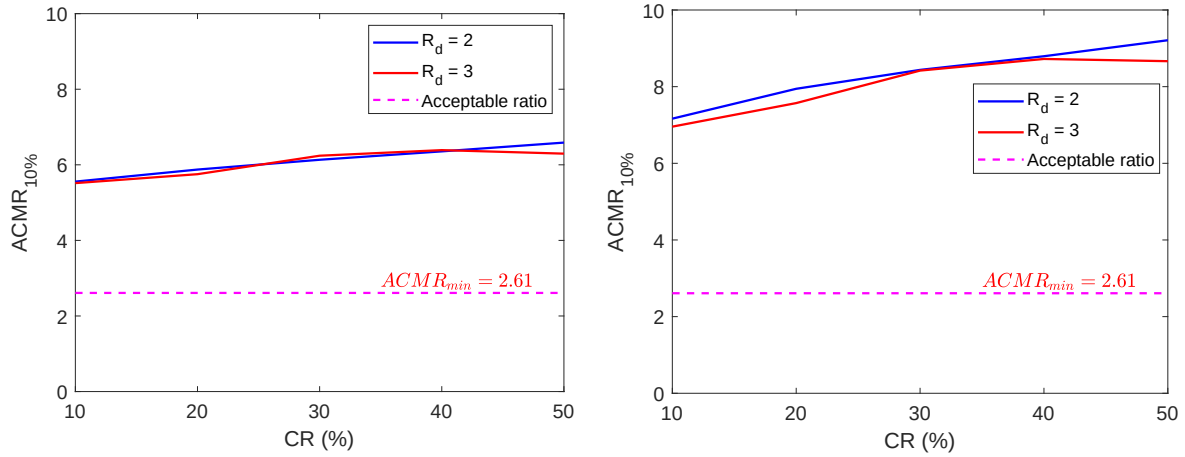

(a) Y direction (b) X direction

Figure 6.6: FEMA P695 acceptability evaluation for 15 Storey CLT-CW system.

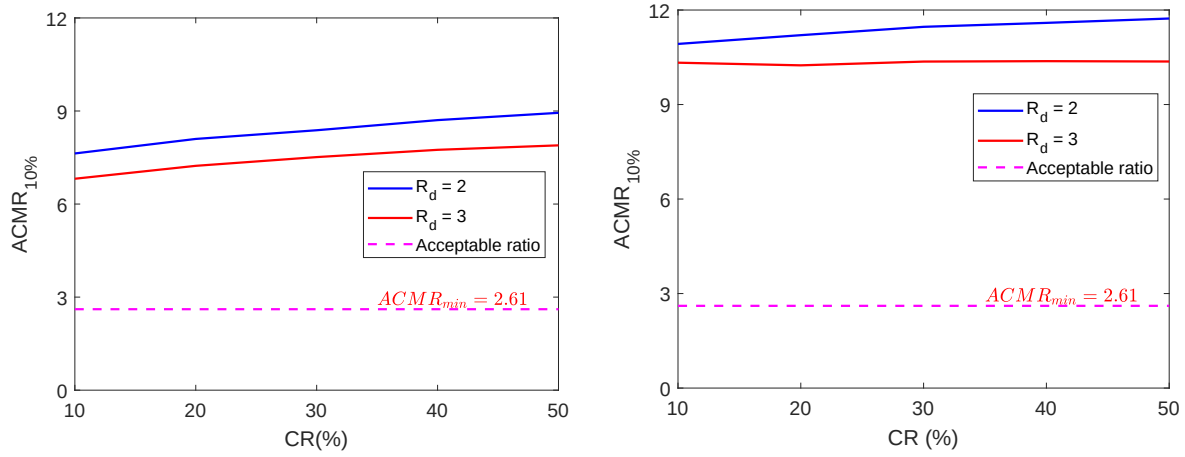

(a) Y direction (b) X direction

Figure 6.7: FEMA P695 acceptability evaluation for 10 Storey CLT-CW system.

Chapter 7

Performance Based Design

The HCW system's performance based design (PBD) procedure outlined in El-Tawil et al. (2010) is used to design the CLT-CW system. FEMA-356 (2000) recommends four analysis procedure types: ELFA, linear dynamic, pushover, and NLTHA. In this report, ELFA and NLTHA are used to determine the initial seismic force parameters and perform the nonlinear performance of the structure, respectively. A CMM is applied to determine the preliminary CLT-CW geometry parameter, and calculate the seismic design forces along the ELFA. The performance of the designed CLT-CW elements are then evaluated using NLTHA under the action of selected GMs.

7.1 Design considerations

The first step in the PBD is to select the desired performance objectives for a given seismic hazard level. The performance objectives can be specified in terms of structural and non-structural damage limit states (e.g. displacement-limit objectives, selection of yield mechanisms), constructability, and post-earthquake repairability (i.e. resiliency) (e.g. (Harries et al., 2004; Harries and McNeice, 2006; Hull and Harries, 2008)). The performance objectives for a different building type may different from one another. For example the key performance objective for conventional CW is to have a contractible coupling beam (Harries and McNeice, 2006).

The North American building code, for example, provides four earthquake design performance limit states. Table 7.1 summarizes the four recommended performance objective levels with their detail description: immediate occupancy (IO), life safety (LS)

and collapse prevention (CP). Harries and McNeice (2006) recommended the three performance objectives (CP, LS and IO) for designing HCW systems (El-Tawil et al., 2010). Accordingly, the performance objective levels used in this report are the two severe performance level conditions (CP and LS). The corresponding drift limits for the selected performance objectives are 2.5% and 1.5%, respectively.

Earthquake design level (Probability of exceedance)	Performance limit states			
	Immediate Occupancy (IO)	Damage Control (DC)	Life Safety (LS)	Collapse Prevention (CP)
Frequent (50% PE in 30 years)	■	×	×	×
Occasional (50% PE in 50 years)	◆	■	×	×
Rare (10% PE in 50 years)	◇	◆	■	×
Very rare (2% PE in 50 years)		◇	◆	■

Legend:
■: Basic Objective – Proposed NBCC Normal Importance
◆: Essential Service Objective - Proposed NBCC High Importance
◇: Safety Critical Objective – No Proposed NBCC Category
×: Unacceptable Performance for New Construction

Figure 7.1: Recommended performance objectives (DeVall, 2003)

7.2 PBD framework

The proposed PBD framework with a 9-step procedure is provided in Figure 7.2. A numerical example is provided for the parametric study reported in Table 7.1 for $R_o R_d = 3$ and $CR = 30\%$.

Step 1. Construct the normalized roof displacement curve

Figure 7.3 shows the plot of roof deflection determined from an elastic analysis (normalized to that of a pair of uncoupled wall piers, F_3) against elastic CR (Harries et al., 2004). The parameters CR and F_3 are closed-form solutions derived from CMM and are provided in Chapter 4, equations 4.6 and 4.12, respectively.

Step 2. Select target drift ratio limit and CR values

Based on the performance level targeted to be achieved, 2.5% is selected as a drift ratio limit ($\frac{y_H}{H}$) and CR = 30% is used to illustrate the procedure. For the selected values of

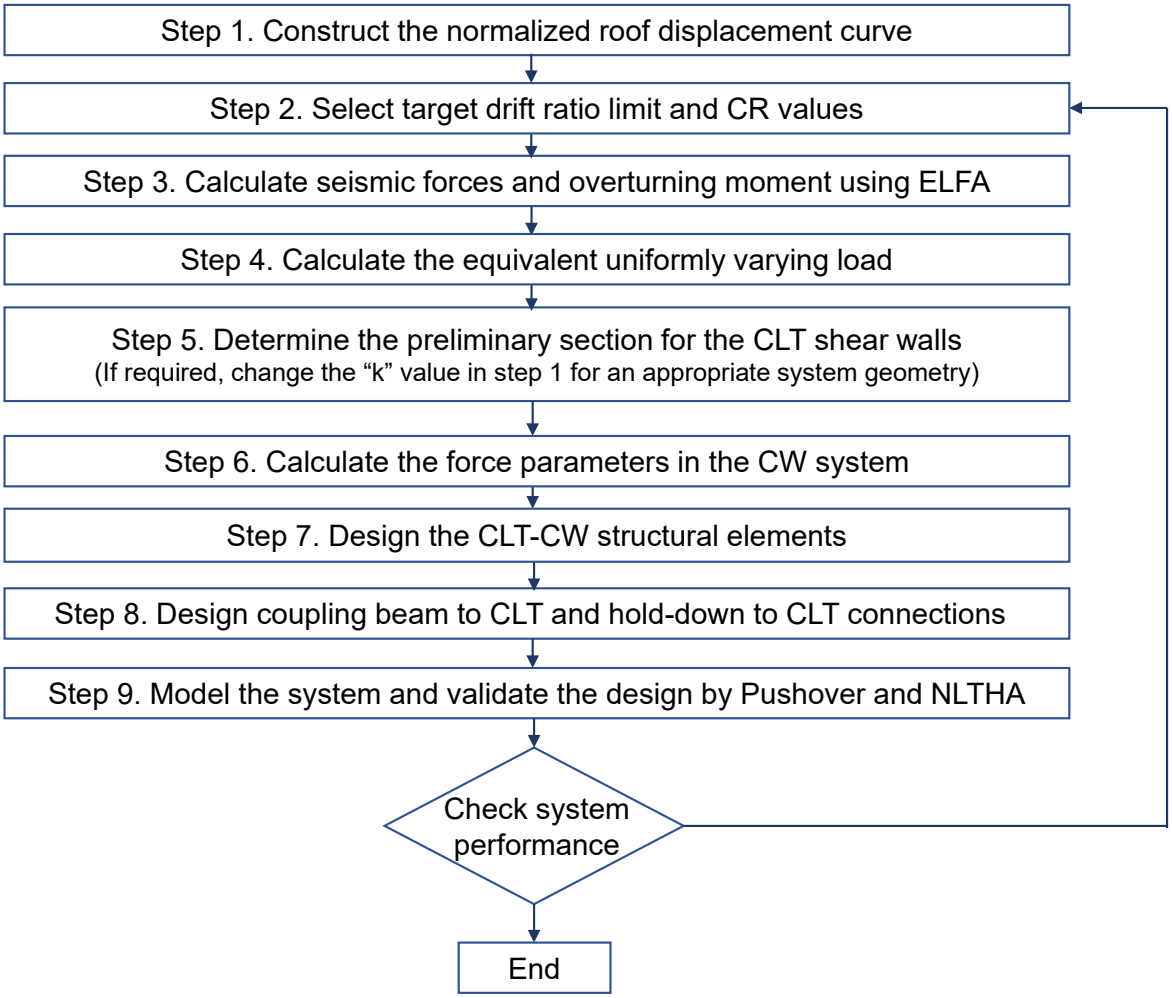

Figure 7.2: Proposed PBD procedure for CLT-CW system

k (step 1) and CR, the corresponding value of F_3 is read from the curve plotted in Step 1 and its value is 0.586, and the corresponding value of $k\alpha H$ will be: $k\alpha H = 1.751$.

Step 3. Calculate seismic forces and overturning moment using ELFA

The total lateral seismic force (V), and the design base shear (F_x) and overturning moment at each storey level (M_x) can be calculated using equations 4.13, 4.15, and 4.17. For the numerical examples considered; the ELFA parameters and the calculated seismic forces and overturning moment are given in Tables 7.2 and 7.3.

Step 4. Calculate the equivalent uniformly varying load

Equation 4.18 can be used to calculate the equivalent triangular lateral load, P, for the lateral seismic forces, obtained in Step 3. Table 7.4 illustrates the procedure and Figure shows the distribution of the seismic force from the ELFA and the corresponding equivalent triangular lateral load.

Table 7.1: Natural periods of the structure under different $R_o R_d$ and CR values.

No.	$R_o R_d$	CR (%)	$L_1 = L_2$ (m)	L_b (m)	$(EI)_{eff}$ (10^9 Nm^2)	T_1 (s)	T_2 (s)	T_3 (s)
1	3	10	4.00	1.25	27.55	3.749	0.847	0.358
2	3	20	3.75	1.25	22.70	3.761	0.820	0.352
3	3	30	3.50	1.25	18.46	3.939	0.823	0.354
4	3	40	3.25	1.25	14.78	4.215	0.848	0.363
5	3	50	3.00	1.25	11.62	4.566	0.887	0.375
6	4.5	10	3.50	1.25	18.46	4.581	1.037	0.432
7	4.5	20	3.25	1.25	14.78	4.555	1.003	0.428
8	4.5	30	3.00	1.25	11.62	4.788	1.011	0.433
9	4.5	40	2.75	1.25	8.95	5.160	1.044	0.446
10	4.5	50	2.50	1.25	6.73	5.659	1.102	0.465

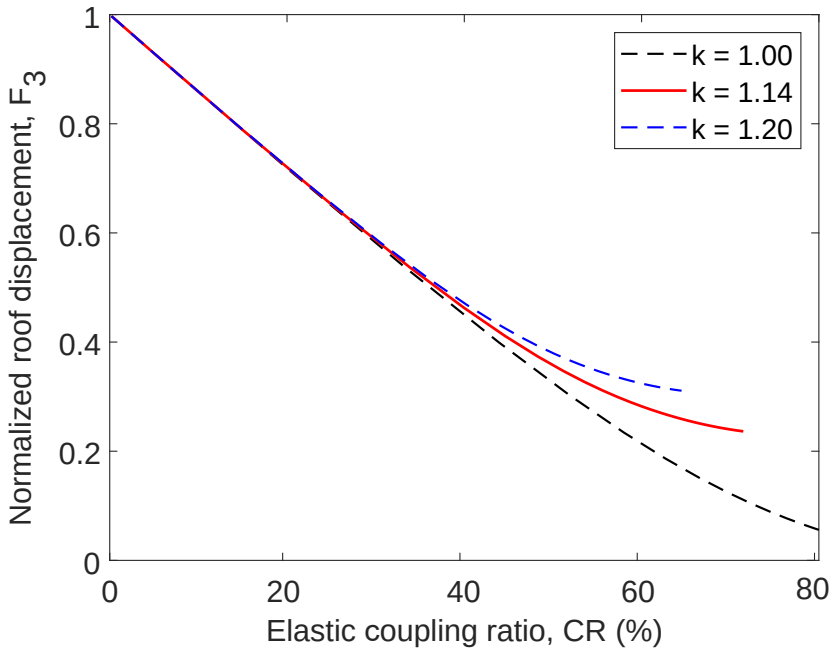

Figure 7.3: Normalized roof displacement curve

Step 5. Determine the preliminary section for the CLT shear walls

The required geometry of the CLT shear wall panels is determined from the targeted roof drift ratio considering the modified deflection equation given by (Smith and Coull, 1991):

Table 7.2: Equivalent lateral force analysis parameters.

T_a	: 3.95 sec
$S(T_a)$	: 0.141
M_v	: 1
I_E	: 1
J_x	: 0.894
$R_o R_d$	: 3
n (number of storeys)	: 20
h_x (height at storey x)	: 3 m
H (total height)	: 60 m
w_x (weight at each storey x)	: 1,100 kN
W (total weight)	: 22,000 kN
F_t	: 259.26 kN
V (total base shear)	: 1,037.04 kN

$$\frac{y_H}{H} = \frac{11PH^3}{120\ \mathbf{EI}} F_3\,(k\alpha H) \tag{7.1}$$

For drift ratio limit, $\frac{y_H}{H} = 0.025$, $P = 34.65\ kN/m$ (calculated from step 4), $H = 60\ m$, and $F_3 = 0.586$ (calculated in step 2); the required effective flexural stiffness, $EI = (EI)_{eff}$, can be determined from equation 7.1 and its value is $15.97E9\ Nm^2$. Considering the contribution of both the longitudinal and transverse CLT layers in the flexural stiffness, the equivalent stiffness, I_{eff}, can be determined from equation 7.2.

$$I_{eff} = \frac{(EI)_{eff}}{E_0} \tag{7.2}$$

For 7-ply CLT Grade E1 panel ($t = 35\ mm$, $E_0 = 11.7\ GPa$, and $E_{90} = 9\ GPa$), the required length of the CLT wall piers is calculated to be $L_1 = L_2 = 3.34\ m \approx 3.50\ m$ (Equation 7.3).

Table 7.3: Base shear and Overturning moment distributions.

Storey, n	Height, H (m)	$w_x h_x$ (kNm)	F_x (kN)	V_x (kN)	J_x	M_x (kNm)
20	60	65,846	332	0	1	0
19	57	62,601	70	332	1	997
18	54	59,356	66	402	1	2,203
17	51	56,111	62	468	1	3,606
16	48	52,866	59	530	1	5,197
15	45	49,621	55	589	1	6,963
14	42	46,376	52	644	1	8,895
13	39	43,131	48	695	1	10,981
12	36	39,886	44	743	1	13,212
11	33	36,641	41	788	1	15,451
10	30	33,396	37	828	0.98	17,760
9	27	30,151	33	865	0.97	20,133
8	24	26,906	30	899	0.97	22,559
7	22	23,661	26	929	0.96	25,024
6	19	20,416	23	955	0.95	27,515
5	16	17,171	19	978	0.94	30,020
4	13	13,926	15	997	0.93	32,527
3	10	10,681	12	1,012	0.92	35,026
2	7	7,436	8	1,024	0.91	37,504
1	4	4,191	5	1,032	0.91	39,951

Table 7.4: Equivalent triangular lateral force.

V	: $1,037.04\ kN$
H	: $60\ m$
P (Load at the top storey)	: $2 \times \frac{V}{H} = 2 \times \frac{1{,}037.04}{60} = 34.65\ \frac{kN}{m}$

$$I_{eff} \cdot E_0 = \sum_{i=1}^{n} E_i \cdot t_i \cdot \frac{L_i^3}{12} + \sum_{i=1}^{n} E_i \cdot t_i \cdot L_i \cdot z_i^2 \tag{7.3}$$

The length of coupling beams can be proportioned from the relation defined in

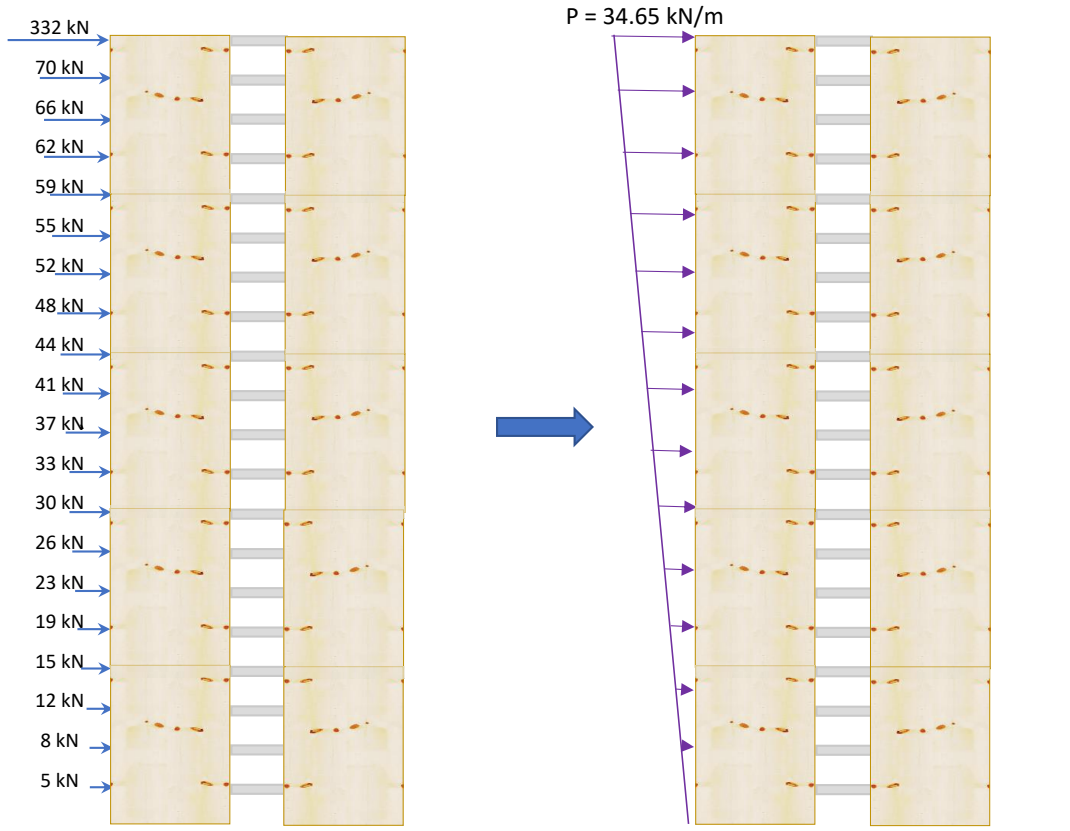

Figure 7.4: ELF and its Equivalent lateral load distribution

equation 4.4. For symmetrical CW system, where: $A_2 = A_1$ and $I = 2I_1$, its simplified form is given by:

$$k = \sqrt{1 + \frac{4\ I_1}{A_1\ L_w^2}} \tag{7.4}$$

Considering the effective axial stiffness of the CLT layers (longitudinal layers only, i.e. $A_1 = A_2 = 4t$), $k = 1.14$ (taken from step 1) and $L_1 = 3.5\ m$ (calculated above), the value of $L_w = 4.64\ m$ and from the relation $L_w = L_1 + L_b$ (for symmetrical system), L_b is calculated to be $1.14\ m \approx 1.25\ m$.

Step 6. Calculate the force parameters in the CW system

The axial load developed at each storey of wall piers (N_z) and shear flow on the continuous medium (q_z) are functions of stiffness parameter $(k\alpha H)$ and relative height parameter $(\frac{z}{H})$, and the closed-form solutions are given by equations 4.7 and 4.8, respectively. The shear force induced on each of the coupling beams (V_z in Figure 7.5)

can be calculated by integrating equation 4.8 over the building height, and is given by:

$$V_z = q_z h \tag{7.5}$$

Figures 7.5 (a) and (b) illustrate the distribution of cumulative axial load developed at each storey of wall piers and induced shear force on the coupling beams, respectively. Figure 7.5 (c) demonstrates the bending moment distribution due to seismic action (M_{max}), the moment converted into wall axial forces by the developed coupling action ($M_{coupling}$), and final or reduced moment on the wall piers ($M_{walls} = 2M_{wall}$ for symmetrical wall piers). Tables 7.5 and 7.6 demonstrate their quantitative values.

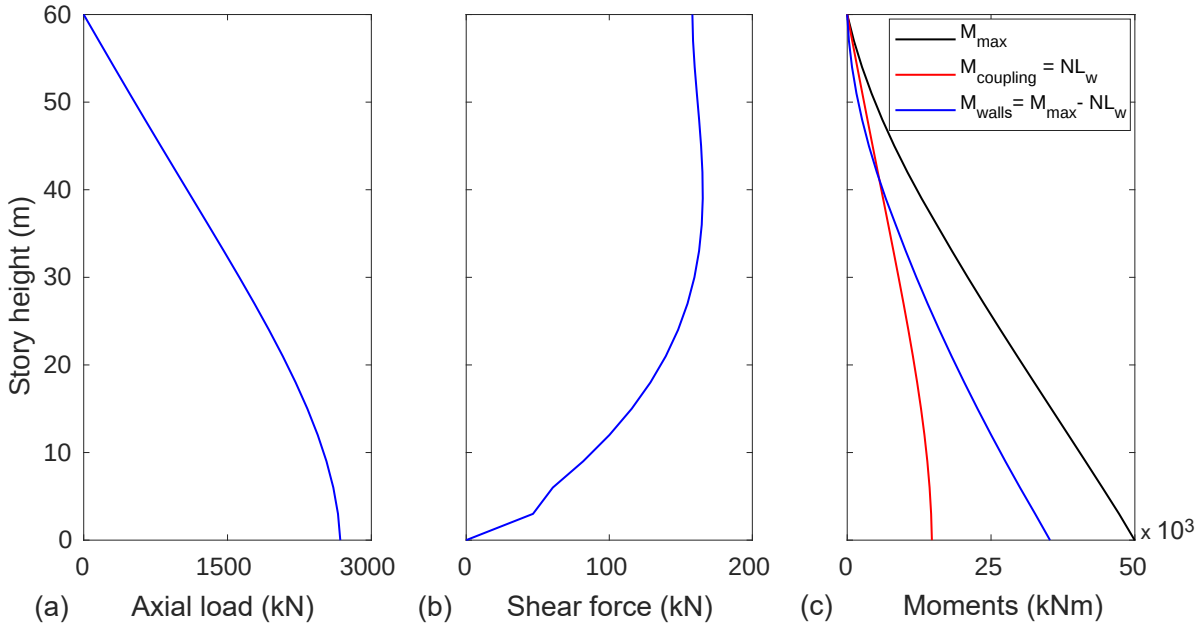

Figure 7.5: CW force parameters for R_d = 2 and CR = 30%: (a) Axial load (kN); (b) Shear force (kN); and (c) Moments (kNm).

Step 7. Design and check the strength of the CLT-CW structural elements

The forces developed on the coupling beams are shear force and end moment. As can be seen in Figure 7.5 (b), the shear induced in the coupling beams is not uniform. For an efficient design, CSA (2014), and Harries and McNeice (2006) recommend up to 20% vertical redistribution of shear forces between coupling beams. However, the total demand provided should not be less than the total required (El-Tawil et al., 2010; Harries and McNeice, 2006). Based on these recommendations, the design strength

Table 7.5: Summary for the distributions of drift, axial and shear forces.

n	z (m)	z/H	F_1	N (kN)	F_2	V (kN)	F_3	y (m)	DR (%)
20	60	1	0	0	0.178	368	0.322	1.342	2.24
19	57	0.95	0.009	370	0.18	374	0.322	1.039	1.83
18	54	0.9	0.019	750	0.187	388	0.322	0.793	1.47
17	51	0.85	0.028	1147	0.197	408	0.322	0.596	1.17
16	48	0.8	0.038	1567	0.209	433	0.322	0.44	0.92
15	45	0.75	0.049	2013	0.221	459	0.322	0.319	0.71
14	42	0.7	0.06	2485	0.234	485	0.322	0.226	0.54
13	39	0.65	0.072	2982	0.246	510	0.322	0.156	0.4
12	36	0.6	0.085	3504	0.257	533	0.322	0.105	0.29
11	33	0.55	0.098	4045	0.265	550	0.322	0.068	0.21
10	30	0.5	0.111	4601	0.271	562	0.322	0.042	0.14
9	27	0.45	0.125	5166	0.274	568	0.322	0.025	0.1
8	24	0.4	0.139	5733	0.272	564	0.322	0.014	0.06
7	21	0.35	0.152	6291	0.266	551	0.322	0.008	0.04
6	18	0.3	0.165	6830	0.254	526	0.322	0.004	0.02
5	15	0.25	0.177	7337	0.235	487	0.322	0.002	0.01
4	12	0.2	0.188	7798	0.209	433	0.322	0.001	0.01
3	9	0.15	0.198	8196	0.174	360	0.322	0.001	0.01
2	6	0.1	0.205	8511	0.129	266	0.322	0.001	0.01
1	3	0.05	0.21	8720	0.071	148	0.322	0.001	0.01
0	0	0	0.212	8796	-0.001	0	0.322	0	0

of the coupling beams (V_{des}) is provided as:

$$V_{des} = max\ (0.8\ V_{max},\ V_{ave}) \tag{7.6}$$

where V_{max} and V_{ave} = maximum and average shear forces, respectively. The values $0.8\ V_{max}$, V_{ave}, and V_{des} for the considered case are $129\ \ kN$, $135\ \ kN$, and $135\ \ kN$, respectively. The force parameters developed at the base of the CLT shear walls are concentrated in two points, the extreme ends of the wall, assuming the shear walls will

Table 7.6: CLT-CW system force parameters.

n	z (m)	N (kN)	M_{max} (kNm)	M_c (kNm)	M_w (kNm)
20	60	0	0	0	0
19	57	370	1255	1664	-205
18	54	750	2950	3374	-212
17	51	1147	5061	5162	-51
16	48	1567	7566	7051	258
15	45	2013	10442	9056	693
14	42	2485	13664	11179	1243
13	39	2982	17211	13418	1897
12	36	3504	21059	15764	2648
11	33	4045	24963	18200	3382
10	30	4601	29043	20704	4170
9	27	5166	33272	23247	5013
8	24	5733	37620	25795	5913
7	21	6291	42060	28306	6877
6	18	6830	46565	30732	7917
5	15	7337	51110	33015	9048
4	12	7798	55668	35090	10289
3	9	8196	60215	36880	11668
2	6	8511	64729	38297	13216
1	3	8720	69185	39237	14975
0	0	8796	73563	39580	16992

exhibit rocking action under the action of seismic load. Hence, the demand in the hold-down is calculated as the maximum design tensile force (F_{des}) developed in the base and is given by the static equilibrium equation:

$$F_{des} = \frac{M_{wall}}{L_1} + \frac{T}{2} = \frac{M_{wall}}{L_1} + \frac{\sum V_{z,i}}{2} \tag{7.7}$$

Step 8. Design coupling beam to CLT and hold-down to CLT connections

The detail calculation performed in this step is same as the one given in section 4.3 of this report. For a design force of $135\ kN$, Table 7.7 summarizes the design force and moment in the connection system.

Table 7.7: Shear, moment and resultant forces on coupling beam to CLT connections.

i	$x(mm)$	$x^2(mm^2)$	$y(m)$	$y^2(mm^2)$	$F_{v,i}$ (kN)	$F_{m,i}$ (kN)	θ	F_R (kN)
1	-135	18225	180	32400	50.96	8.44	126.87	46.39
2	-45	2025	180	32400	42.02	8.44	104.04	40.81
3	45	2025	180	32400	42.02	8.44	75.96	44.82
4	135	18225	180	32400	50.96	8.44	53.13	56.43
5	-135	18225	60	3600	33.46	8.44	156.04	25.98
6	-45	2025	60	3600	16.99	8.44	126.87	13.7
7	45	2025	60	3600	16.99	8.44	53.13	23.06
8	135	18225	60	3600	33.46	8.44	23.96	41.31
9	-135	18225	-60	3600	33.46	8.44	156.04	25.98
10	-45	2025	-60	3600	16.99	8.44	126.87	13.7
11	45	2025	-60	3600	16.99	8.44	53.13	23.06
12	135	18225	-60	3600	33.46	8.44	23.96	41.31
13	-135	18225	-180	32400	50.96	8.44	126.87	46.39
14	-45	2025	-180	32400	42.02	8.44	104.04	40.81
15	45	2025	-180	32400	42.02	8.44	75.96	44.82
16	135	18225	-180	32400	50.96	8.44	53.13	56.43

Same steel bolts with steel side plates, (Figure 4.6) is used in the design. The only difference with the design in section 4.3, is $25.4\ mm$ (1") diameter ASTM A307 bolt is used. The corresponding lateral strength resistance for modes of failure "a", "c", "d", and "g", are calculated (in terms of kN/ shear plane/ bolt) as 153.16, 43.87, 47.92, and 34.58 respectively. Mode failure "g" governs and the factored lateral strength resistance (N_r) for each bolt = $63.63\ kN$. Similarly, same bolt diameters and steel plate thicknesses are adopted for the connection in the hold-down, and for the design axial load of $4067\ kN$, a minimum of 64 bolts are required in the proposed rectangular arrangement of bolts (Figure 4.6 (b)). Welded connections are used to connect the steel plates with both the coupling beams and the BRB hold-downs.

Step 9. Model the system and validate the design through Pushover and

NLTHA

The proposed PBD method was validated by analyzing the CLT-CW system using pushover and NLTHA. The details are discussed in the next sections.

7.3 Result and discussion

7.3.1 Pushover analysis

Pushover analyses are carried out to evaluate the nonlinear response of the CLT-CW system. Incrementally increasing inverse-triangular loads, distributed along the height of the structure, are applied to continually traces the shear-deformation relationship of the system up to collapse. For this system, collapse is considered to occur either at model instability or 5% drift ratio (Deng et al., 2019; Tesfamariam et al., 2019b; van de Lindt et al., 2020). Figures 7.6 (a) and 7.6 (b) show the pushover curve for CLT-CW systems designed considering R_d = 2 and 3, respectively. The resulting responses are the sum of the frame response resulting from the coupling beams, the axial responses of the hold-downs, and the individual CLT panel flexural responses.

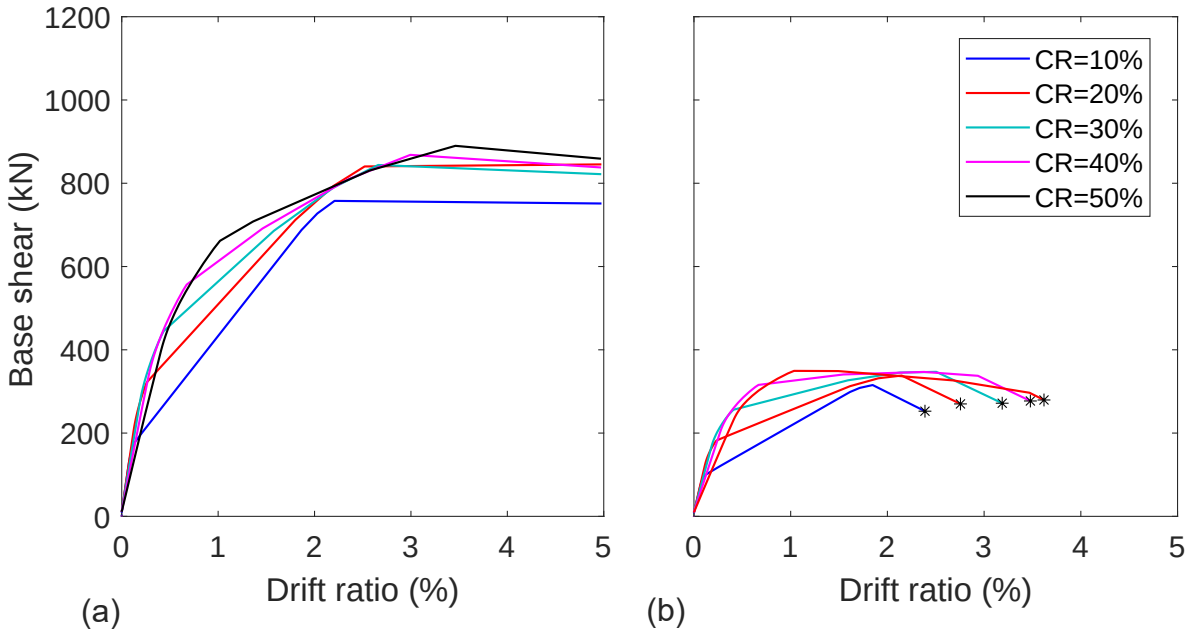

Figure 7.6: Pushover analysis for: (a) R_d = 2 and (b) R_d = 3.

Significant increase in strength and stiffness of the system is demonstrated for the CLT-CW system designed with R_d = 2 (Figure 7.6 (a)) compared to those designed

with R_d = 3 (Figure 7.6 (b)). The CLT-CW system designed with R_d = 3 exhibits a steep degradation once it reaches the peak point and therefore fails before it reaches a drift ratio of 5%. The asterisk in Figure 7.6 (b) shows the failure point at which the structure is deformed up to a displacement which is characterised by a 20% base shear reduction. An increase in strength of the system is also observed when using higher values of CR. It should be noted that the observed difference is due to the combined effect that arises from the difference in both CR values and the stiffness of the CLT shear-walls. In fact, the later counter-acted the significant difference that one might expect from the pushover analysis.

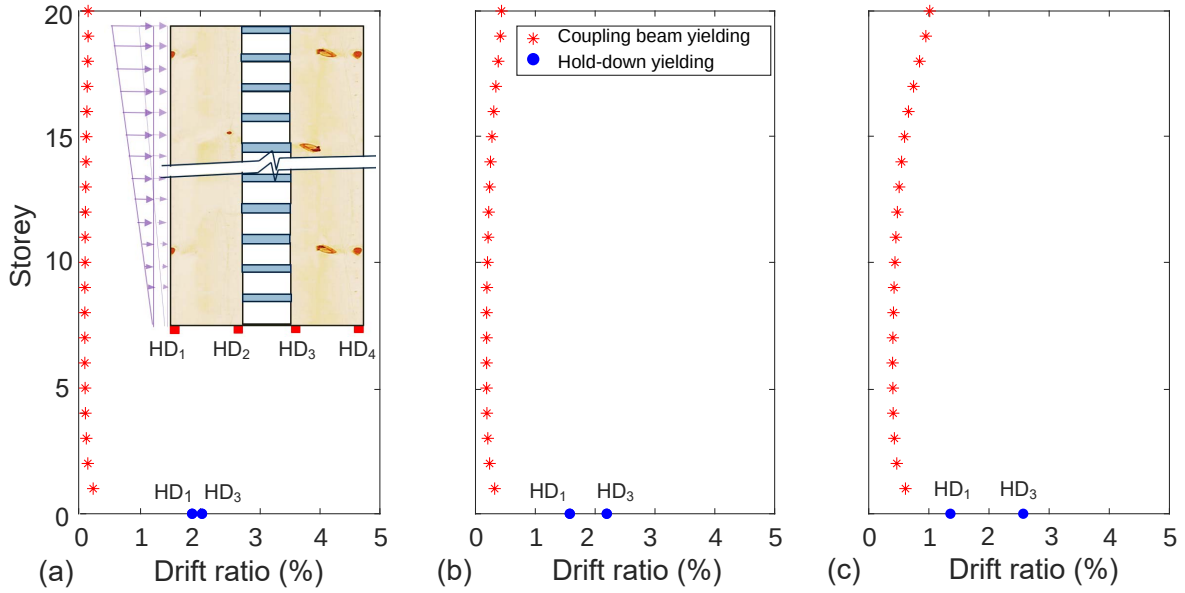

Figure 7.7: Sequence of yielding for the case R_d = 2 and (a) CR = 10%; (b) CR = 30%; and (c) CR = 50%.

The successive yielding of two ductile elements, the coupling-beams and the hold-down, for R_d = 2 is shown in Figure 7.7. The figure illustrates a fairly consistent sequence of yielding between coupling beams and hold-downs. In all the cases, the coupling beams yield prior to the hold-downs and this matches with the preferred sequence of yielding in CW systems (El-Tawil et al., 2010). In the process, the hold-down yielding is more delayed for the cases with CR = 10% (Figure 7.7 (a)) comparing with those designed with CR value of 30% (Figure 7.7 (b)) and 50% (Figure 7.7 (c)). The progression of coupling beam yielding differs from case to case and is governed by the actual demand from CMM and provided strength (Figure 7.8). Except on the first two floors, almost all the coupling beams yield simultaneously for the case CR = 10% (Figure 7.7 (a)). With small variation, the shear force profile from CMM can

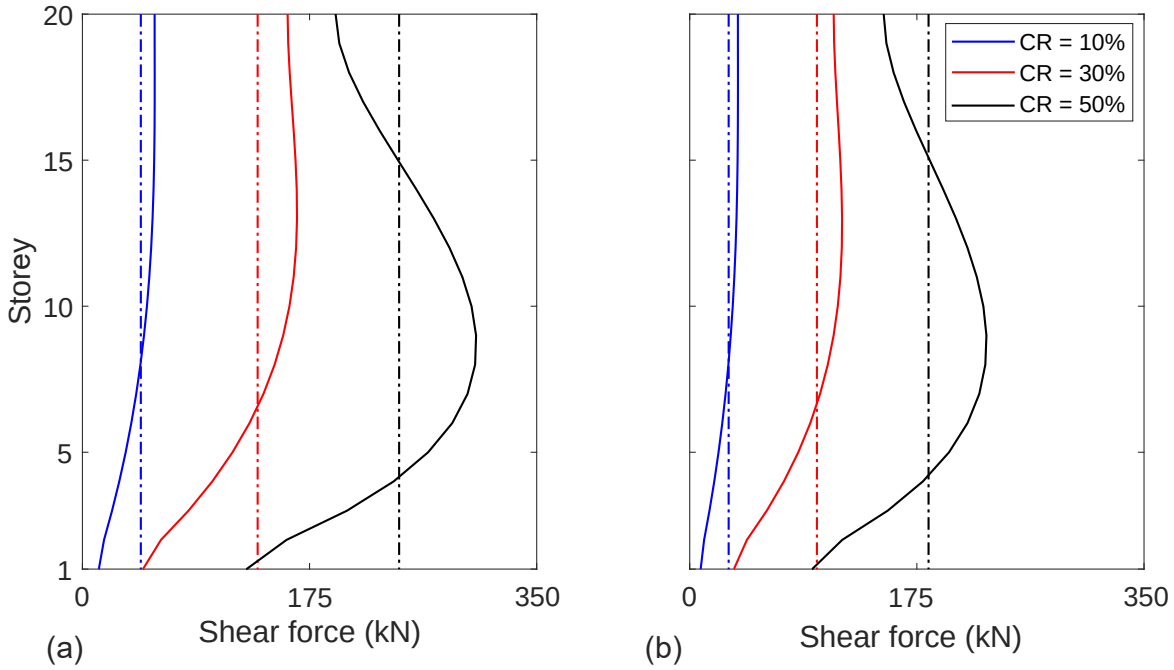

Figure 7.8: Coupling beams actual shear force demand (all solid lines) and provided strength (all broken lines) for: (a) R_d = 2 and (b) R_d = 3.

clearly explain the reason. As can be seen from Figure 7.8 (a) (for CR= 10%), the provided strength for coupling beams above the 7^{th} floor is smaller than the actual demand and this is why (with the exception of those from 3^{rd} to 6^{th} floor) they yield prior to those at the first two floors. This simultaneous yielding of the coupling beams (for CR = 10%) also results in sharp decrease in the stiffness of the system (Figure 7.6 (a)) at approximately 0.2% drift ratio. The CLT-CW systems designed with CR = 50% is another extreme case, where the coupling beams yield at different drift ratio values. Coupling beam yielding is initiated at floor levels 5 to 8 and progressed both upwards and downwards (Figure 7.7 (c)). The sequence of the yielding in Figure 7.7 (c) almost matches with the actual demand and provided strength of the coupling beams, Figure 7.8 (a) for CR= 50%, in which the beams within the middle $2/3$ of the building were provided with smaller strength and hence, yielded prior to the top and bottom level coupling beams. This sequential yielding of the coupling beams result in curved (gradual) decrease in the stiffness of the system (Figure 7.6 (a)) with the sharp edge occurs at approximately 1% drift ratio. For all the designed systems, hold-down HD_1 (HD_4, for a pushover performed in opposite direction) yields first compared to hold-down HD_3 (HD_2, for a pushover performed in opposite direction). As in the coupling beams, the hold-downs at CR= 10% (Figure 7.7 (a)) yields close to one-another compared to these at CR= 50% (Figure 7.7 (c)). The yielding point

of the first hold-downs is not distinguishable in the pushover curves. However, the yielding point of the second hold-downs correspond to a further (sharp) reduction in stiffness of the CLT-CW system (Figures 7.6 (a) and 7.6 (b)). The sequence of yielding, both for the coupling beam and hold-down, for the CLT-CW systems designed with CR = 30% (Figure 7.7 (b)) lies between the two extreme cases (CR= 10% and 50%). Unlike with CR= 10% and 50%, where the sequence of yielding of coupling beam and CMM shear profile matches, quite significant difference is observed for the CLT-CW systems designed with CR = 30% (Figures 7.7 (b) and 7.8 (a)). Figure 7.8 (b) illustrates the shear force profile of coupling beams for CLT-CW systems designed with R_d = 3. Exactly same sequence of yielding is observed and hence, same conclusion can be presented.

7.3.2 Nonlinear time history analysis

Peak responses of the CLT-CW system

To assess the nonlinear response of the systems under the action of seismic excitation, NLTHA is carried out using 30 GM records (30 records, 2 components each) at the design 2% PE in 50 years earthquake level (section 5.2). Maximum inter-storey drift ratio (MaxISDR), residual inter-storey drift ratio (ResISDR), and horizontal peak floor acceleration (PFA) are computed to access the performance of the designed CLT-CW systems. As per NBC (2015), the MaxISDR for 2% PE in 50 years and collapse prevention limit state is 2.5%. The mean value for the MaxISDRs, for R_d = 2 and R_d = 3 along the height of the buildings, are shown in Figures 7.9 (a) and 7.10 (a), respectively. From the figures, it is evident that the average MaxISDR demands are well below the NBC limit of 2.5% and the design structural systems demonstrate satisfactory performance.

Another important performance measuring parameter is ResISDR, a parameter that measures the permanent or non-reversible deformation of the buildings at the end of the applied GM. The same data as the MaxISDR were recorded in the NLTHA analysis, considering 30 GMs. Figures 7.9 (b) and 7.10 (b) illustrate the values of the ResISDR throughout the height of the building and their values are below 0.2% and 0.3% for the cases R_d = 2 and R_d = 3 (except at 50% CR where it closes to 0.6%), respectively. Again the values of the ResISDR are within the intended limit of 1%, a value provided by TBI (2017) to protect excessive post-earthquake deformations that likely will cause

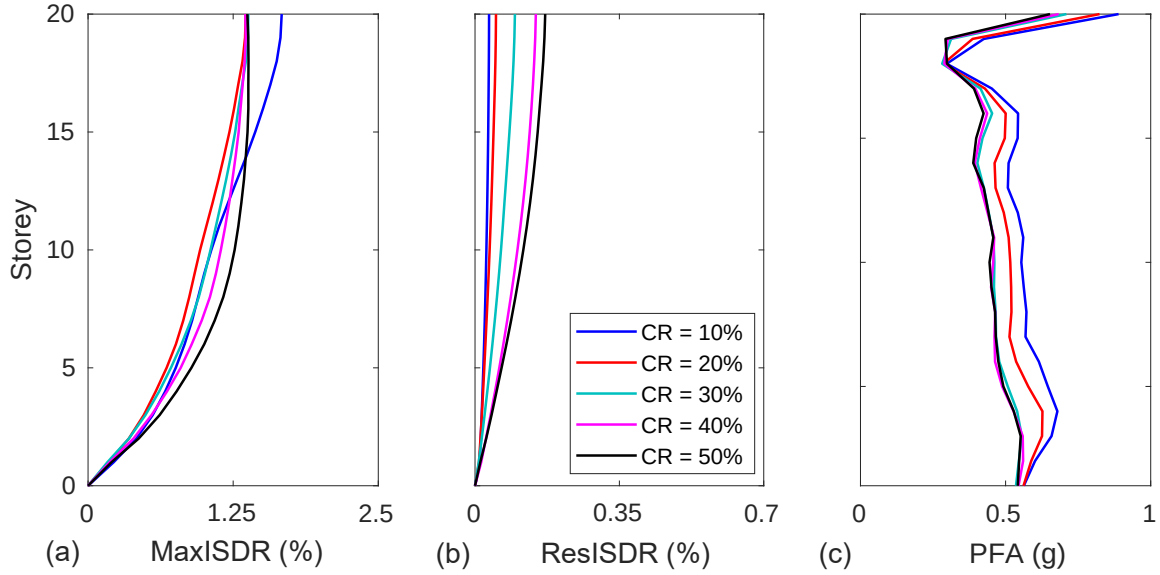

Figure 7.9: NLTHA results for R_d = 2: (a) MaxISDR (%); (b) ResISDR (%); and (c) PFA (g).

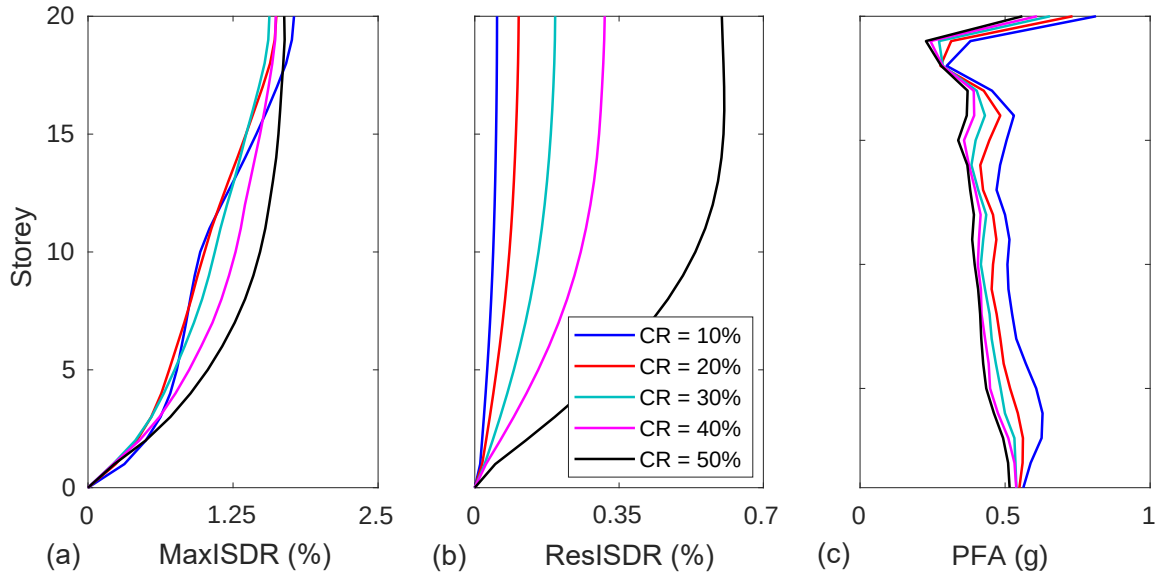

Figure 7.10: NLTHA results for R_d = 3: (a) MaxISDR (%); (b) ResISDR (%); and (c) PFA (g).

condemnations or excessive downtime repairs of buildings. Figures 7.9 (c) and 7.10 (c) also show the distribution of the PFA throughout the height of the building, in terms of gravitational acceleration (g) units. As can be seen from the Figures, the PFA values remain close to 0.5g for stories 1 to 16, and achieves their maximum value at the top floor.

Coupling beam and hold-down behaviors

The force-displacement response for selected coupling beams throughout the storey of the building, for R_d = 2 and R_d = 3, are shown in Figures 7.11 and 7.12 respectively. The figures illustrate the response of the coupling beams at GM #28, a GM that corresponds to the maximum response of the coupling beams and hold-downs. The response of the coupling beams is dictated by the shear force profile of the CMM analysis and the provided strength (Figure 7.8). For example, for $R_d = 2$ and $CR = 10\%$, the shear force profile increases with the increase in the height of the structure (Figure 7.8 (a)). As the provided strength is an average of the actual demand, the response shown in Figure 7.11 (for CR = 10%) increases with the increase in the height of the building. Similar observation can be made for the rest of the cases (eg. Figure 7.11 for the case R_d = 2 and CR values 30% and 50%).

The energy dissipation contribution of the coupling beams, for R_d = 2 and R_d = 3, are shown in Figures 7.13 and 7.14, respectively. The figures illustrate the energy dissipation of the coupling beams for GM #28. The figures demonstrate the difference between the actual demand and provided strength of the coupling beams, as presented in Figure 7.8. For example, for coupling beam at storey level 20, the provided strength is smaller than the actual demand and hence, dissipates more energy compared with those coupling beam at the other storey levels (Figure 7.13). Conversely, coupling beam at 1^{st} storey is provided higher strength than the actual demand and hence, exhibits smaller energy dissipation (Figure 7.13). Exactly the same behavior is seen R_d = 3. Since the strengths (Figures 7.8 (a) and 7.8 (b)) and displacements (Figures 7.11 and 7.12) of coupling beams designed with R_d = 2 are higher, they dissipate more seismic energy than the coupling beams designed with R_d = 3 (Figures 7.13 and 7.14).

The axial load-displacement plot of the BRB hold-downs, for R_d = 2 and 3, at GM #28 are shown in Figures 7.15 and 7.16, respectively. The plots (a), (b), (c), and (d) in both Figures 7.15 and 7.16 represent the response of the hold-downs HD_1, HD_2, HD_3, and HD_4, respectively (Figure 7.7 (a)). From the figures, it can be observed that the responses of the hold-downs are significantly high for the lower values of CR. This is attributed to the fact that the coupling beams with lower CR values are less stiff than these with higher CR values and hence, the coupling action of beams begin to degrade and the lateral forces are redistributed to the corresponding hold-downs. For each CR values, same capacity were provided. Consequently, a symmetric response is

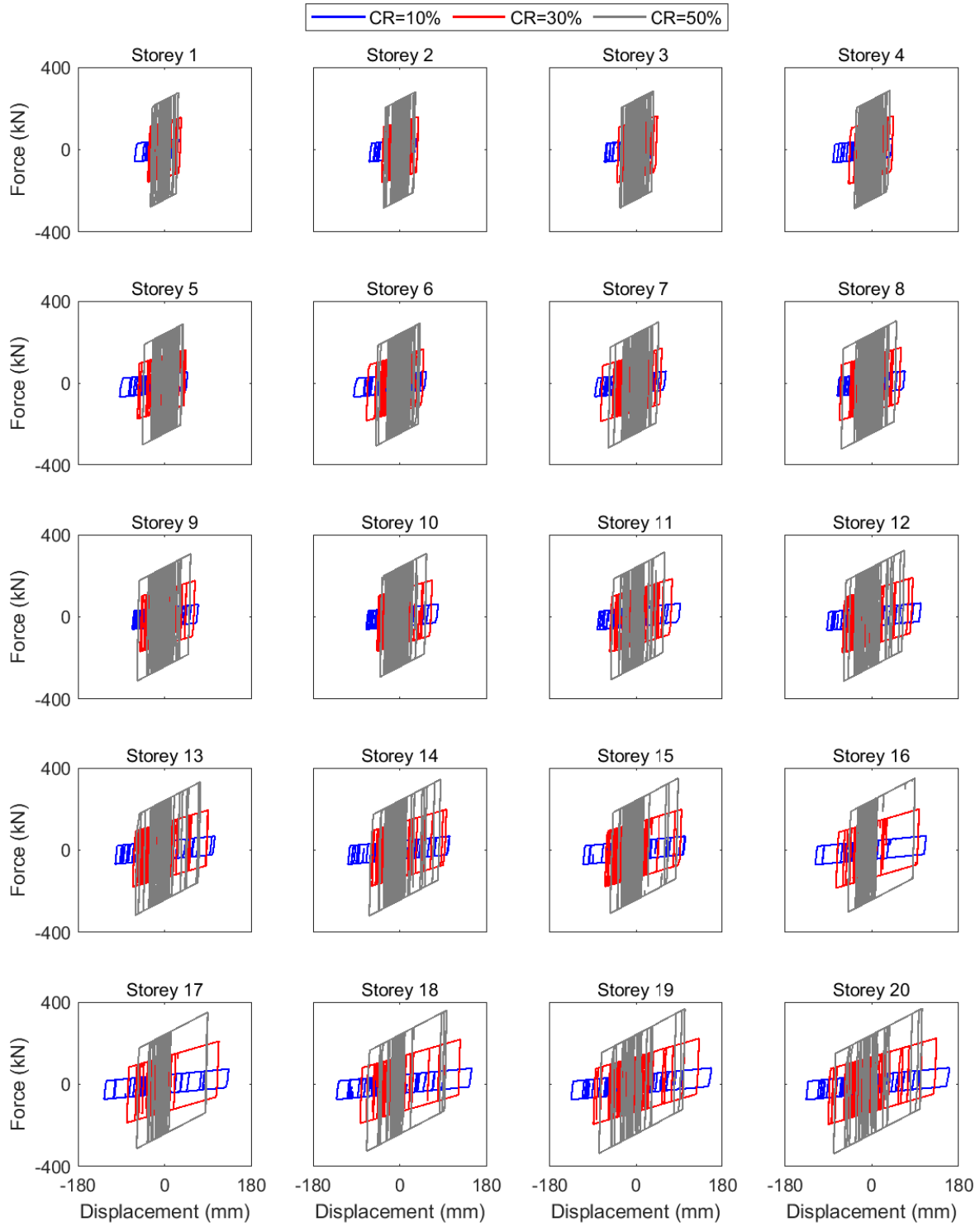

Figure 7.11: Coupling beam response for R_d = 2 and GM #28.

observed from the axial displacement of the hold-downs. Moreover, the hold-downs at the right side of the CLT walls (Figures 7.15 (b) and 7.15 (d)) are exhibiting higher responses compared to those in the left side of the CLT walls (Figures 7.15 (a) and 7.15 (c)) for R_d = 2). The opposite is happening for the hold-downs in the CLT-CW systems

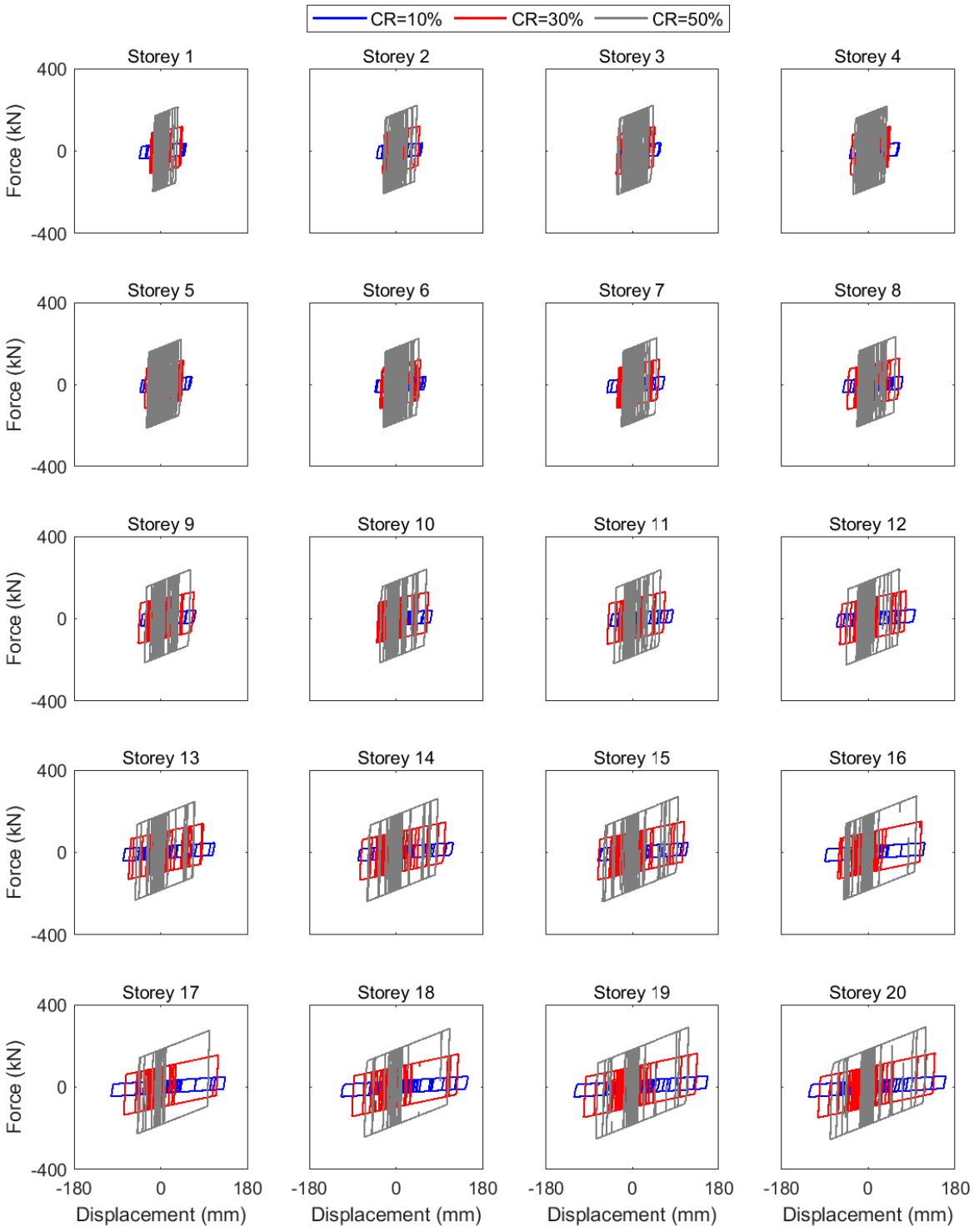

Figure 7.12: Coupling beam response for R_d = 3 and GM #28.

designed with R_d = 3 (Figure 7.16). For most of the GMs, the response of the hold-downs is limited within the linear or elastic limit. As a result, the energy dissipation of the hold-downs become small. The energy dissipation of the hold-downs for R_d = 2 and 3, considering CR = 10%, 30%, and 50%, are shown in Figures 7.17 and 7.18,

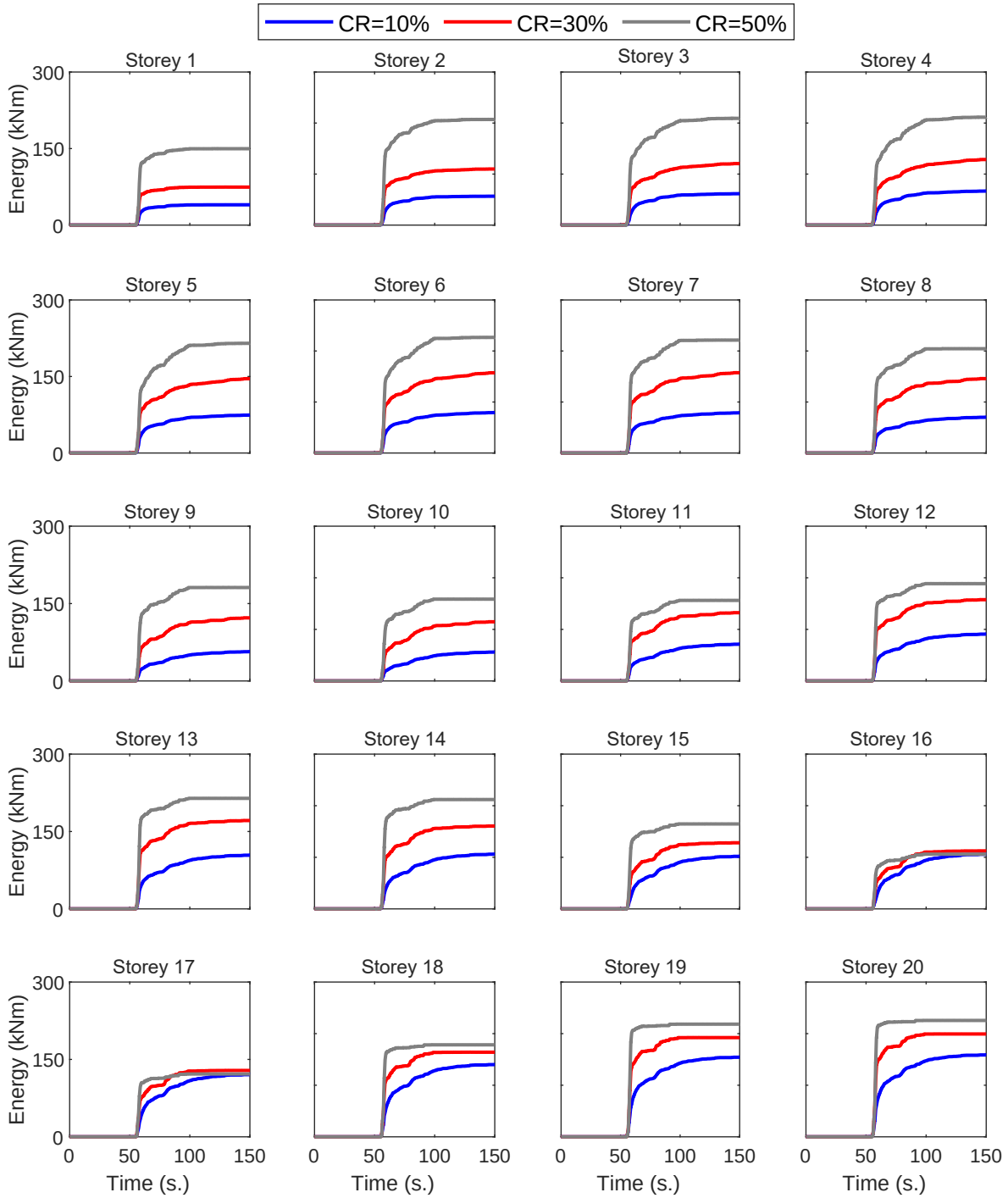

Figure 7.13: Coupling beam energy dissipation for R_d = 2 and GM #28.

respectively. The hold-downs dissipate less seismic energy compared to the dissipation of the coupling beams (Figures 7.13 and 7.14). Moreover, it can be noted that hold-downs at CR = 10% dissipates more energy than hold-downs at CR = 30% and 50% (Figures 7.17 and 7.18).

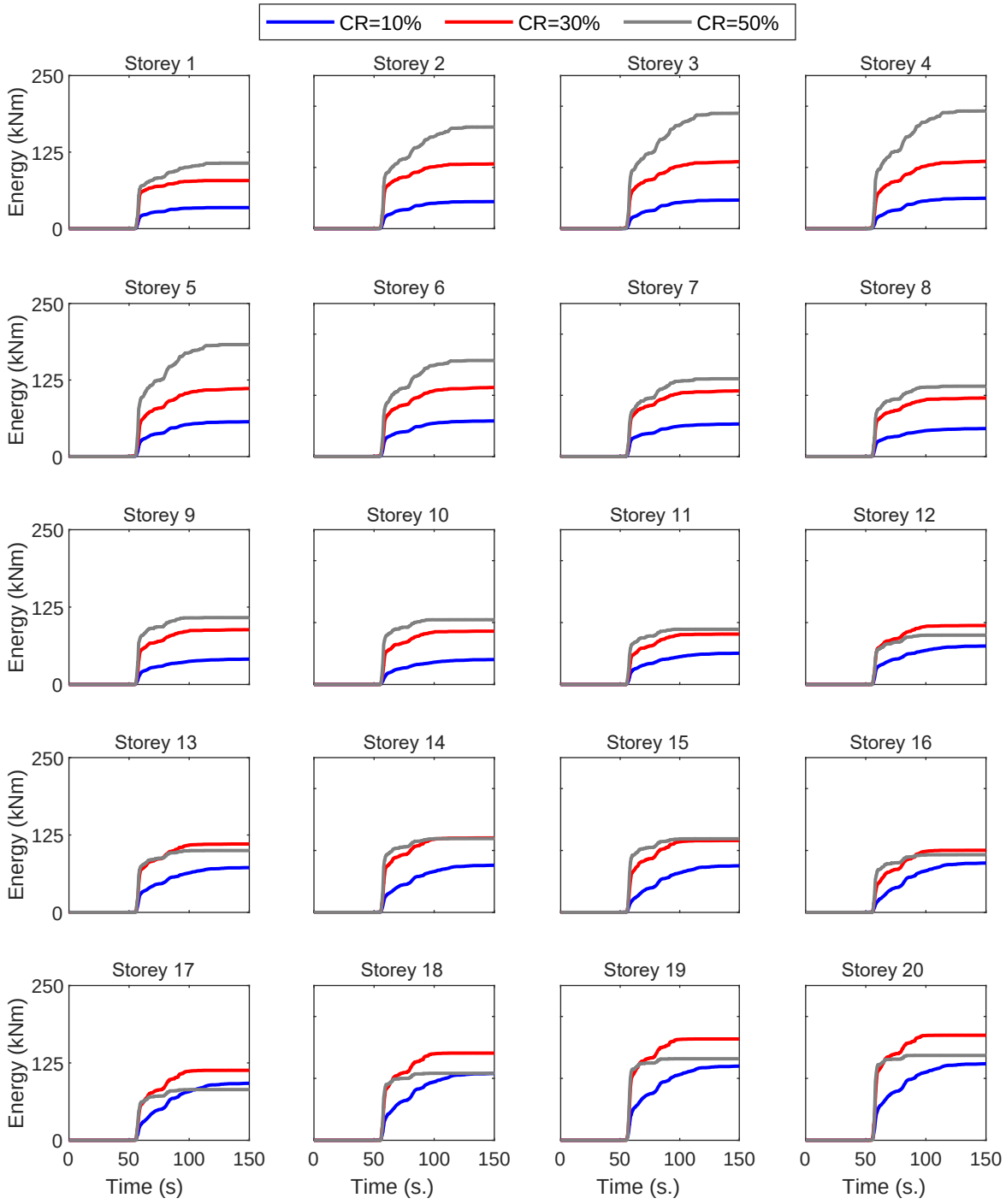

Figure 7.14: Coupling beam energy dissipation for R_d = 3 and GM #28.

7.3.3 Effect of seismic modification factor

In this study, an over-strength factor R_o = 1.5, as given in CSA 086-14 (CSA, 2016), was adopted and two seismic modification factors, R_d = 2 and 3, were examined. The result for the fundamental geometric design of the CLT-CW system for the considered R_d values is summarized in Table 7.1 and Figure 7.19 (d). The length of the CLT shear-walls

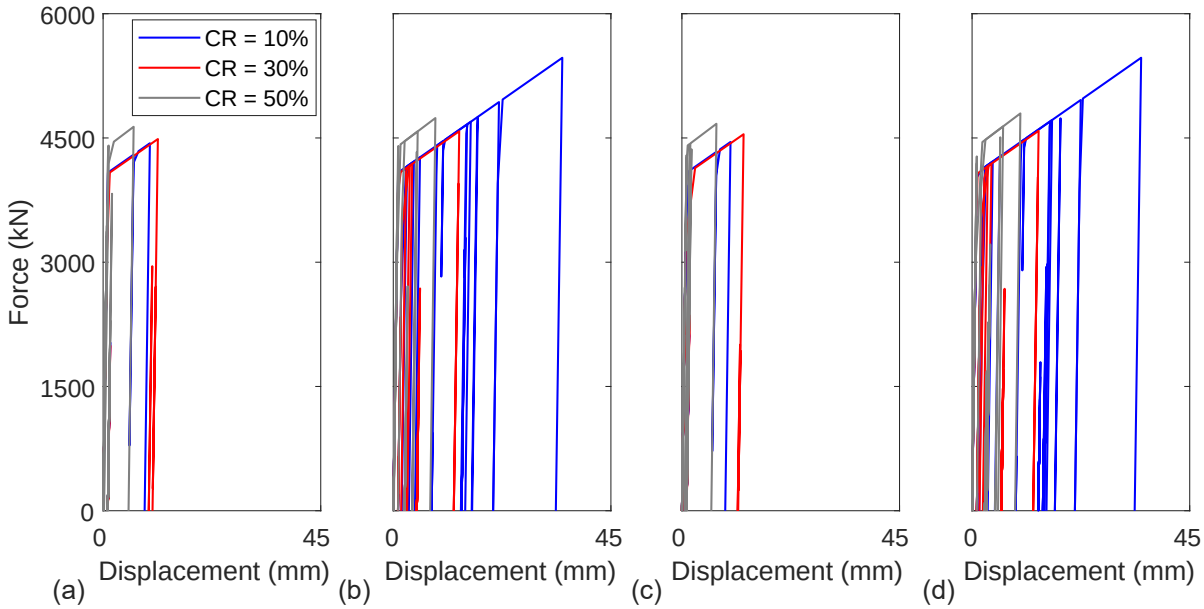

Figure 7.15: Hold-down response for R_d = 2 considering GM #28: (a) HD_1; (b) HD_2; (c) HD_3; and (d) HD_4.

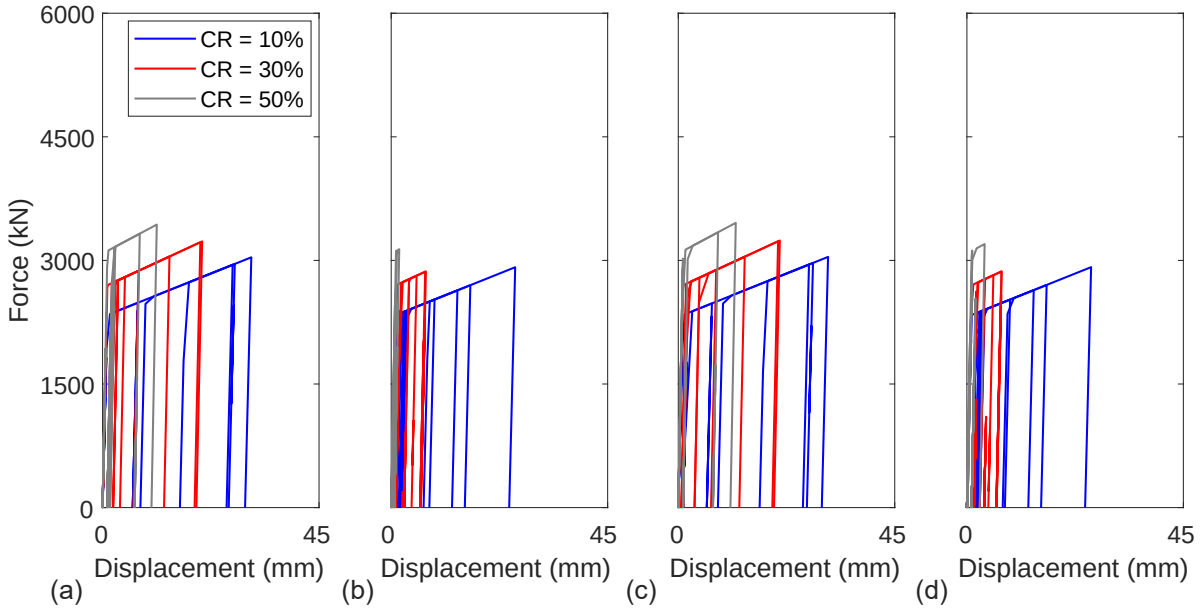

Figure 7.16: Hold-down response for R_d = 3 considering GM #28: (a) HD_1; (b) HD_2; (c) HD_3; and (d) HD_4.

designed by R_d = 3 are relatively short and hence, the walls become slender with large fundamental periods (Table 7.1 and Figure 7.19 (d)). Accordingly, higher MaxISDR and ResISDR are developed comparing to the cases designed with R_d = 2 (Figures 7.19 (a) and 7.19 (b), respectively). Figure 7.19 (c) illustrates the computed PFA of the buildings and it is observed that CLT-CW systems designed with R_d = 3 exhibits less PFA values compared to these designed with R_d = 2.

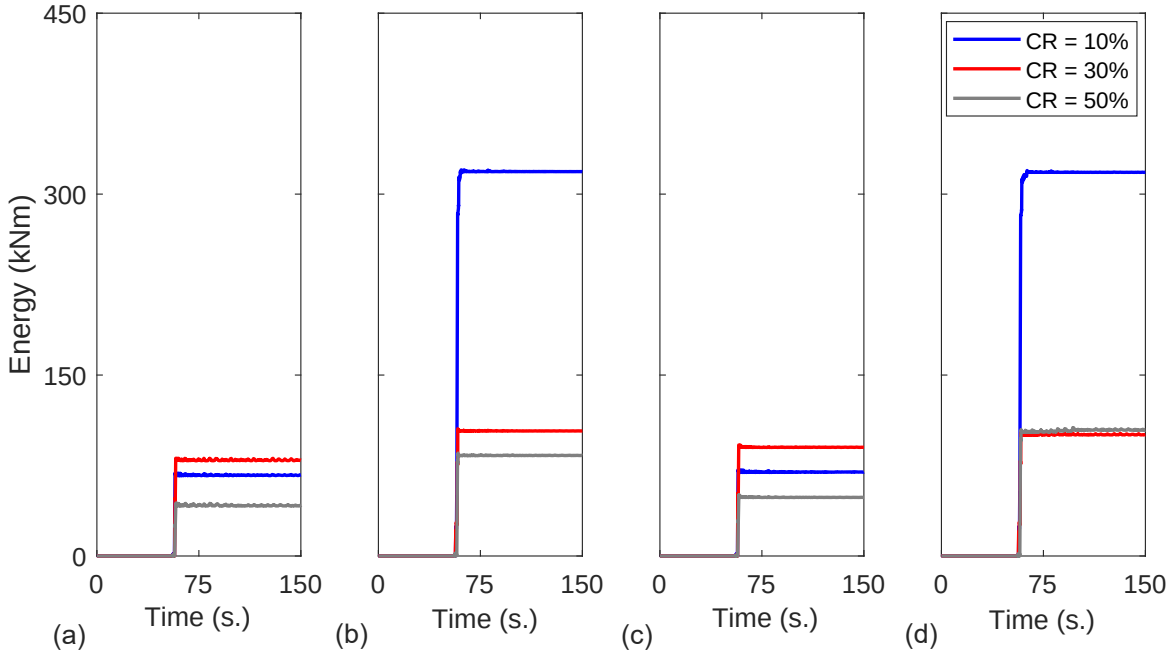

Figure 7.17: Hold-down energy dissipation for R_d = 2 and GM #28: (a) HD_1; (b) HD_2; (c) HD_3; and (d) HD_4.

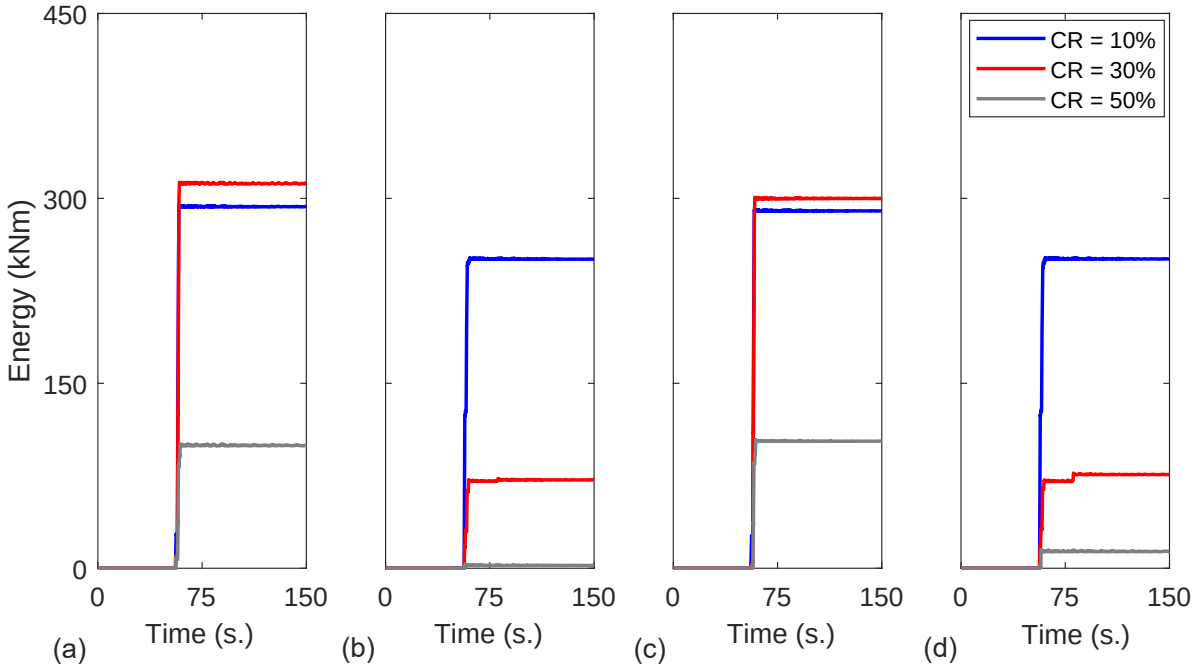

Figure 7.18: Hold-down energy dissipation for R_d = 3 and GM #28: (a) HD_1; (b) HD_2; (c) HD_3; and (d) HD_4.

7.3.4 Effect of coupling ratio

The behaviour of the CLT-CW system was examined under five CR values 10%, 20%, 30%, 40%, and 50%. Figure 7.19 can not explicitly investigate the effect of CR values,

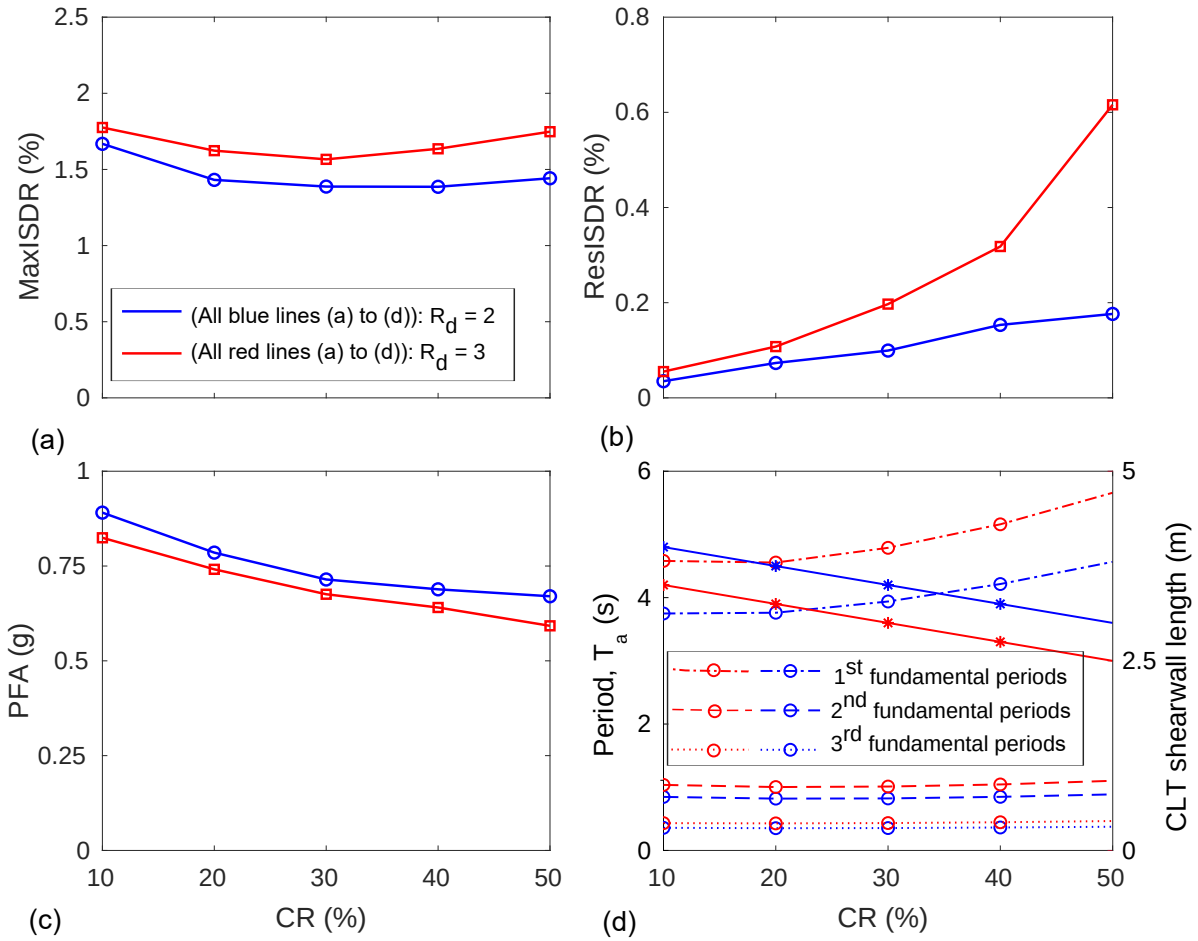

Figure 7.19: Effect of R_d and CR on: (a) MaxISDR (%); (b) ResISDR (%); (c) PFA (g); and (d) fundamental periods in second (left axis) and CLT shear-wall length in meters (right axis).

as the design cases were developed considering different CLT panel stiffness's (Table 7.1 and Figure 7.19 (d)). In order to explicitly study the behaviour of the system under different CR values, fixed wall cases were developed and simulated. Five CLT shear-wall lengths $3.00\ m$, $3.25\ m$, $3.50\ m$, $3.75\ m$, and $4.00\ m$ (initially designed for R_d = 2) are examined, each for different values of CR (10% to 50%). With those additional 20 (25 - 5) simulations, the effect of CR on the behaviour of the CLT-CW system can be clearly noticed from Figure 7.20. Now, for fixed wall length condition, systems with higher CR value reveal higher stiffness and strength. As can be seen from Figures 7.20 (a) and 7.20 (b), the values of MaxISDR and ResISDR significantly decreases and increases with the increase in the value of CR, respectively. The PFA exhibits a slight decrease with the increase in the CR value (Figure 7.20 (c)). As expected, the fundamental periods of the CLT-CW system decreases with increase in the value of CR (Figure 7.20 (d)). Note that Figure 7.20 illustrates for the CLT shear-wall cases

initially designed for R_d = 2. However, the same observation and conclusion can be drawn for the cases designed with R_d = 3.

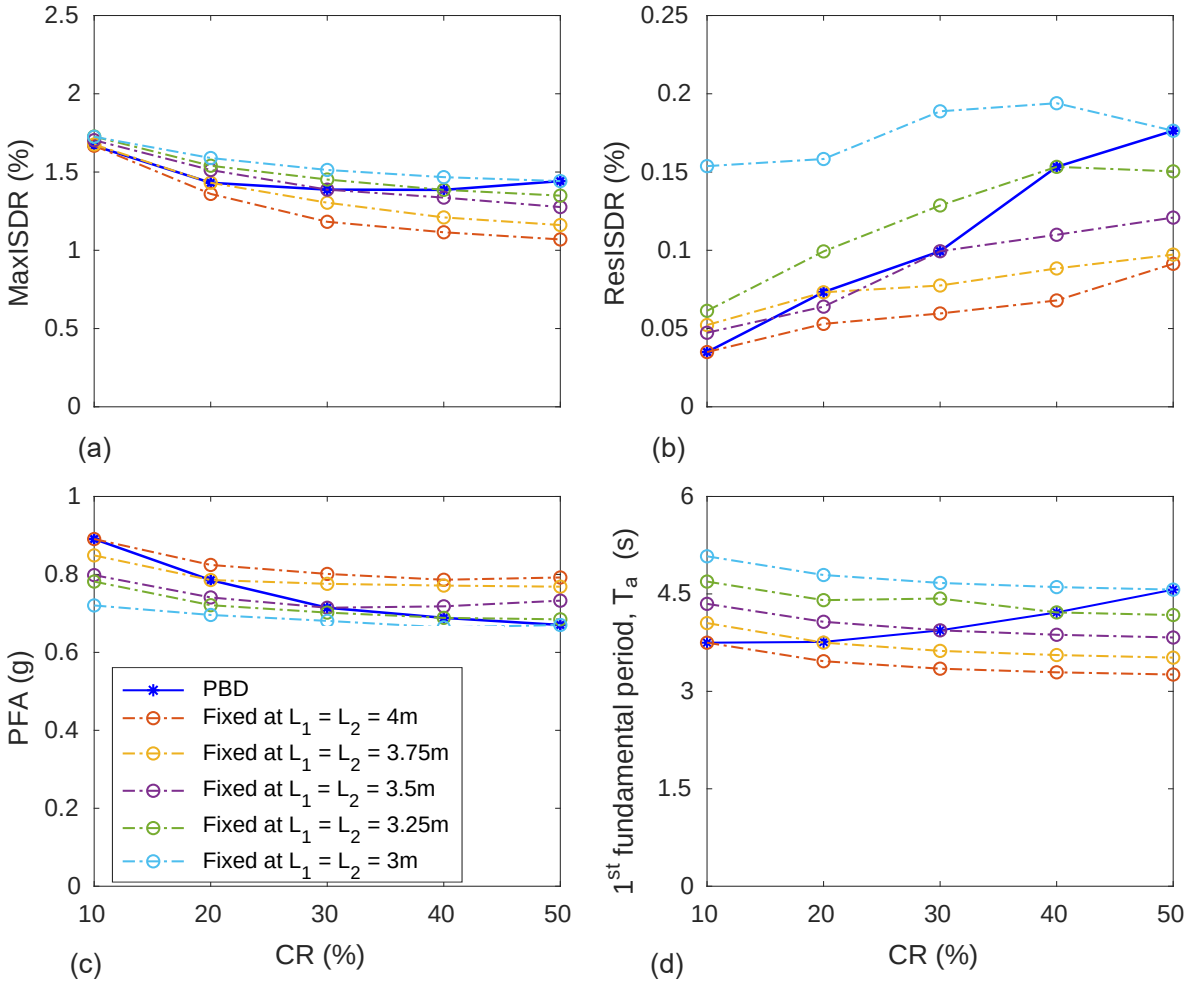

Figure 7.20: Effect of CR (for R_d = 2) on: (a) MaxISDR (%); (b) ResISDR (%); (c) PFA (g); and (d) First fundamental period (s).

Chapter 8

Conclusions and Future Recommendations

8.1 Conclusions

The construction of mass-timber structures have been increased in Canada due to the support that have been done by the wood industry and provincial governments in Canada. Although timber is sustainable construction material and is easily available, the use of mass-timber building was limited to low building heights due to its light-weight and relatively high flexibility. However, this height limit has been revised with the state-of-the-art studies that have been done recently. To take part in this contribution, this report has examined the behavior of tall-mass-timber building with coupled CLT shear wall system. In a conventional reinforced concrete CW system, this system reduces the moments that must be resisted by the individual walls which results in a more efficient structural system. The coupling beams provide an alternative frame-resisting mechanism for lateral load resistance in addition to bending-beam-resisting of individual walls and dissipate the seismic energy by their high ductility properties. This report has taken conventional CW systems and provide design guideline for CLT CW system.

Twenty-storey mass-timber-building is considered as a prototype in this study. The model is then examined with three different values of ductility modification factor (R) and five coupling ratio (CR) values. Performance-based design procedure formulated for conventional and hybrid CW system is implemented to analyse and design the CW

system parameters. As the proposed location of the building is Vancouver - British Columbia, Canada; the structure is examined for collapse prevention performance limit state by performing NTHA. The NTHA is conducted on OpenSees by considering 60 ground motions and stated parametric study conditions. In OpenSees, the CLT walls are modelled as a linear elastic *quad* elements, while connections are modelled with nonlinear springs. The shear coupling beams are modelled using elastic beam elements as rigid offsets and a nonlinear vertical spring. Moreover, the BRB hold-downs are modelled as *Steel01* uniaxial material. Besides, the contact between the base of the CLT ballon shear walls and the ground was modeled as a parallel system using elastic no-tension (ENT) spring element.

The result from the NTHA shows that the structural behaviour of the system is enhanced by provided coupling beams. The calculated maximum inter-storey drift ratio are well-below the target drift limits. Moreover, the residual inter-storey drift ratio values are small exhibiting a weak storey at the first level attributed to the height difference and the existence of hold-downs. The force-displacement response of the hold-downs and coupling beams various depending on the values of R and CR. Generally, as the values of R increase, the hysteresis curve for both the hold-downs and coupling beams increases as the strength demand for large R value is small as dictated by the ELF and CMM analysis.

8.2 Future work

The provided design guideline for two-wall coupling system can be extended for three-wall systems. Moreover, coupling beams with different ductility behavior can be examined based on the proposed design guideline. The analysis and design can also extend for different archetype buildings.

By establishing damped coupling system, the optimization of the system can be performed under uncertainties for robust performances. For this purpose, reliability based design optimization should be performed by using different surrogate models.

Appendix - Contents

Appendix A

Response of CLT walls: Parametric analyses

A.1 Single CLT wall

A.1.1 Description

The applied forces and kinematics for a single CLT wall are shown in Fig. A.1. A distributed vertical load w and an horizontal force F are applied at the upper side of the wall. The wall is anchored to the ground with hold-down and shear connections. The hold-down connections bear the vertical tensile forces that result from uplifting (rocking) of the wall, while the shear connection bears the horizontal force F. The intended kinematics of the wall are shown in Fig. A.1b, and they correspond to rocking of the wall with respect to either of its lower corners. For the rocking to take place, the following conditions should be satisfied.

- For the rocking to initiate, the base overturning moment generated by the lateral force should surpass the stabilizing moment from the vertical load, i.e.: $FH > w\frac{L^2}{2}$. It is obvious that apart from the relative magnitude between the two forces, the geometrical dimensions of the wall also have an effect.
- The hold-down should yield in tension and provide with adequate ductility, as required by seismic design guidelines.
- The shear connection should have adequate strength to resist the wall shear F, without yielding (i.e. the shear connection should be capacity-designed).

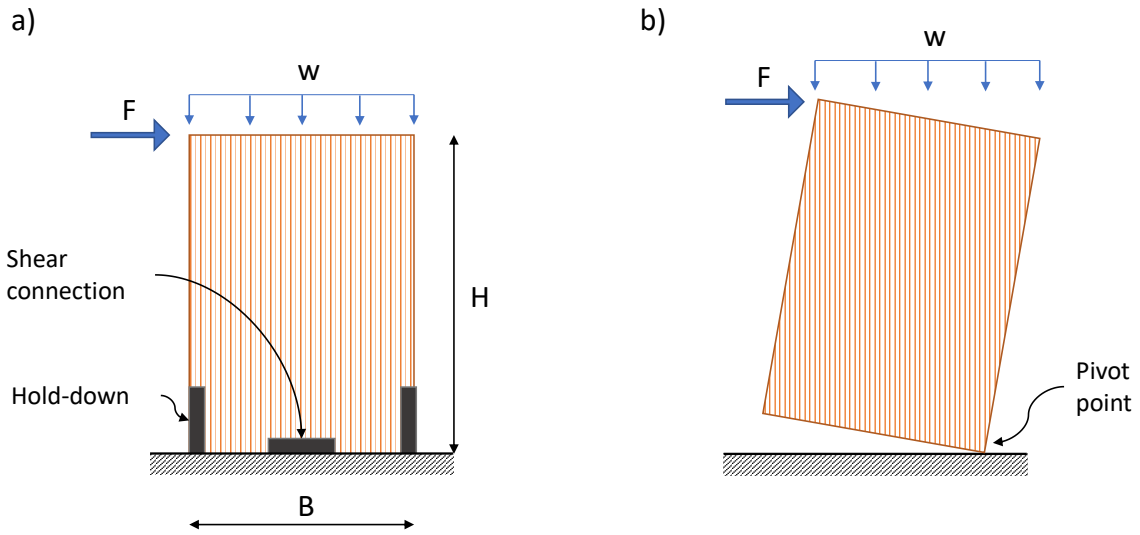

Figure A.1: Single CLT wall

- The shear connection should allow rocking of the wall without imposing a restraint in the vertical direction (i.e. uncoupled horizontal and vertical response). If this is not the case, the vertical contribution as well as the interaction in the two directions of the shear connection should be accounted for.

Rocking is the preferable mode of deformation for seismic design applications because of its self-centering property. On the other hand, CLT walls deforming in sliding mode (shearing of the shear connections) have been associated with large permanent deformations and progressive withdrawal of fasteners in the hold-down and shear connections (Gavric et al., 2015) during cyclic response. Other modes of deformation, such as bending and shear of the CLT panels have a relatively small contribution, and therefore, the wall can be idealized as a rigid block (Gavric et al., 2015; Pei et al., 2013). Therefore, the elastic modulus and thickness of the CLT panels are not influencing parameters for the lateral deformation of the wall, whereas the wall aspect ratio H/B is.

A.1.2 Parametric analysis

In order to study the hysteretic behavior of a single CLT wall in rocking, parametric analyses are conducted by varying the influencing parameters of the problem. For this purpose, a single CLT wall is studied with nominal dimensions: $H = 3315mm$ and

$B = 2025mm$. The nominal imposed vertical load is: $w \cdot B = 11.77kN$. The nominal hold-down yield strength is: $F_y^{HD} = 20kN$. The CLT panel has a thickness of $170mm$ and it is modelled as elastic isotropic material with modulus of elasticity of $8GPa$ and a Poisson ratio of 0.16. A simple cyclic displacement protocol is applied with four incrementally increasing displacement amplitudes up to $100mm$ (3% wall drift ratio), wherein each displacement amplitude is repeated three times before proceeding to the next amplitude. The open-source finite element framework Opensees (Mazzoni et al., 2006) is used for all modelling and analysis.

The examined parameters are the type of hold-down connection used, the imposed vertical load ($w \cdot B$), the hold-down yield strength (F_y^{HD}) and the aspect ratio of the wall (H/B). The effect of each one of these parameters is individually assessed in the following.

(A) Hold-down type

Three types of hold-down connections are examined. A steel bracket with nailed fasteners (Popovski et al., 2010) is examined, which is a conventional type for CLT walls. The *Pinching4* uniaxial material model of Opensees is used, while the model parameters have been calibrated with experimental results in a previous study (Shen et al., 2013). The first point in the backbone curve is taken as the yield strength, which is $19.7kN$, close to the value of $20kN$, which is the considered nominal strength of this parametric study.

Furthermore, the flag-shaped model is examined, which is implemented herein with Opensees *SelfCentering* uniaxial material model. This model represents a number of real-world materials and structural elements, such as shape-memory alloy (SMA) tendons and unbonded post-tensioned tendons. Recently, the resilient slip-friction joint (RSFJ) (Hashemi et al., 2018) has been developed for use as a hold-down in timber walls, which is a self-centering friction-dissipating connection. The parameters of the *SelfCentering* Opensees model are based on the calibration study of (Hashemi et al., 2018).

Finally, a BRB hold-down is examined with the familiar bilinear hysteretic response, which is characteristic of steel materials. It is implemented using the Opensees *Steel02* and it is also representative of a number of other steel connections and dampers, such as modified HSK connection (Zhang et al., 2018), multi-plate flexural devices

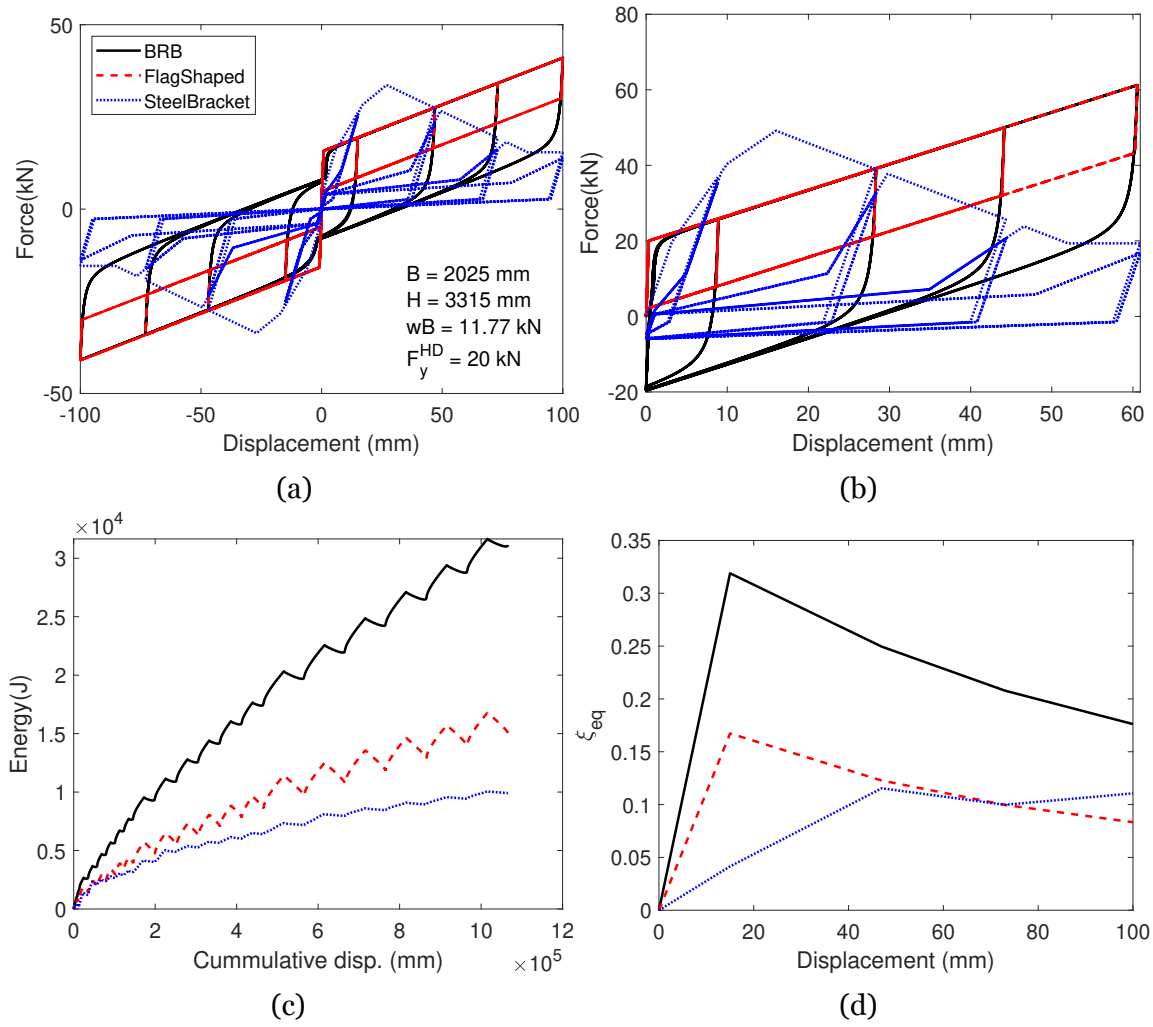

Figure A.2: Single CLT wall subjected to cyclic load; (a) Wall response; (b) Hold-down response; (c) Energy plot; (d) Equivalent damping ratio

(Blomgren et al., 2019) and U-shaped flexural plate (UFP) dampers (Akbas et al., 2017). The properties of the BRB hold-down (strength, stiffness, post-elastic stiffness ratio) are the same as the flag-shaped hold-down, for comparative purposes.

The response of the wall with the three different hold-downs is shown in Fig. A.2.

(B) Vertical load

Vertical load acts as a stabilizing factor for rocking walls, by increasing the uplift shear capacity of the wall. This is illustrated in Fig. A.3, where it is shown that increasing vertical load leads to increasing base shear capacity. This should taken into account in the capacity design of the shear connections. Moreover,it should be verified whether the increased vertical load prevents the the wall from yielding and dissipating energy when subjected to strong seismic motions. It is further observed from Fig. A.3 that

increased vertical load is associated with reduced residual displacement and enhanced self-centering capacity of the wall. Although the dissipated energy does not change with increasing vertical load (Fig. A.3(c)), the equivalent damping ratio decreases (Fig. A.3(d)).

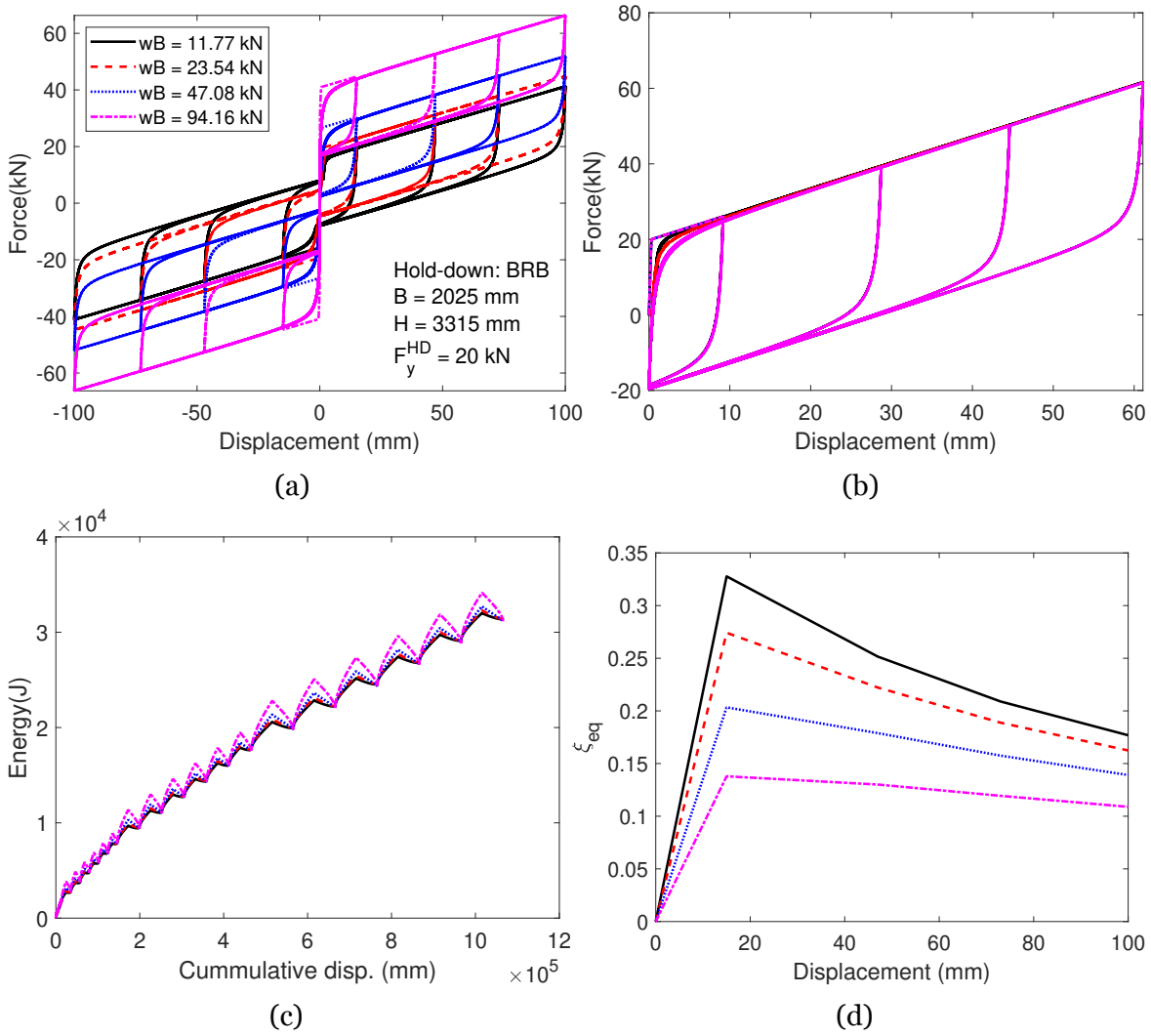

Figure A.3: Single CLT wall subjected to cyclic load; (a) Wall response; (b) Hold-down response; (c) Energy plot; (d) Equivalent damping ratio

A.2 Coupled CLT walls

A.2.1 General

CLT walls coupled with energy-dissipating connections can increase the amount of dissipating energy for seismic design applications. Fig. A.6 shows the reference case of two walls coupled with a shear connection. The desirable lateral mechanism is the

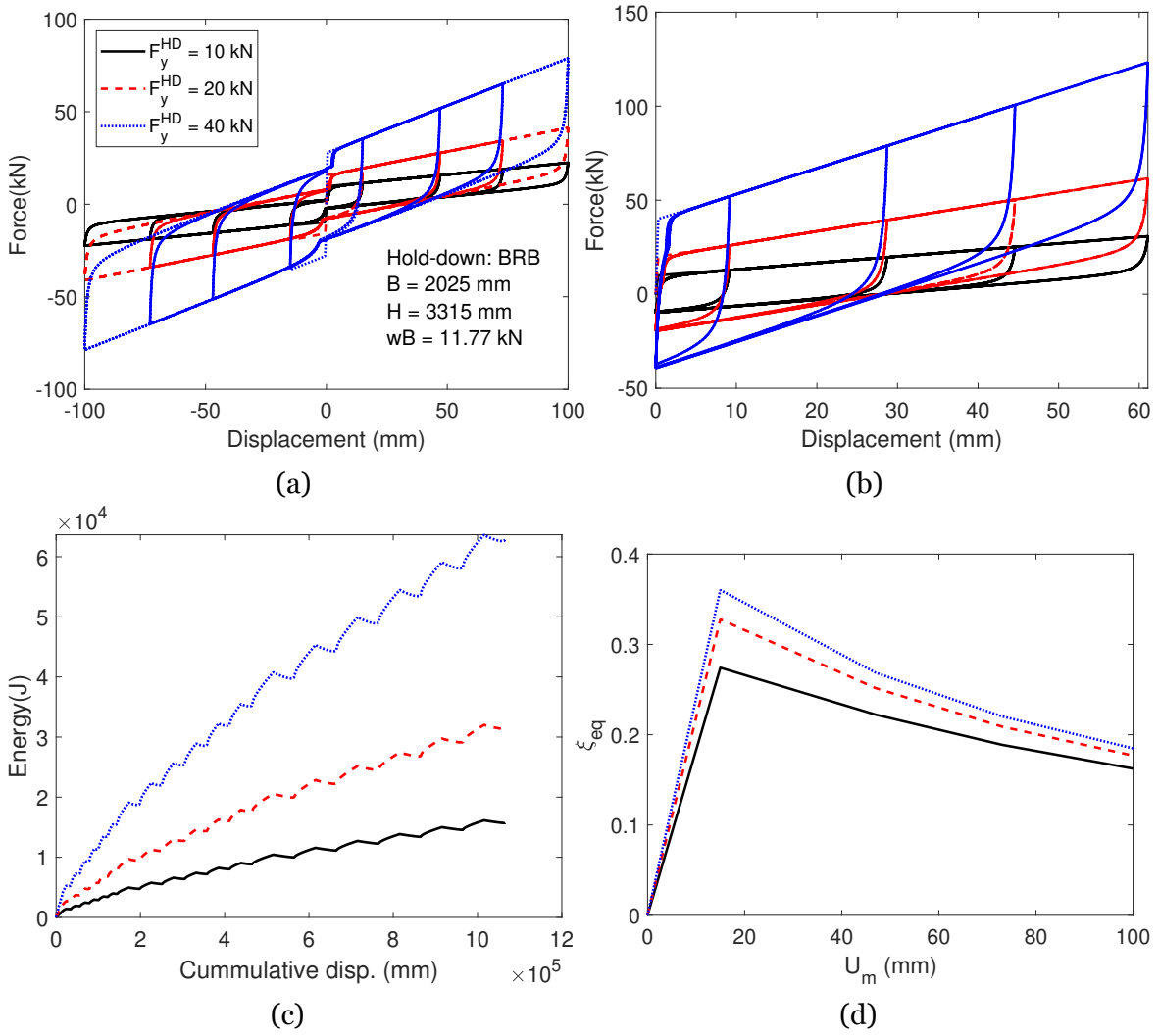

Figure A.4: Single CLT wall subjected to cyclic load; (a) Wall response; (b) Hold-down response; (c) Energy plot; (d) Equivalent damping ratio

coupled rocking shown in Fig. A.6[b]. For this mechanism to happen the strength ratio between hold-down and wall-to-wall shear connection must not surpass a certain limit. Analytical formulations have been derived for multiple coupled CLT walls with linear (Casagrande et al., 2018) and elasto-plastic (Nolet et al., 2019) connections. In this study, numerical parametric analyses are conducted to verify the qualitative response characteristics presented in the aforementioned studies.

A.2.2 Parametric analysis

The parameters examined here are the hold-down yield strength (F_y^{HD}), the vertical shear connection yield strength (F_y^{VSC}) and the vertical load ($w \cdot 2B$). For the sake of simplification, BRB material is used for both the hold-down and the vertical shear

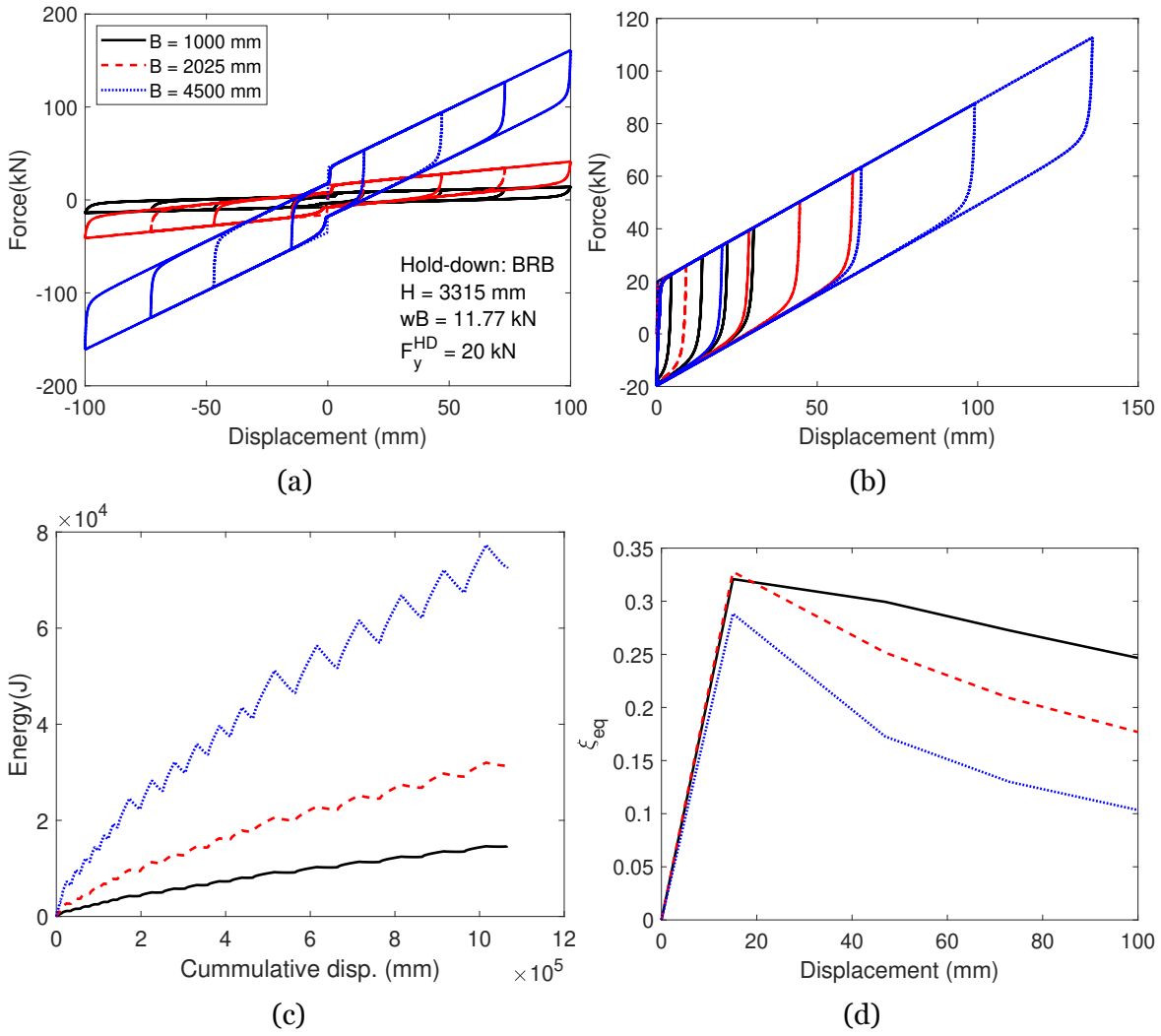

Figure A.5: Single CLT wall subjected to cyclic load; (a) Wall response; (b) Hold-down response; (c) Energy plot; (d) Equivalent damping ratio

connection. The nominal assumed values are: $F_y^{HD} = 20kN$, $F_y^{VSC} = 20kN$ and $w \cdot 2B = 23.54kN$.

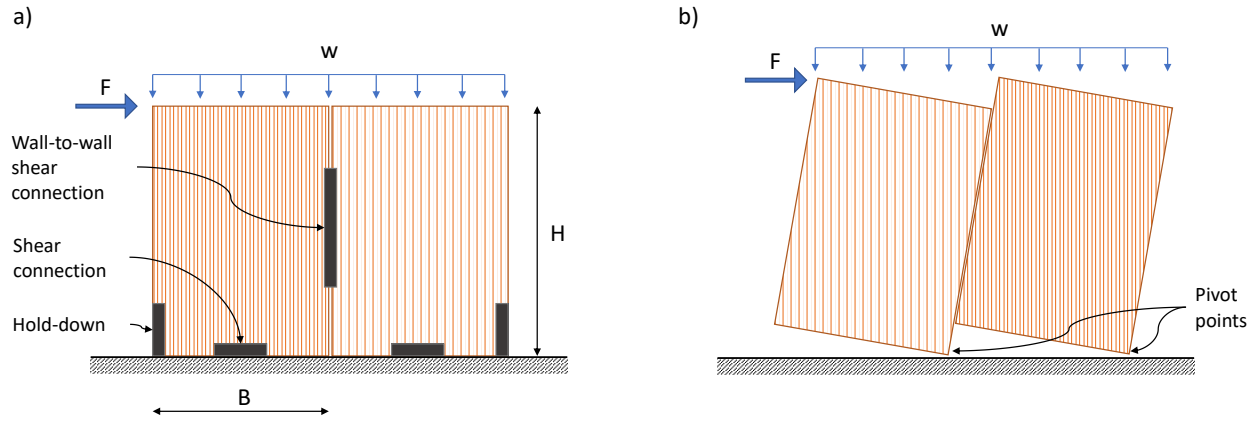

Figure A.6: Single CLT wall

(A) Hold-down strength

Cyclic pseudo-static analysis results for varying hold-down yield strength are shown in Fig. A.7. The displaced shapes for static pushover analysis are shown in Fig. A.8. It is observed, that for low values of F_y^{HD}, the walls behave as a single body, as is expected, because the hold-down yields before the shear connection. This is associated with increased hold-down displacement demand for fixed wall drift (Fig. A.8[b]) and decreased equivalent damping ratio (Fig. A.8[e]). Therefore, it is desirable to have a large enough ratio of hold-down strength to shear-connection strength, so that the walls respond as coupled walls with the shear connection yielding and dissipating energy.

(B) Vertical shear connection yield strength

For varying shear-connection yield strength, the trend is reversed with respect to hold-down strength, i.e. increasing shear connection strength corresponds to increasing hold-down demand and decreasing equivalent damping ratio. It is interesting that with increasing F_y^{VSC}, the damping ratio first increases, due to the larger hysteresis loop of the shear connection. By further increasing F_y^{VSC}, the walls start to respond as rigid body leading to abrupt decrease of the damping ratio (Fig. A.9(e)).

A.3 Two-storey CLT building

In this section, parametric analysis for a 2-storey CLT building are conducted. The purpose is to demonstrate the effect of the boundary condition between the 2 stories to lateral response.

A.4 Walls coupled with coupling beams

In this study, platform-type CLT construction is examined. There are two approaches in the literature for modelling multi-storey CLT platform buildings. In the first approach, the CLT floors are not simulated and the walls at one storey are directly connected to the lower and upper storey walls. In the second approach, the CLT floor diaphragm is explicitly or implicitly simulated. This automatically accounts for the geometric and kinematic constraints imposed by the diaphragm to the lower and

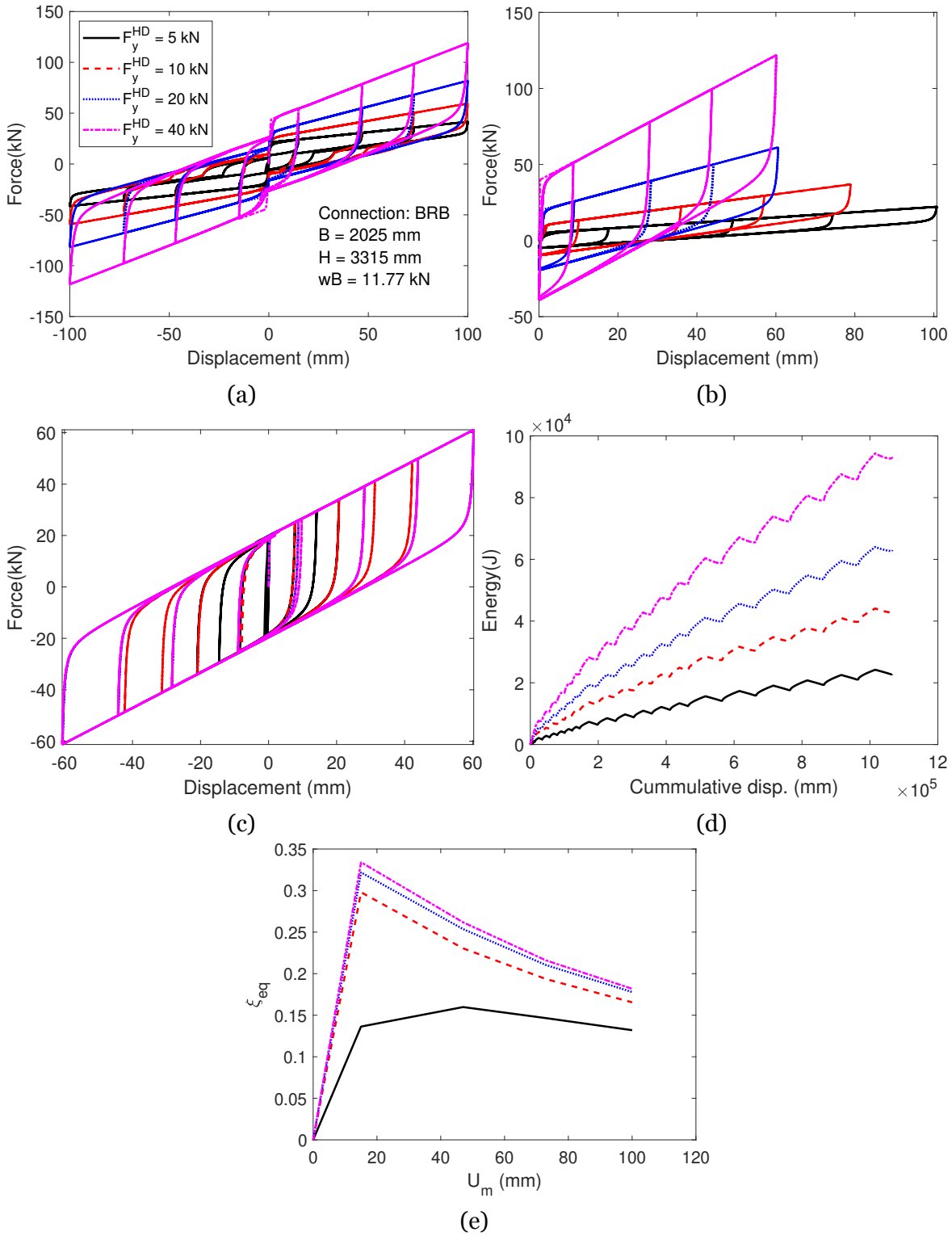

Figure A.7: Coupled CLT walls subjected to cyclic load; (a) Wall response; (b) Hold-down response; (c) Energy plot; (d) Equivalent damping ratio

upper storey CLT walls. Fig. A.15 and Fig. A.16 show the exaggerated deformed shape of a 3-storey building subjected to incremental displacement-controlled lateral load (pushover analysis), while Fig. A.17 shows the comparison between the two resulting

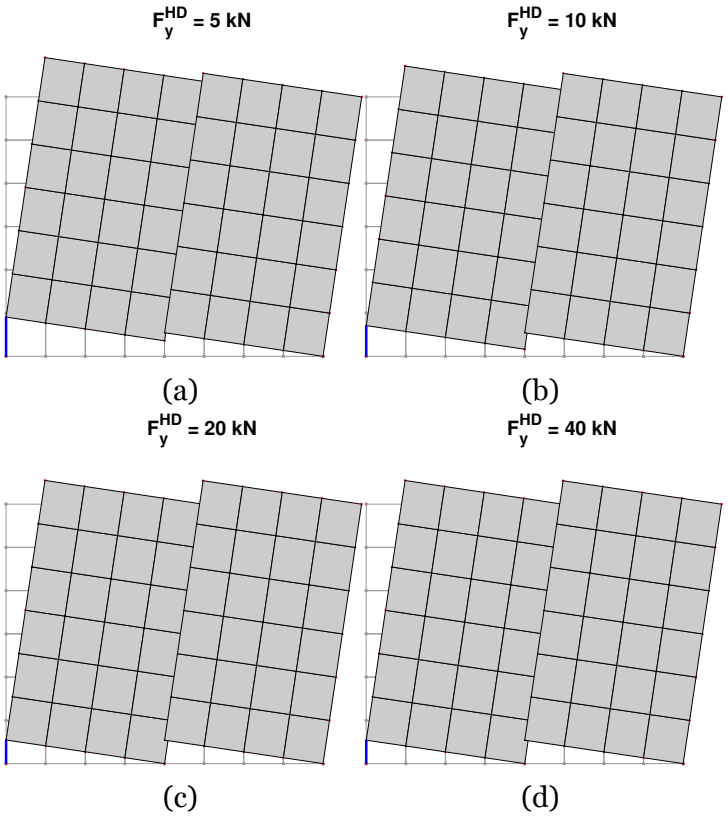

Figure A.8: Displaced shape of coupled walls for different values of the hold-down yield strength

pushover curves. The following remarks can be made:

- In the building without simulated floor diaphragms, a more uniform height-wise distribution of inelasticity is attained by yielding of the vertical shear connections at all floors. However, this is accompanied by kinematic incompatibilities between the different floors at the floor diaphragm locations.

- On the other hand, in the building with simulated diaphragms, the largest part of the lateral deformation is concentrated at the first storey (soft-storey formation). While the upper stories are displaced as a rigid body.

- The building with diaphragms is stiffer and has a larger lateral strength. This is due to the constraining action of the simulated floor diaphragms and despite the larger number of (flexible) connections utilized.

- Due to the latter, the building with diaphragms has a larger sliding displacement (activation of the shear brackets in the horizontal direction), because rocking action is constrained from the action of the diaphragms.

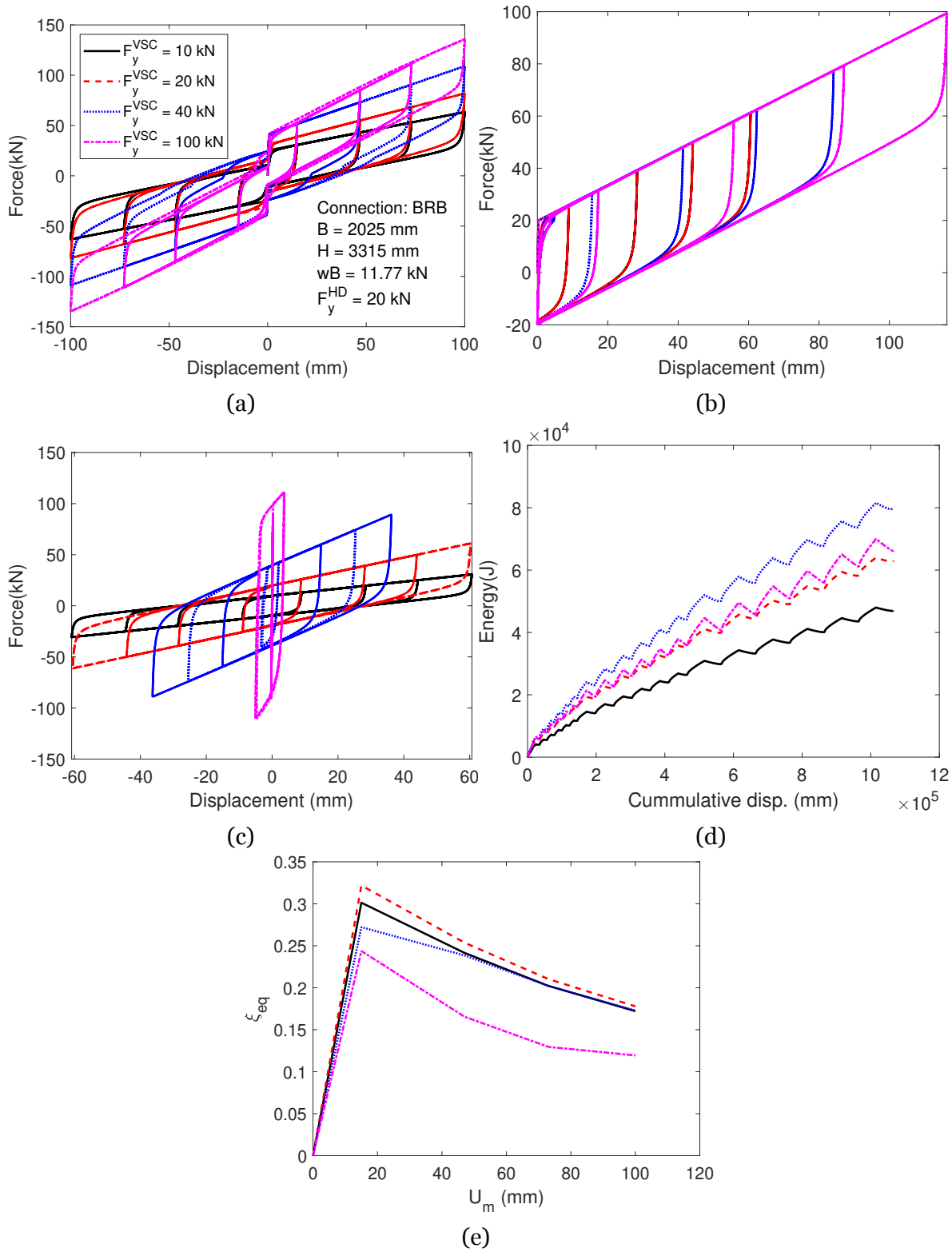

Figure A.9: Coupled CLT walls subjected to cyclic load; (a) Wall response; (b) Hold-down response; (c) Energy plot; (d) Equivalent damping ratio

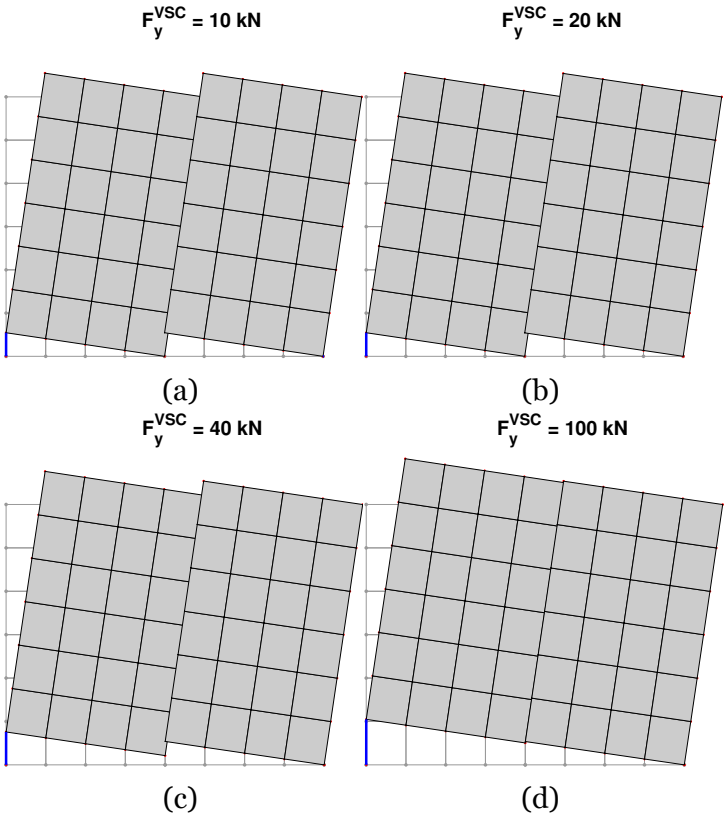

Figure A.10: Displaced shape of coupled walls for different values of hold-down yield strength

A.5 Modelling approaches of multi-storey coupled CLT buildings

Different approaches have been developed for modelling CLT buildings. It is noted that the modelling approach depends on the structural system which is further influenced by the construction type of the building. For multi-storey CLT buildings two distinct types of construction exist, namely platform-type (Izzi et al., 2018) and balloon-type (Chen and Popovski, 2020) construction. In platform-type construction the floor of each storey is used as base for the structural walls of the next storey. Whereas, in balloon-type construction the structural walls are first erected for the whole building and, subsequently, the floors are connected to the walls.

There are several distinct differences between platform-type and balloon-type CLT buildings. In multi-storey platform buildings, the accumulated vertical load is transferred from structural walls to lower floors perpendicular to the grain, thus inducing a critical stress condition. On the other hand, balloon buildings subjected to lateral load have a bending-type lateral deformation profile, with wall rotations

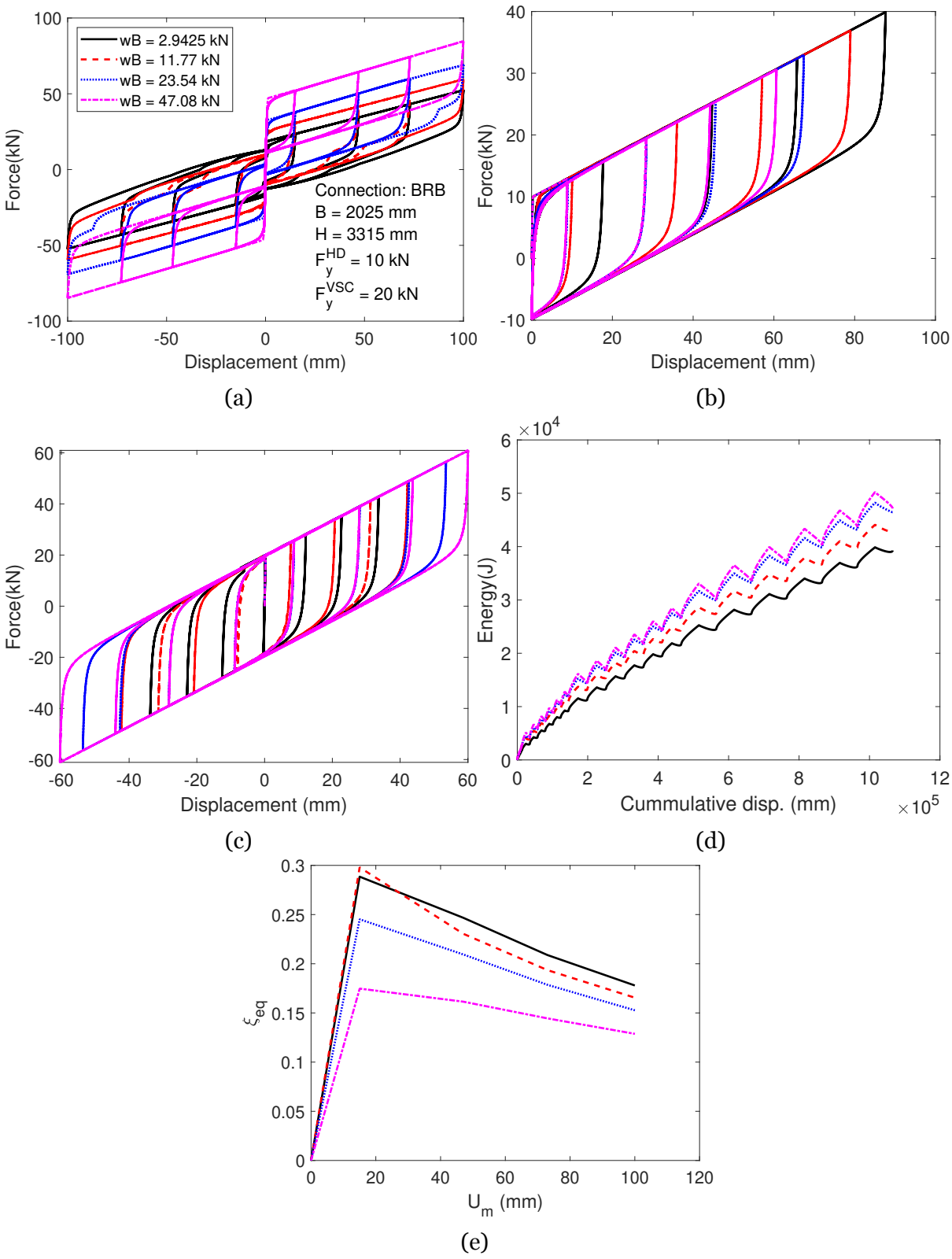

Figure A.11: Coupled CLT walls subjected to cyclic load; (a) Wall response; (b) Hold-down response; (c) Energy plot; (d) Equivalent damping ratio

accumulated from the base to the highest storey. These rotations are associated with large vertical displacement components that can induce large stresses to the

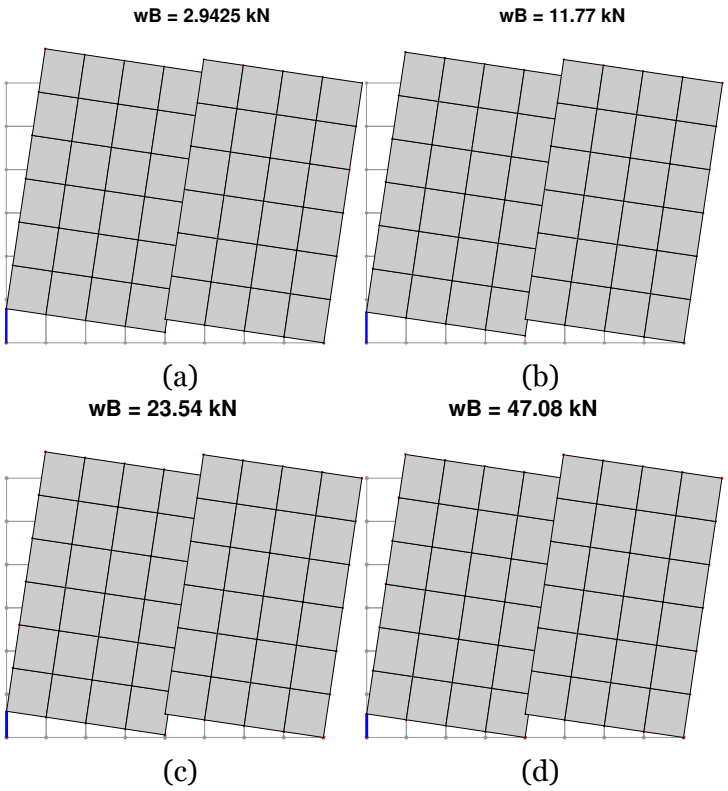

Figure A.12: Displaced shape of coupled walls for different values of vertical weight

floors. Therefore, a decoupling between the lateral and vertical load resisting system is desirable, which is challenging from a practical point of view.

Modelling of a multi-storey CLT building strongly depends on whether the building is platform or balloon type. A difference is that in platform buildings the constraining action of the floors and the wall-to-ceiling connections should be explicitly taken into account. The distinct variation in lateral response profile is illustrated in Fig. A.15 (balloon) and Fig. A.16 (platform). Explicitly simulating the constraining action of the floor diaphragm increases the stiffness of the system as is shown in Fig. A.17.

Notwithstanding the differences in response, the effect of simulated floor diaphragms are usually not taken into account when modelling platform buildings. For instance, Demirci et al. (2018) modelled platform buildings without explicitly modelling the floor diaphragms. Likewise, Shahnewaz et al. (2020) conducted fragility analysis of multi-storey CLT buildings without explicitly modelling the floor action.

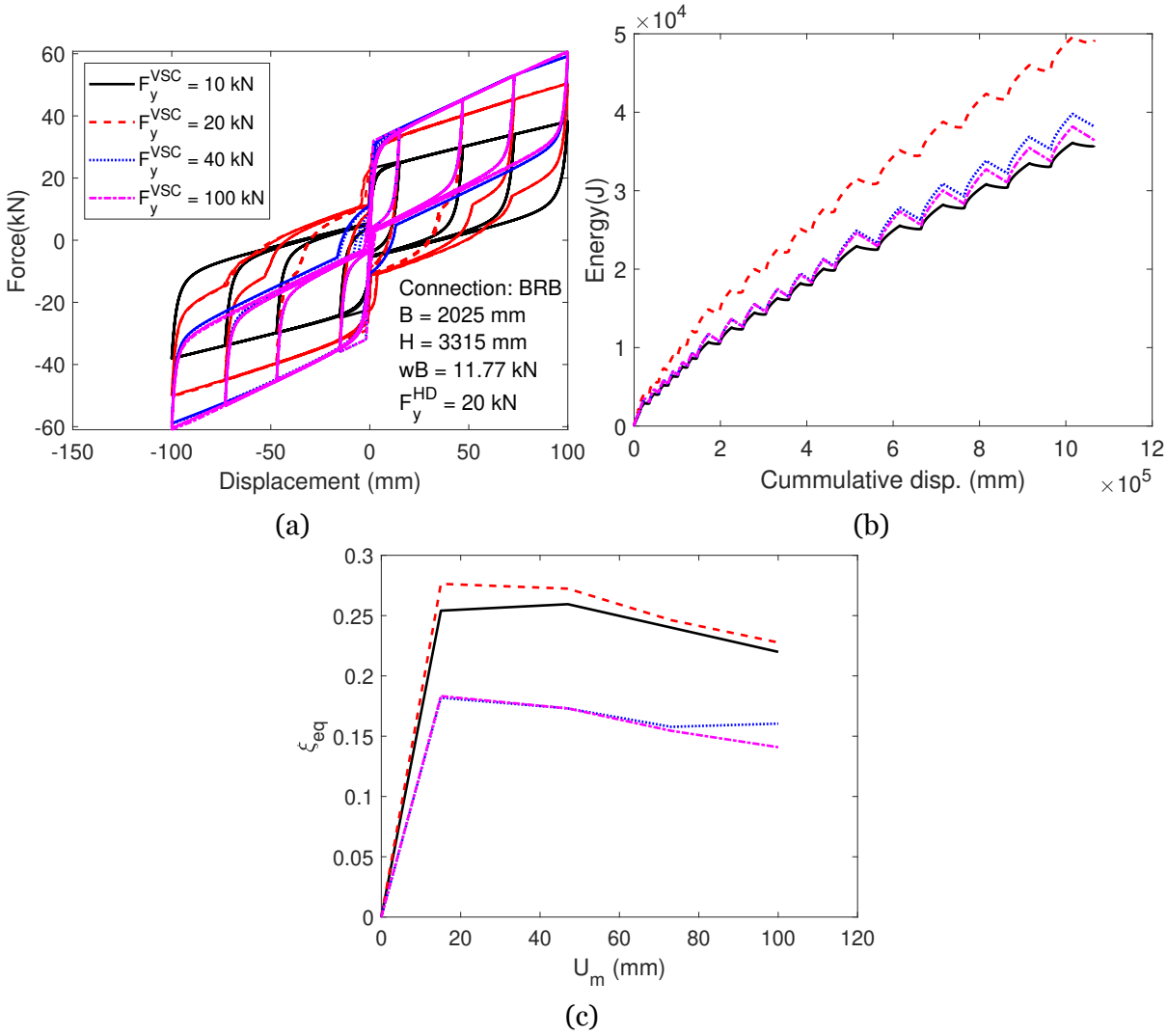

Figure A.13: Coupled (2-storey) CLT walls subjected to cyclic load; (a) Wall response; (b) Hold-down response; (c) Energy plot; (d) Equivalent damping ratio

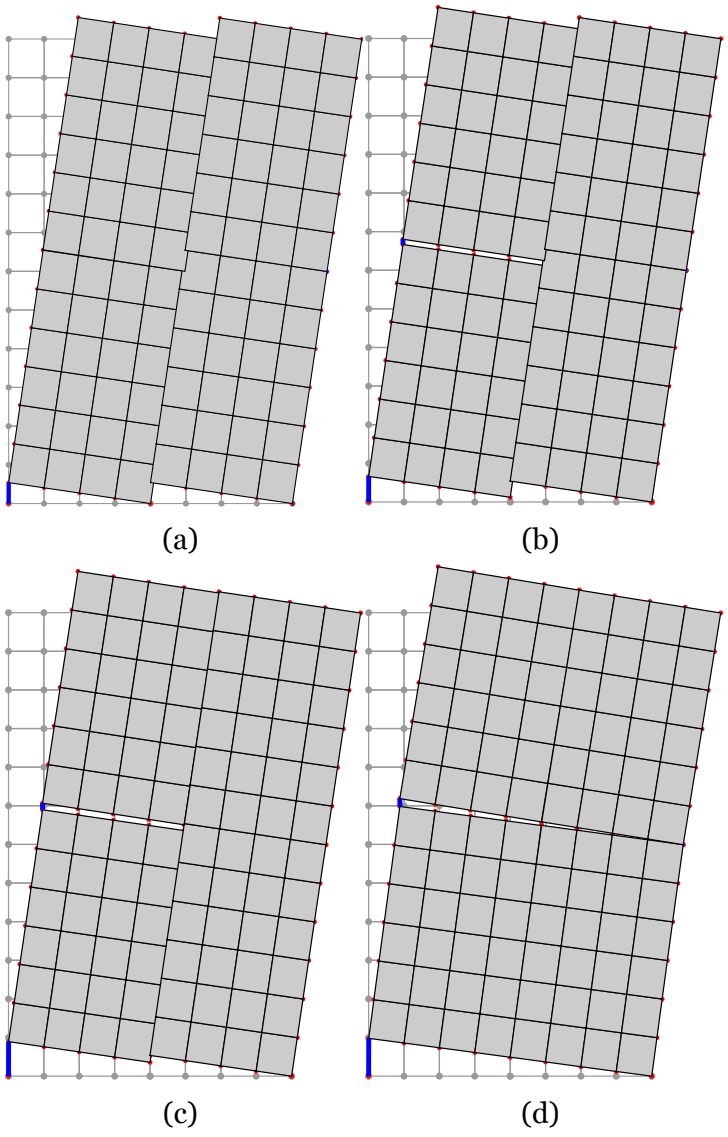

Figure A.14: Displaced shape of 2-storey coupled walls for different values of vertical weight

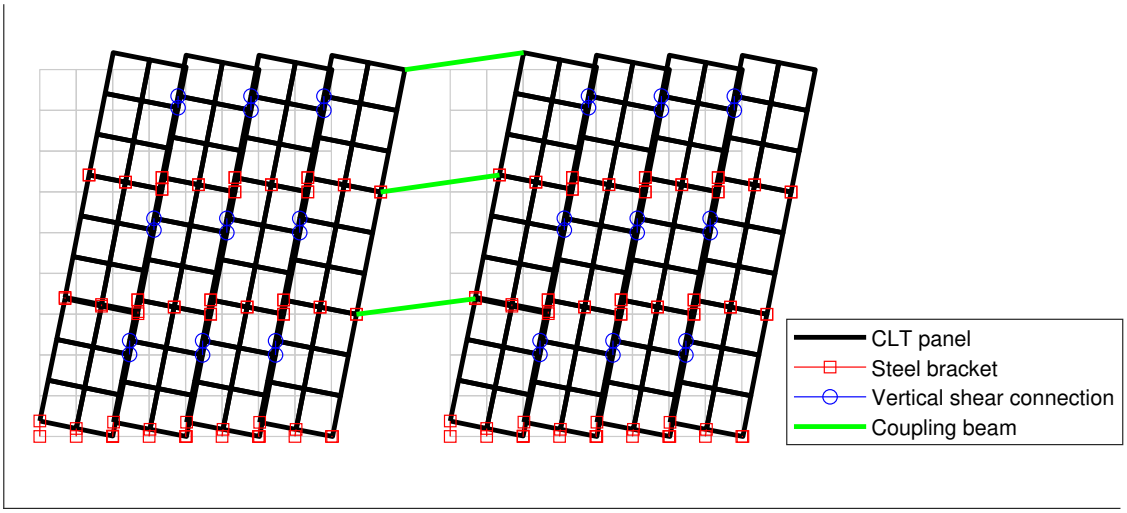

Figure A.15: Exaggerated view of 3-storey building without floor diaphragms in pushover analysis

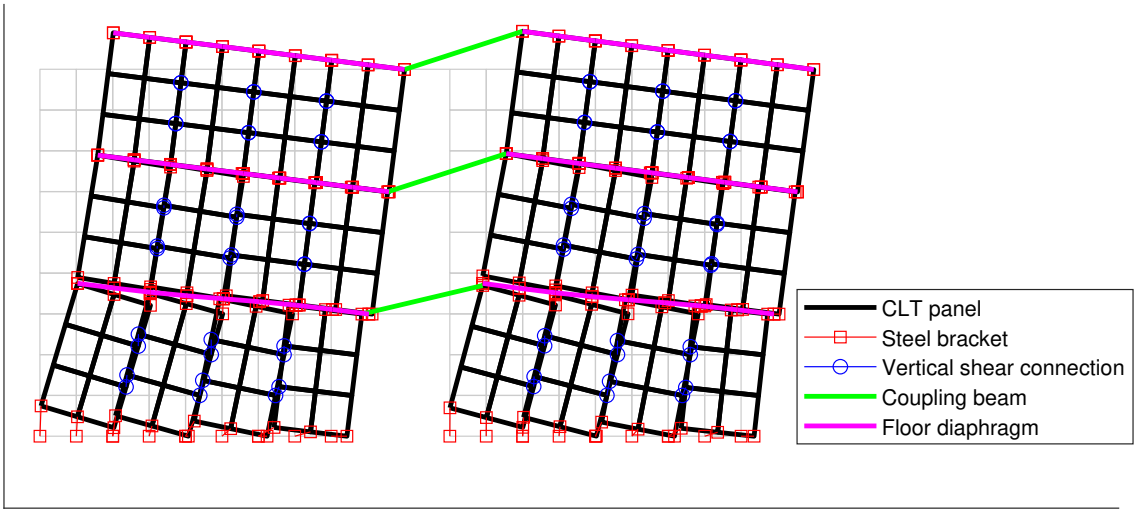

Figure A.16: Exaggerated view of 3-storey building with floor diaphragms in pushover analysis

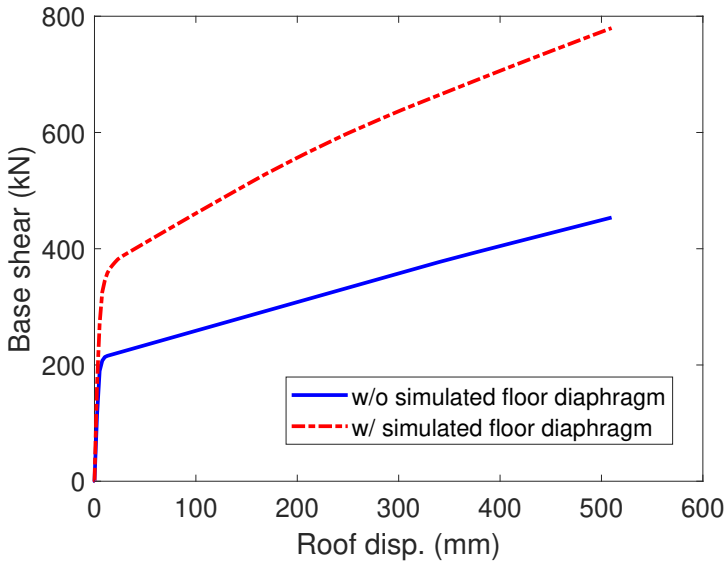

Figure A.17: Pushover curves for 3-storey buildings with and without simulated floor diaphragms

References

Akbas, T., Sause, R., Ricles, J. M., Ganey, R., Berman, J., Loftus, S., Dolan, J. D., Pei, S., van de Lindt, J. W., and Blomgren, H.-E. (2017). Analytical and experimental lateral-load response of self-centering posttensioned CLT walls. *Journal of Structural Engineering*, 143(6):04017019.

Ali, M. M. and Moon, K. S. (2018). Advances in structural systems for tall buildings: Emerging developments for contemporary urban giants. *Buildings*, 8(8):1–34.

ANSI, A. (2012). *ANSI/APA PRG 320–2012 Standards for Performance-Rated Cross-Laminated Timber*. American National Standards Institute (ANSI)/APA, Tacoma, US.

Atkinson, G. M. and Goda, K. (2011). Effects of seismicity models and new ground-motion prediction equations on seismic hazard assessment for four Canadian cities effects of seismicity models and ground-motion prediction equations on seismic hazard assessment. *Bulletin of the Seismological Society of America*, 101(1):176–189.

Baltzopoulos, G., Grella, A., and Iervolino, I. (2021). Seismic reliability implied by behavior-factor-based design. *Earthquake Engineering & Structural Dynamics*, 50(15):4076–4096.

Blomgren, H.-E., Pei, S., Jin, Z., Powers, J., Dolan, J. D., van de Lindt, J. W., Barbosa, A. R., and Huang, D. (2019). Full-scale shake table testing of cross-laminated timber rocking shear walls with replaceable components. *Journal of Structural Engineering*, 145(10):04019115.

Brandner, R., Flatscher, G., Ringhofer, A., Schickhofer, G., and Thiel, A. (2016). Cross laminated timber (CLT): overview and development. *European Journal of Wood and Wood Products*, 74(3):331–351.

Casagrande, D., Doudak, G., Mauro, L., and Polastri, A. (2018). Analytical approach to establishing the elastic behavior of multipanel CLT shear walls subjected to lateral loads. *Journal of Structural Engineering*, 144(2):04017193.

Chaallal, O., Gauthier, D., and Malenfant, P. (1996). Classification methodology for coupled shear walls. *Journal of Structural Engineering*, 122(12):1453–1458.

Chaallal, O. and Nollet, M.-J. (1997). Upgrading the degree of coupling of coupled shear walls. *Canadian Journal of Civil Engineering*, 24(6):986.

Chen, Z. and Popovski, M. (2020). Mechanics-based analytical models for balloon-type cross-laminated timber (CLT) shear walls under lateral loads. *Engineering Structures*, 208:109916.

Cheng, F., Mertz, G., Sheu, M., and Ger, J. (1993). Computed versus observed inelastic seismic low-rise RC shear walls. *Journal of Structural Engineering*, 119(11):3255–3275.

Chitty, L. (1947). On the cantilever composed of a number of parallel beams interconnected by cross bars. *Philosophical Magazine*, 38(285):685–699.

Christopoulos, C. and Montgomery, M. (2013). Viscoelastic coupling dampers (VCDs) for enhanced wind and seismic performance of high-rise buildings. *Earthquake Engineering & Structural Dynamics*, 42(15):2217–2233.

Colotti, V. (1993). Shear behavior of RC structural walls. *Journal of Structural Engineering*, 119(3):728–746.

Cornell, C. and Krawinkler, H. (2000). *Progress and challenges in seismic performance assessment*. PEER Center News 3, University of California, Berkeley.

Coull, A. and Choudhury, J. (1967a). Analysis of coupled shear walls. In *Journal Proceedings*, volume 64, pages 587–593.

Coull, A. and Choudhury, J. (1967b). Stresses and deflections in coupled shear walls. *Proceedings of the American Concrete Institute*, 64(2):65–72.

CSA (2014). *Standard CSA A23.3: Design of Concrete Structures*. Canadian Standards Association, Mississauga, Canada.

CSA (2016). *Standard CSA o86-14: Engineering design in wood (Supplement)*. Canadian Standards Association, , Mississauga, Canada.

CSA (2019). *Standard CSA o86-19: Engineering Design in Wood*. Canadian Standards Association, Mississauga, Canada.

Demirci, C., Málaga-Chuquitaype, C., and Macorini, L. (2018). Seismic drift demands in multi-storey cross-laminated timber buildings. *Earthquake Engineering & Structural Dynamics*, 47(4):1014–1031.

Deng, P., Pei, S., van de Lindt, J. W., Amini, M. O., and Liu, H. (2019). Lateral behavior of panelized CLT walls: A pushover analysis based on minimal resistance assumption. *Engineering Structures*, 191:469–478.

DeVall, R. H. (2003). Background information for some of the proposed earthquake design provisions for the 2005 edition of the National Building Code of Canada. *Canadian Journal of Civil Engineering*, 30(2):279–286.

Dowden, D. M. and Tatar, A. (2019). Seismically resilient self-centering cross-laminated rocking walls with coupling beams. In *Structures Congress 2019: Buildings and Natural Disasters*, pages 151–161. American Society of Civil Engineers Reston, VA.

Dubois, J.-M., Frappier, J., and Gallagher, S. (2020). Pushing the boundaries of mass timber construction and building codes. *International Journal of High-Rise Buildings*, 9(3):261–271.

El-Tawil, S. and Kuenzli, C. M. (2002). Pushover of hybrid coupled walls. II: Analysis and behavior. *Journal of Structural Engineering*, 128(10):1282–1289.

El-Tawil, S., Fortney, P., Harries, K., Shahrooz, B., Kurama, Y., Hassan, M., and Tong, X. (2009). *Recommendations for Seismic Design of Hybrid Coupled Wall Systems*. American Society of Civil Engineers.

El-Tawil, S., Harries, K. A., Fortney, P. J., Shahrooz, B. M., and Kurama, Y. (2010). Seismic design of hybrid coupled wall systems: State of the art. *Journal of Structural Engineering*, 136(7):755–769.

Eljadei, A. (2012). *Performance based design of coupled wall structures*. PhD thesis, University of Pittsburgh.

Eljadei, A. A. and Harries, K. A. (2014). Design of coupled wall structures as evolving structural systems. *Engineering Structures*, 73:100–113.

FEMA (2000). *Prestandard and commentary for the seismic rehabilitation of buildings, FEMA-356*. Federal Emergency Management Agency, Washington, D.C.

FEMA (2003). *NEHRP recommended provisions for seismic regulations for new buildings and other structures*. Federal Emergency Management Agency.

FEMA (2009). *Quantification of Building Seismic Performance Factors, FEMA P-695*. prepared by the Applied Technology Council for the Federal Emergency Management Agency, Washington, D.C.

Gavric, I., Fragiacomo, M., and Ceccotti, A. (2015). Cyclic behavior of CLT wall systems: Experimental tests and analytical prediction models. *Journal of Structural Engineering*, 141(11):04015034.

Goda, K. (2019). Nationwide earthquake risk model for wood-frame houses in Canada. *Frontiers in Built Environment*, 5:128.

Ha, K. H. and Tan, T. (1999). An efficient analysis of continuum shear wall models. *Canadian Journal of Civil Engineering*, 26(4):425–433.

Halchuk, S., Allen, T. I., Adams, J., and Rogers, G. C. (2014). *Fifth Generation Seismic Hazard Model Input Files as Proposed to Produce Values for the 2015 National Building Code of Canada*, volume 7576. Geological Survey of Canada, Open File.

Harries, K. A., Mitchell, D., Redwood, R. G., and Cook, W. D. (1997). Seismic design of coupled walls-a case for mixed construction. *Canadian Journal of Civil Engineering*, 24(3):448–459.

Harries, K. A., Moulton, J. D., and Clemson, R. L. (2004). Parametric study of coupled wall behavior—implications for the design of coupling beams. *Journal of Structural Engineering*, 130(3):480–488.

Harries, K. A. and McNeice, D. S. (2006). Performance-based design of high-rise coupled wall systems. *The Structural Design of Tall and Special Buildings*, 15(3):289–306.

Hashemi, A., Zarnani, P., Masoudnia, R., and Quenneville, P. (2018). Experimental

testing of rocking cross-laminated timber walls with resilient slip friction joints. *Journal of Structural Engineering*, 144(1):04017180.

Hull, D. H. and Harries, K. A. (2008). On the applicability of fixed point theory to the behavior of coupled core walls. *International Journal of Structural Stability and Dynamics*, 8(01):161–186.

Iqbal, A., Pampanin, S., Palermo, A., and Buchanan, A. (2015). Performance and design of LVL walls coupled with UFP dissipaters. *Journal of Earthquake Engineering*, 19(3):383–409.

Izzi, M., Casagrande, D., Bezzi, S., Pasca, D., Follesa, M., and Tomasi, R. (2018). Seismic behaviour of Cross-Laminated Timber structures: A state-of-the-art review. *Engineering Structures*, 170:42–52.

Ji, X., Liu, D., and Hutt, C. M. (2018). Seismic performance evaluation of a high-rise building with novel hybrid coupled walls. *Engineering Structures*, 169:216–225.

Ji, X. and Hutt, C. M. (2020). Seismic design and application of hybrid coupled walls with replaceable steel coupling beams in high-rise buildings. *The Structural Design of Tall and Special Buildings*, 29(8):e1727.

Kabeyasawa, T. (1982). Analysis of the full-scale seven story reinforced concrete test structure: Test PSD3. *Proceedings, 3rd Joint Technical Coordinationg Committee, US-Japan Cooperative Earthquake Research Program*.

Kurama, Y. C. and Shen, Q. (2004). Posttensioned hybrid coupled walls under lateral loads. *Journal of Structural Engineering*, 130(2):297–309.

Li, Y., Liu, Y., and Chen, Z. (2020). Seismic response assessment of a hybrid coupled wall structure with novel self-centering steel truss coupling beams. *Bulletin of Earthquake Engineering*, 18:1–24.

Liu, J. and Lam, F. (2014). Numerical simulation for the seismic behaviour of mid-rise CLT shear walls with coupling beams. In *2014 World Conference on Timber Engineering*.

Loo, W. Y., Quenneville, P., and Chouw, N. (2016). Rocking timber structure with slip-friction connectors conceptualized as a plastically deformable hinge within a multistory shear wall. *Journal of Structural Engineering*, 142(4):E4015010.

Lu, X., Chen, C., Jiang, H., and Wang, S. (2018). Shaking table tests and numerical analyses of an RC coupled wall structure with replaceable coupling beams. *Earthquake Engineering & Structural Dynamics*, 47(9):1882–1904.

Mazzoni, S., McKenna, F., Scott, M. H., Fenves, G. L., et al. (2006). OpenSees command language manual. *Pacific Earthquake Engineering Research (PEER) Center*, 264.

Mitchell, D., Tremblay, R., Karacabeyli, E., Paultre, P., Saatcioglu, M., and Anderson, D. L. (2003). Seismic force modification factors for the proposed 2005 edition of the National Building Code of Canada. *Canadian Journal of Civil Engineering*, 30(2):308–327.

Moon, K.-S., Connor, J. J., and Fernandez, J. E. (2007). Diagrid structural systems for tall buildings: characteristics and methodology for preliminary design. *The Structural Design of Tall and Special Buildings*, 16(2):205–230.

NBC (2015). *National Building Code of Canada, 2015*. National Research Council Canada, Ottawa, Canada.

Nolet, V., Casagrande, D., and Doudak, G. (2019). Multipanel CLT shearwalls: An analytical methodology to predict the elastic-plastic behaviour. *Engineering Structures*, 179:640–654.

Panagiotakos, T. B. and Fardis, M. N. (2001). Deformations of reinforced concrete members at yielding and ultimate. *Structural Journal*, 98(2):135–148.

Park, W.-S. and Yun, H.-D. (2005). Seismic behaviour of coupling beams in a hybrid coupled shear walls. *Journal of Constructional Steel Research*, 61(11):1492–1524.

PEER (2017). *Guidelines for Performance-Based Seismic Design of Tall Buildings*. Pacific Earthquake Engineering Research Center, University of California, Berkeley (PEER Report 2017/06).

Pei, S., van de Lindt, J. W., and Popovski, M. (2013). Approximate R-factor for cross-laminated timber walls in multistory buildings. *Journal of Architectural Engineering*, 19(4):245–255.

Pei, S., Lenon, C., Kingsley, G., and Deng, P. (2017). Seismic design of cross-laminated timber platform buildings using a coupled shearwall concept. *Journal of Architectural Engineering*, 23(3):06017001.

Petrone, C., Rossetto, T., and Goda, K. (2017). Fragility assessment of a RC structure under tsunami actions via nonlinear static and dynamic analyses. *Engineering Structures*, 136:36–53.

Popovski, M., Schneider, J., and Schweinsteiger, M. (2010). Lateral load resistance of cross-laminated wood panels. In *World Conference on Timber Engineering*, pages 20–24.

Porteous, J. and Kermani, A. (2013). *Structural Timber Design to Eurocode 5*. John Wiley & Sons.

Porter, K. A. (2003). An overview of PEER's performance-based earthquake engineering methodology. In *Proceedings of ninth international conference on applications of statistics and probability in civil engineering*, pages 1–8.

Priestley, M. N. (1993). Myths and fallacies in earthquake engineering. *Bulletin of the New Zealand Society for Earthquake Engineering*, 26(3):329–341.

Priestley, M. N., Calvi, G. M., and Kowalsky, M. J. (2007). *Displacement-based seismic design of structures*. IUSS press.

Rinaldin, G. and Fragiacomo, M. (2016). Non-linear simulation of shaking-table tests on 3-and 7-storey X-Lam timber buildings. *Engineering Structures*, 113:133–148.

Shahnewaz, M., Pan, Y., Shahria Alam, M., and Tannert, T. (2020). Seismic Fragility Estimates for Cross-Laminated Timber Platform Building. *Journal of Structural Engineering*, 146(12):04020256.

Shahrooz, B. M., Remmetter, M. E., and Qin, F. (1993). Seismic design and performance of composite coupled walls. *Journal of Structural Engineering*, 119(11):3291–3309.

Shen, Q. and Kurama, Y. C. (2002). Nonlinear behavior of posttensioned hybrid coupled wall subassemblages. *Journal of Structural Engineering*, 128(10):1290–1300.

Shen, Y.-L., Schneider, J., Tesfamariam, S., Stiemer, S. F., and Mu, Z.-G. (2013). Hysteresis behavior of bracket connection in cross-laminated-timber shear walls. *Construction and Building Materials*, 48:980–991.

Smith, B. S., Kuster, M., and Hoenderkamp, J. (1981). A generalized approach to

the deflection analysis of braced frame, rigid frame, and coupled wall structures. *Canadian Journal of Civil Engineering*, 8(2):230–240.

Smith, S. B. and Coull, A. (1991). *Tall Building Structures: Analysis and Design*. John Wiley amp; Sons, Inc.

Spacone, E. and El-Tawil, S. (2004). Nonlinear analysis of steel-concrete composite structures: State of the art. *Journal of Structural Engineering*, 130(2):159–168.

Tesfamariam, S., Stiemer, S. F., Bezabeh, M., Goertz, C., Popovski, M., and Goda, K. (2015). *Force Based Design Guideline for Timber-Steel Hybrid Structures: Steel Moment Resisting Frames with CLT Infill Walls*. UBC Faculty Research and Publications. `http://dx.doi.org/10.14288/1.0223405`.

Tesfamariam, S., Madheswaran, J., and Goda, K. (2019a). Displacement-based design of hybrid RC-timber structure: Seismic risk assessment. *Journal of Structural Engineering*, 145(11):04019125.

Tesfamariam, S., Bezabeh, M., Skandalos, K., Martinez, E., Dires, S., Bitsuamlak, G., and Goda, K. (2019b). *Wind and Earthquake Design Framework for Tall Wood-Concrete Hybrid System*. UBC Faculty Research and Publications. `http://dx.doi.org/10.14288/1.0380777`.

Tesfamariam, S., Skandalos, K., Goda, K., Bezabeh, M. A., Bitsuamlak, G., and Popovski, M. (2021). Quantifying the ductility-related force modification factor for 10-Story timber–RC hybrid building using FEMA P695 procedure and considering the 2015 NBC seismic hazard. *Journal of Structural Engineering*, 147(5):04021052.

Tesfamariam, S. and Das, S. (2021). *Resilient Tall Timber Building Design : Damped-Outrigger System*. UBC Faculty Research and Publications. `https://dx.doi.org/10.14288/1.0403816`.

Vamvatsikos, D. and Cornell, C. A. (2002). Incremental dynamic analysis. *Earthquake Engineering & Structural Dynamics*, 31(3):491–514.

Vamvatsikos, D., Bakalis, K., Kohrangi, M., Pyrza, S., Castiglioni, C. A., Kanyilmaz, A., Morelli, F., Stratan, A., D'Aniello, M., Calado, L., et al. (2020). A risk-consistent approach to determine EN1998 behaviour factors for lateral load resisting systems. *Soil Dynamics and Earthquake Engineering*, 131:106008.

van de Lindt, J. W., Amini, M. O., Rammer, D., Line, P., Pei, S., and Popovski, M. (2020). Seismic performance factors for cross-laminated timber shear wall systems in the United States. *Journal of Structural Engineering*, 146(9):04020172.

Veilleux, L., Gagnon, S., and Dagenais, C. (2015). *Mass Timber Buildings of Up to 12 Storeys: Directives and Explanatory Guide*. Régie du bâtiment du Québec.

Whittaker, A., Hart, G., and Rojahn, C. (1999). Seismic response modification factors. *Journal of Structural Engineering*, 125(4):438–444.

Xuan, G. (2006). *Performance-based design of a 15-story reinforced concrete coupled core wall structure*. PhD thesis, University of Cincinnati.

Yang, T., Xu, H., and Tobber, L. (2020). Mechanism and experimental validation of innovative self-centering conical friction damper. *Structural Control and Health Monitoring*, 27(10):e2609.

Zhang, X., Popovski, M., and Tannert, T. (2018). High-capacity hold-down for mass-timber buildings. *Construction and Building Materials*, 164:688–703.

Zona, A., Degée, H., Leoni, G., and Dall'Asta, A. (2016). Ductile design of innovative steel and concrete hybrid coupled walls. *Journal of Constructional Steel Research*, 117:204–213.

Zona, A., Tassotti, L., Leoni, G., and Dall'Asta, A. (2018). Nonlinear seismic response analysis of an innovative steel-and-concrete hybrid coupled wall system. *Journal of Structural Engineering*, 144(7):04018082.